

**ANALYSIS ON MRI BRAIN TUMOR SEGMENTATION USING
OPTIMIZATION - BASED DEEP LEARNING CLASSIFIER**

**A THESIS SUBMITTED IN PARTIAL FULFILLMENT OF THE
REQUIREMENTS FOR THE DEGREE OF
DOCTOR OF PHILOSOPHY**

PRAVIN SHIVAJI BIDKAR

MZU REGISTRATION NO.: 1900181

Ph. D. REGISTRATION NO.: MZU/Ph. D. /1558 of 24.07.2019



**DEPARTMENT OF ELECTRONICS & COMMUNICATION
ENGINEERING
SCHOOL OF ENGINEERING AND TECHNOLOGY
MARCH 2025**

**ANALYSIS ON MRI BRAIN TUMOR SEGMENTATION USING
OPTIMIZATION - BASED DEEP LEARNING CLASSIFIER**

BY

PRAVIN SHIVAJI BIDKAR

**DEPARTMENT OF ELECTRONICS & COMMUNICATION
ENGINEERING**

Name of Supervisor : DR. ABHIJYOTI GHOSH

Name of Joint Supervisor : DR. RAM KUMAR

Submitted

**In partial fulfillment of the requirement of the Degree of Doctor of Philosophy
in Electronics & Communication Engineering of Mizoram University, Aizawl**




Department of Electronic and Communication Engineering
School of Engineering and Technology
MIZORAM UNIVERSITY
(A Central University)
Tanhri, Aizawl - 796 004, Mizoram

CERTIFICATE

This is to certify that the thesis entitled “**Analysis on MRI Brain Tumor Segmentation using Optimization - Based Deep Learning Classifier**” submitted to Mizoram University for the award of the degree of **Doctor of Philosophy in Electronics and Communication Engineering** by **Pravin Shivaji Bidkar, Ph.D.** Registration No. **MZU/Ph.D./1558 of 24.07.2019**, is a Ph.D. scholar in the Department of Electronics and Communication Engineering, under our guidance and supervision, and has not been previously submitted for the award of any degree in any Indian or foreign University. He has fulfilled all criteria prescribed by the UGC (Minimum Standard and Procedure governing Ph.D. Regulations). He has fulfilled the mandatory publication (Publication enclosed) and completed Ph.D. coursework. It is also certified that the scholar has been admitted to the Department through an entrance test, followed by an interview as per the UGC Regulation of 2018.

Date:
GHOSH)
Place: Aizawl

(Dr. ABHIJYOTI
Supervisor


(Dr. RAM KUMAR)
Joint Supervisor

DECLARATION
MIZORAM UNIVERSITY
MARCH, 2025

I **PRAVIN SHIVAJI BIDKAR**, hereby declare that the subject matter of this thesis is the record of work done by me, that the contents of this thesis did not form basis of the award of any previous degree to me or to do the best of my knowledge to anybody else, and that the thesis has not been submitted by me for any research degree in any other University/Institute.

This is being submitted to the Mizoram University for the **Degree of Doctor of Philosophy in Electronics and Communication Engineering**.

(PRAVIN SHIVAJI BIDKAR)
Candidate

(Dr. ACHINTA BAIDYA)
Head of the Department

(Dr. ABHIJYOTI GHOSH)
Supervisor

Acknowledgement

I would like to express my sincere, heartfelt gratitude and indebtedness to my supervisors, **Dr. Abhijyoti Ghosh**, Assistant Professor, Department of Electronics and Communication Engineering, Mizoram University, Aizawl, Mizoram, and joint supervisor, **Dr. Ram Kumar**, Assistant Professor, Department of Electrical and Electronics Engineering, Katihar Engineering college, Katihar, Bihar for their support, effective guidance, timely motivation, and constant encouragement throughout this research work. I am also thankful to **Prof. Reshmi Maity**, Head of the Department of Electronics and Communication Engineering, Mizoram University, Aizawl, Mizoram, and to **Prof. Sudipta Chattopadhyay**, Professor, Department of Electronics and Communication Engineering, Mizoram University, for his valuable inputs during research work.

I thank my doctoral committee members, for their suggestions and comments that have enabled me to complete the research work. I would like to mention special thanks to my friends **Dr. Jayendra Kumar**, **Dr. Pritam Nikam** and **Dr. Akshay Bhosale** for their endless support during this journey.

I extend my heartfelt gratitude to my late grandparents, **Yashvant Bidkar**, and **Sonabai**, whose legacy has enriched my journey. I appreciate the love, efforts, and sacrifices of my father, **Mr. Shivaji Bidkar**, and mother, **Mrs. Anandi**, for educating and preparing me for my future. I owe my thanks to my sister, **Mrs. Justice Poonam Gaikwad**, and Brother-in-Law, Tahsildar **Mr. Dipak Gaikwad**, as well as my wife, **Mrs. Bhagyashree**, for their support during research work. I dedicate this work to my niece, **Tanisha** and **Vedanshi** and my children, **Samarjeet** and **Bhargav**, who have made me stronger, better, and motivate me to keep moving forward.

Lastly, I place on record, my sense of gratitude to one and all who, directly or indirectly have lent their helping hand in this venture.

(PRAVIN SHIVAJI BIDKAR)

Table of Contents

| | |
|--|----------------|
| Acknowledgement | i |
| Table of Contents | ii |
| List of Figures | v |
| List of Tables | vii |
| List of Abbreviations | viii |
| List of Symbols | ix |
| Chapter 1 Introduction and Literature Review | 1 - 22 |
| 1.1 Introduction | 1 |
| 1.2 Literature review | 2 |
| 1.3 Motivation | 20 |
| 1.4 Objective | 20 |
| 1.5 Summary | 21 |
| Chapter 2 Robust and Adaptable SWO-based DBN for Brain Tumor Segmentation and Classification | 23 - 59 |
| 2.1 Introduction | 23 |
| 2.2 Challenges | 24 |
| 2.3 Proposed Salp Water Optimization-based Deep Belief Network for brain tumor segmentation and classification | 25 |
| 2.3.1 Pre-processing | 26 |
| 2.3.2 Segmentation of pre-processed image with SegNet | 27 |
| 2.3.3 Feature extraction with CNN features | 30 |
| 2.3.4 Brain tumor classification with the developed Salp Water Optimization-based Deep Belief Network | 31 |
| 2.4 Results and discussion | 35 |
| 2.4.1 Evaluation metrics | 35 |
| 2.4.2 Simulation results | 36 |
| 2.4.3 Performance analysis using dataset 2018 | 39 |
| 2.4.4 Performance analysis using BRATS 2020 dataset | 43 |
| 2.4.5 Comparative methods | 46 |
| 2.4.6 Comparative analysis using dataset 2018 | 47 |

| | | |
|------------------|--|----------|
| 2.4.7 | Comparative analysis using dataset 2020 | 52 |
| 2.4.8 | Comparative discussion | 56 |
| 2.5 | Summary | 59 |
| Chapter 3 | Enhanced Brain Tumor Recognition with Adam-based Techniques for Clinical Diagnosis | 60 - 88 |
| 3.1 | Introduction | 60 |
| 3.2 | Challenges | 61 |
| 3.3 | Proposed Adam SWO-DCNN for BT Segmentation and Classification | 62 |
| 3.3.1 | Image acquisition | 62 |
| 3.3.2 | Image pre-processing | 63 |
| 3.3.3 | BT segmentation using Unet++ | 64 |
| 3.3.4 | Feature extraction | 69 |
| 3.3.5 | BT classification using Adam SWO-DCNN | 72 |
| 3.4 | Results and discussion | 78 |
| 3.4.1 | Performance metrics | 78 |
| 3.4.2 | Experimental result | 79 |
| 3.4.3 | Competitive analysis | 79 |
| 3.4.4 | Segmentation analysis | 87 |
| 3.4.5 | Comparative discussion | 87 |
| 3.5 | Summary | 88 |
| Chapter 4 | Optimizing Brain Health with ASO-DRN Technique for MRI based Brain Tumor Classification | 89 - 107 |
| 4.1 | Introduction | 89 |
| 4.2 | Challenges | 91 |
| 4.3 | Proposed ASO-DRN for brain tumor classification | 92 |
| 4.3.1 | Image acquisition | 92 |
| 4.3.2 | Pre-processing of image | 92 |
| 4.3.3 | Segmentation of image | 93 |
| 4.3.4 | Feature extraction | 94 |
| 4.3.5 | Classification of brain tumor | 95 |
| 4.4 | Results and discussion | 101 |
| 4.4.1 | Experimental results | 101 |

| | | |
|------------------|---|-----------|
| 4.4.2 | Comparative assessment | 102 |
| 4.4.3 | Comparative discussion | 106 |
| 4.5 | Summary | 107 |
| Chapter 5 | Maximizing Accuracy in Brain Tumor Classification using Adaptive ASWO_DbneAlexnet Approach | 108 - 124 |
| 5.1 | Introduction | 108 |
| 5.2 | Challenges | 109 |
| 5.3 | Proposed adaptive ASWO_Dbnealexnet for brain tumor classification | 110 |
| 5.3.1 | Acquisition of input MRI | 110 |
| 5.3.2 | Adaptive biateral filter-based pre-processing | 110 |
| 5.3.3 | Tumor segmentation using U-Net++ | 111 |
| 5.4 | Result and discussion | 118 |
| 5.4.1 | Experimental results | 118 |
| 5.4.2 | Comparative evaluation | 118 |
| 5.5 | Summary | 123 |
| Chapter 6 | Conclusion and Scope of Future Studies | 125 - 126 |
| | References | 127 - 138 |
| | Brief Bio-data of candidate | 139 |
| | List of Publications | 140 |
| | Particulars of the candidate | 141 |

List of Figures

| | | |
|-------------|--|----|
| Figure 1.1 | Sample MR images with tumor | 2 |
| Figure 2.1 | Schematic representation of the devised SegNet+SWO-based DBN model for tumor segmentation and classification | 26 |
| Figure 2.2 | CNN feature extraction | 30 |
| Figure 2.3 | DBN classifier architecture | 32 |
| Figure 2.4 | Experimental results using BRATS dataset 2018, (a) input image (b) ground truth image (c) segmented output image | 37 |
| Figure 2.5 | Experimental results using BRATS dataset 2018, (a) Input image, (b) ground truth image, and (c) segmented output image | 38 |
| Figure 2.6 | Performance analysis with hidden neurons (a) specificity, (b) accuracy, (c) and sensitivity | 40 |
| Figure 2.7 | Performance analysis with batch size (a) specificity, (b) accuracy, (c) and sensitivity | 42 |
| Figure 2.8 | Performance analysis with hidden neurons (a) specificity, (b) accuracy, (c) and sensitivity | 44 |
| Figure 2.9 | Performance analysis with batch size (a) specificity, (b) accuracy, (c) and sensitivity | 46 |
| Figure 2.10 | Analysis of methods for Dataset 2018 using (a) dice coefficient, (b) segmentation accuracy | 48 |
| Figure 2.11 | Analysis of methods considering training data (a) specificity, (b) accuracy, (c) sensitivity, and (d) ROC | 51 |
| Figure 2.12 | Analysis of methods for Dataset 2020 using (a) Dice coefficient, (b) Segmentation accuracy | 53 |
| Figure 2.13 | Analysis of methods using dataset 2020 considering training data (a) specificity, (b) accuracy, (c) sensitivity, and d) ROC | 56 |
| Figure 2.14 | Comparative plot of classification accuracy of different methods | 58 |
| Figure 3.1 | Block diagram of Adam SWO-DCNN for BT classification | 63 |
| Figure 3.2 | Structure of UNet++ | 64 |
| Figure 3.3 | Extracted CNN feature from CNN | 70 |
| Figure 3.4 | Structure of DCNN | 71 |
| Figure 3.5 | Experimental result of AdamSWO-DCNN a) Input images, b) Pre-processed images, c) Segmented images, d) LGP feature, e) Loop feature | 80 |
| Figure 3.6 | Analysis of evaluation metrics with respect to training data a) Accuracy, b) NPV, c) PPV, d) TNR, e) TPR | 83 |

| | | |
|------------|--|-----|
| Figure 3.7 | Analysis of evaluation metrics with respect to k-value a) Accuracy, b) NPV, c) PPV, d) TNR, e) TPR | 86 |
| Figure 3.8 | Analysis of segmentation based on dice coefficient | 86 |
| Figure 4.1 | Illustrative diagram of the devised ASO-DRN for classifying brain tumors | 93 |
| Figure 4.2 | SegNet architecture | 93 |
| Figure 4.3 | DRN architecture | 97 |
| Figure 4.4 | Image results showing (a) Input MRI image, (b) Pre-processed image, (c) Segmented image | 102 |
| Figure 4.5 | Comparative investigation of (a) accuracy, (b) TPR, and (c) TNR of the implemented ASO-DRN with other techniques on the basis of the training data | 104 |
| Figure 4.6 | Analyzation of a) accuracy, b) TPR, and c) TNR of various techniques on the basis of k-value | 106 |
| Figure 5.1 | Diagrammatic illustration of proposed Adaptive ASWO_DbneAlexnet for brain tumor classification | 111 |
| Figure 5.2 | Overview of U-Net++ | 113 |
| Figure 5.3 | Architecture of DbneAlexnet | 115 |
| Figure 5.4 | Experimental outcomes, a) Input image, b) Pre-processed result, c) Segmented outcome, d) LOOP feature | 118 |
| Figure 5.5 | Estimation with training data, (a) Accuracy, (b) TPR, (c) TNR | 120 |
| Figure 5.6 | Estimation with K-value, (a) Accuracy, (b) TPR, (c) TNR | 122 |

List of Tables

| | | |
|-----------|---|-----|
| Table 2.1 | Segmentation accuracy using the proposed method and existing methods for BRATS 2018 dataset | 48 |
| Table 2.2 | Segmentation accuracy using the proposed method and existing methods for BRATS 2020 dataset | 53 |
| Table 2.3 | Comparative discussion for segmentation | 57 |
| Table 2.4 | Comparative discussion based on training data percentage | 58 |
| Table 2.5 | Comparative discussion of classification accuracy | 58 |
| Table 3.1 | Comparative discussion | 87 |
| Table 3.2 | Analysis of Segmentation technique | 88 |
| Table 4.1 | Comparative discussion of the proposed technique | 106 |
| Table 5.1 | Comparative discussion | 123 |

List of Abbreviations

| | |
|-------------|--|
| ABF | Adaptive Bilateral Filter |
| ASM | Angular Second Moment |
| ASO | Adaptive Salp Swarm Optimization |
| ASWO | Adaptive Salp Water Optimization |
| AdamSTBO | Adam Sewing Training Based Optimization |
| AdamSWO | Adam Salp Water Wave Optimization |
| AvgPool | Average Pooling |
| BRATS | Brain Tumor Segmentation |
| BT | Brain Tumor |
| CNN | Convolutional Neural Network |
| CRF | Conditional Random Field |
| DCNN | Deep Convolutional Neural Network |
| DNN | Deep Neural Network |
| DRN | Deep Residual Network |
| DbneAlexnet | Deep Belief Network Extension of AlexNet |
| ED | Peritumoral Edema |
| ET | Enhancing Tumor |
| FC | Fully Connected |
| FCNN | Fully Convolutional Neural Network |
| FLAIR | Fluid-Attenuated Inversion Recovery |
| GCNN | Graph Convolutional Neural Network |
| GLCM | Gray-Level Co-Occurrence Matrix |
| IDM | Inverse Difference Moment |
| LGP | Local Gradient Pattern |
| LOOP | Local Optimal Oriented Pattern |
| MLP | Multilayer Perceptron |
| MRI | Magnetic Resonance Imaging |
| NCR/NET | Necrotic and Non-Enhancing Tumor Core |
| NPV | Negative Predictive Value |
| PHOG | Pyramid Histogram of Oriented Gradients |
| PPV | Positive Predictive Value |
| RBM | Restricted Boltzmann Machine |
| ROC | Receiver Operating Characteristic |
| ReLU | Rectified Linear Unit |
| SSA | Salp Swarm Algorithm |
| STBO | Sewing Training Based Optimization |
| SWO | Salp Water Optimization |
| SegNet | Segmentation Network |
| TNR | True Negative Rate |
| TPR | True Positive Rate |
| U-Net++ | Enhanced U-Net |
| WWO | Wavelet Weighted Optimization |
| eLU | Exponential Linear Unit |

List of Symbols

| | |
|----------------------|--|
| \approx | Approximately equal to |
| \neq | Not equal to |
| \leq | Less than or equal to |
| \geq | Greater than or equal to |
| \pm | Plus, or minus |
| \sum | Summation symbol |
| $\sqrt{}$ | Square root |
| ∞ | Infinity |
| \int | Integral |
| Δ | Change in |
| μ | Mean or Micro |
| σ | Standard deviation |
| λ | Wavelength or Lambda |
| π | Pi, ratio of circumference to diameter |
| α | Alpha |
| β | Beta |
| γ | Gamma |
| Ω | Ohm or Omega |
| θ | Theta |
| Ξ | Zai |

CHAPTER

1

Introduction and Literature

Review

1.1 Introduction

A digital image is a set of numbers arranged in a form of a matrix, which are known as grey levels. The smallest part of the digital image is called a pixel. Digital image processing is a branch of engineering that processes captured digital data. Digital image processing focuses on two major tasks first, is the improvement of pictorial information for better human interpretation. The professionals like doctors, photographers and film makers etc. uses these improved images for their applications. Second, is the processing of image data for extracting object attributes to give inputs for autonomous machine processing [1, 2]. Here the processed images are segmented in different parts, these different parts of images are compared with the pre-defined shapes and separation is made depending on the application. Different attributes of these shapes like area, perimeter, diameter etc. are measured. This is achieved using different image transforms and processes like segmentation, morphological image processing etc. [3].

Magnetic Resonance Imaging (MRI) image is a digital image. The procedure to capture the MRI is as follows. Human body contains around 55% to 60% of water. It is un-uniformly spread in the entire body. Different tissues contain different percentage of water, like muscle tissues contain 75% and adipose tissues i.e. body fat contains 10% [4]. Water molecules are combinations of hydrogen and oxygen atoms. Hydrogen atom has Proton at its center which is highly sensitive to magnetic field. During MR image capturing these protons are aligned with a strong magnetic field of MRI scanner. After that radio waves are passed through that particular body part e.g.

brain, heart etc. Different tissues containing protons, react differently to these radio waves. These radiation from tissues are captured as a MR image. So, it is clear that, as each tissue has different number of protons gives different grey level in MR image. So different parts of tissues can be identified [5].

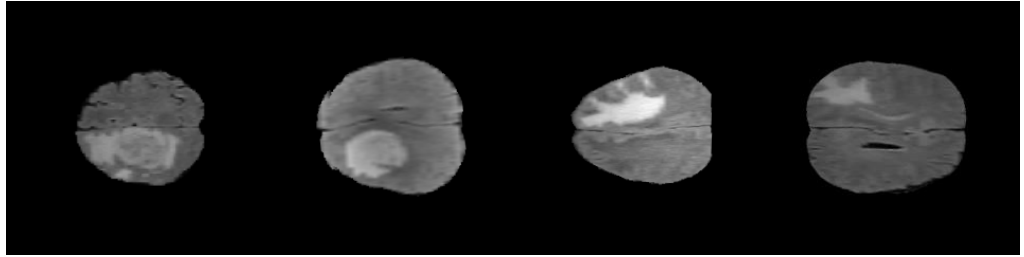


Figure 1.1: Sample MRI images with tumor

Soft tissues of the brain are significantly identified by the MRI. Thus, for tumor detection MRI can be used effectively. As well as MRI provides the various output images for dissimilar soft tissues of the human brain. Thus, MRI image can collect information about the presence of tumors and other tissues of the brain [6]. Brain MRI is the effective sources of detecting the infected tissues, their growth and stage of tumor, giving the guideline to the doctors about the exact use of drug to be used for the medication of patient. The researchers and the experts get plenty amount of information from the availability of MRI images and their processing technology [7]. Brain MRIs are sorted out for detecting the information about the brain and the arrangement of infected tissues in the brain. Processing of MRI is carried out for the detection of tumor and medication planning of the patient. Multiple modalities are used for the MRI image. Different modality shows different image information from different angles and gives different contents. There are various ways to differentiate between the infected cell and usual cells. Brain tumor has an irregular shape. For a human being, there is a limitation to detect the tumor because of time requirement and accuracy. Also, the experienced manpower is required for the same [8].

Glioma is a common malignant tumor in the brain with rapid dispersion and high mortality. For this tumor, immediate treatment is needed at the early stage [9]. A brain tumor is an uncontrolled condition in the brain, which leads to forming an abnormal group of cells in the brain or the neighboring areas [10]. This abnormal cell formation abrupt brain's normal processing with adverse effects on the patient's life.

Brain MRI images become very popular to detect brain tumors for the treatment process. Based on the availability and technology of MRI images, the researchers collect a large amount of information for taking decisions corresponding to brain tumors [11, 12]. With high-resolution MRI images, the formation of the abnormalities is easily determined [13, 14]. From several techniques, MRI is considered as the best one for studying the human brain to get valuable information about the soft tissue.

For improving the extracted information from the MR images, several MRI modalities, like T2-weighted spin-spin relaxation (T2), T1-weighted MRI with contrast improvement (T1c), T1-weighted spin-lattice relaxation (T1), and T2-weighted MRI with fluid attenuation inversion recovery (T2flair) are employed [15, 16]. The multiple modalities offer different patterns and intensity levels for similar tumor regions. The segmentation in MRI brain tumor images is significant to evaluation, treatment planning as well as early diagnosis. While segmenting brain tumors, a huge effort is needed to develop brain tumor segmentation approaches automatically.

The purpose of brain tumor segmentation is to partition brain tumors into edema, necrosis, enhancing, and non-enhancing tumor. The edema provides the involvement to be explored during the surgery. Thus, the tumor type and malignant degree of the tumor are determined effectively. Segmentation plays a major role in brain tumor classification for extracting the infected region of brain MRI images [17]. Segmentation of brain tumors accurately from MRI sequences is very significant in treatment planning as well as clinical diagnostics. Thus, a huge amount of irregular data created by the MRI avoids the manual segmentation precise at the particular time. The semi-automatic and automatic brain tumor segmentation methods are commonly classified as either generative models or methods. The generative model-driven tumor segmentation approaches with suitable information gained using probabilistic image atlases [18]. Therefore, the tumor segmentation issue is modelled as the detection issue. Moreover, this model solves the segmentation problem in the pattern classification setting by classifying the image voxels as the tumor or the normal tissues with the help of image feature [19, 20].

1.2 Literature review

Recent advancements in MRI-based medical image analysis for brain tumors are driven by the need for efficient and objective evaluation of large datasets. The evolution of automated methods over the past two decades, highlighting their increasing applicability in routine clinical settings are discussed in [4]. The focus is on segmentation, registration, and modelling techniques, particularly for gliomas, aiming to outline tumor boundaries and address morphological changes. Emphasis is placed on approaches compatible with standard clinical protocols, with a critical evaluation of current methods and a discussion of future trends, including updates in radiological tumor assessment guidelines.

MRI-based brain tumor segmentation methods, emphasizing the growing popularity of deep learning techniques due to their ability to achieve state-of-the-art results and handle large datasets efficiently has been reported in [8]. Manual segmentation of brain tumors from MRI images is time-consuming, necessitating automatic segmentation methods. The literature provides an overview of deep learning algorithms for brain tumor segmentation, discussing their advantages over traditional methods and addressing future developments for integrating these techniques into clinical practice.

In [11], a stochastic model for characterizing brain tumor texture in MR images, employing multifractional Brownian motion (mBm). The model is applied for patient-independent tumor texture feature extraction and segmentation in MRIs, utilizing a novel algorithm to extract multifractal features. A multifractal feature-based segmentation method is developed and compared with existing approaches, demonstrating superior performance. Additionally, a patient-independent segmentation scheme based on modified AdaBoost algorithm is proposed and evaluated, showing efficacy in automatic tumor segmentation in brain MRIs, outperforming other state-of-the-art methods on publicly available datasets.

An automated brain tumor segmentation algorithm employing a deep convolutional neural network (DCNN) to address the challenging task of detecting gliomas with irregular shapes and ambiguous boundaries is studied in [12]. The

algorithm utilizes a patch-based approach with an inception module and incorporates recent advancements in deep neural networks to mitigate overfitting. Pre-processing includes normalization and bias field correction, followed by patch extraction and classification by the DCNN. A two-phase weighted training method is introduced, enhancing performance on BRATS 2013 and BRATS 2015 datasets compared to existing techniques.

The study in [15] focuses on segmenting infant brain tissue images during the isointense stage, a challenging task due to similar intensity levels of white matter (WM) and grey matter (GM) in T1 and T2 MR images. Using deep convolutional neural networks (CNNs) and multi-modality MR images (T1, T2, and fractional anisotropy), the proposed method achieves superior segmentation performance compared to existing techniques. The CNN architecture employs trainable filters and pooling operations to extract complex features from the input images, demonstrating the effectiveness of integrating multi-modality information for improved segmentation accuracy.

A fully automated method for detecting and segmenting brain tumor tissue from FLAIR MRI images using a super pixel-based approach is implemented in [16]. Various novel image features are utilized for robust classification, including intensity-based, Gabor textons, fractal analysis, and curvatures. Evaluation on clinical and BRATS 2012 datasets shows high performance with an extremely randomized trees (ERT) classifier, achieving average detection sensitivity, balanced error rate, and Dice overlap measure close to expert delineation across different grades of glioma, offering potential for faster and more reproducible tumor detection and delineation in clinical settings.

A generative approach for registering a probabilistic atlas of healthy brain populations to MRI scans showing glioma and segmenting them into tumor and healthy tissue labels is discussed in [19]. The method utilizes the expectation maximization (EM) algorithm, incorporating a glioma growth model for atlas seeding and refinement. Results from segmenting 10 MR scans demonstrate superior performance compared to reference methods, with similar accuracy to human raters.

Additionally, the method is applied to 122 patient scans, allowing estimation of tumor model parameters and construction of a statistical atlas of glioma.

In [21], the challenges of manually segmenting and detecting brain tumors on MRI scans, prompting the development of automatic systems for accurate results. The proposed method comprises five stages, including image acquisition, pre-processing, segmentation using Fuzzy C Means technique, tumor extraction, and evaluation based on criteria like area and circularity. Validation against manually segmented ground truth shows promising results, with an average Dice coefficient value of 0.729 indicating the method's effectiveness.

The study in [22] focuses on developing deep learning models for efficient segmentation of brain tumors in multi-sequence MR images, particularly glioblastomas with varying properties. Three incremental deep convolutional neural network models are proposed, differing from previous approaches by avoiding trial-and-error hyper-parameter tuning and incorporating ensemble learning for enhanced efficiency. Results from experiments on the BRATS-2017 dataset show state-of-the-art performance, with an average Dice score of 0.88 and quick segmentation averaging 20.87 seconds. These models offer accurate and rapid segmentation, potentially aiding physicians in expediting diagnostic processes.

The use of image processing techniques on MRI scans to potentially detect Alzheimer's disease (AD) early, focusing on assessing total brain and hippocampal atrophy, which are strong indicators of AD is explored in [23]. Various techniques such as K-means clustering, wavelet transform, and a customized algorithm are applied to T1 weighted MRIs. Implemented on open-source platforms like OpenCV and Qt, the developed product could assist doctors in early AD detection, correlating with psychiatric results and aiding in understanding and treating AD progression.

An image segmentation method aimed at identifying brain tumors in MRI scans, given the significance of brain tumor research due to its high prevalence is introduced in [24]. While existing thresholding methods yield varying results, this study proposes a set of segmentation algorithms tailored for consistent tumor detection across different images. The proposed algorithms demonstrate satisfactory

performance in segmenting brain tumor images, offering potential for more reliable and uniform tumor detection.

While grey matter has historically received more attention, white matter, comprising half of the human brain, has been overlooked in cognition and learning studies. However, emerging research using imaging and cellular/molecular approaches suggests that white matter plasticity may have significant implications for cognitive function and psychological disorders. This shift in perspective highlights the potential importance of white matter in understanding normal brain function and related pathologies [25].

The study in [26] introduces an adaptive convolutional neural network architecture designed to segment brain tumors from Multimodal Magnetic Resonance Images (MRIs) with improved efficacy. The model autonomously selects local and global features from the image data using interacting sub paths, while mitigating overfitting through dropout mechanisms. Evaluation on the MICCAI BraTS 2018 dataset demonstrates the model's effectiveness, yielding high scores in metrics such as Dice coefficient, Mean Intersection over Union, Sensitivity, and Specificity, surpassing some state-of-the-art methods.

Accurate segmentation of brain tumors is crucial for effective treatment, given their diverse locations and characteristics. The study in [27] introduces a deep convolutional neural network (CNN) tailored for segmenting brain tumors in MRIs, leveraging the BRATS segmentation challenge dataset. The proposed network architecture, an extension of existing models, exhibits superior performance compared to non-deep learning techniques, as evidenced by experimental results on the BRATS 2015 benchmark data.

A fully automatic brain tumor segmentation method using Deep Neural Networks (DNNs), designed for glioblastomas observed in MR images is discussed in [28]. Given the diverse nature of these tumors, the study explores a machine learning solution using flexible, high-capacity DNNs for efficient segmentation. Novel CNN architectures are presented, leveraging both local and global contextual features simultaneously, along with a unique convolutional implementation of fully

connected layers for accelerated processing. Additionally, a 2-phase training procedure and a cascade architecture are proposed to address label imbalance and enhance segmentation accuracy, achieving significant improvements over existing methods while offering substantial speed enhancements.

The study in [29] proposes an enhanced automated brain tumor segmentation and identification method utilizing Artificial Neural Networks (ANN) from MR images, aiming to overcome the challenges posed by the diverse shapes and intensities of brain tumors. The approach integrates K-means clustering for initial image enhancement, followed by ANN-based object selection and texture feature extraction for precise tumor segmentation. Grayscale features are then leveraged for tumor diagnosis, distinguishing between benign and malignant cases. Results demonstrate the effectiveness of the ANN approach, achieving high accuracy and sensitivity in brain tumor classification compared to alternative methods like SVM segmentation.

In [30], stacked sparse auto-encoder (SSAE), a semi-supervised deep learning technique, is presented for RNA-seq data-based cancer prediction. Using a sparsity penalty term and greedy layer-wise pre-training, the SSAE technique efficiently classifies samples and extracts relevant information from high-dimensional data. Testing on three public RNA-seq datasets for different cancer types demonstrates that SSAE outperforms other classification methods, highlighting its promising ability for accurate cancer prediction.

The study in [31] introduces a novel method utilizing transfer learning to correct sampling selection errors in automated tumor segmentation caused by sparse annotations during supervised learning. Traditional approaches are hindered by labor-intensive and error-prone manual segmentation requirements. The proposed method effectively derives high-quality classifiers from sparse annotations and employs domain adaptation techniques to correct sampling errors. Validation on multi-modal MR images demonstrates significant reductions in labelling and training time without sacrificing accuracy, easing the establishment and extension of annotated databases and advancing the practical applicability of learning-based tissue classification approaches.

A learning-based framework for robust and automatic nucleus segmentation in histopathology images, crucial for disease detection like brain tumor and breast cancer is introduced in [32]. The proposed method utilizes a deep convolutional neural network (CNN) for probability map generation, followed by an iterative region merging approach and a novel segmentation algorithm. Notably, the framework demonstrates superior performance across various staining histopathology images, outperforming recent state-of-the-art methods in comparative experiments on large-scale pathology datasets.

A novel methodology that integrates human brain connect omics and parcellation for brain tumor segmentation and survival prediction is discussed in [33]. The segmentation process utilizes existing brain parcellation atlas data mapped to individual subjects, employing deep neural network architectures with hard negative mining for voxel-level classification. For survival prediction, the method combines connect omics data, brain parcellation information, and brain tumor masks, leveraging features from the Human Connectome Project to compute tractographic features indicating potential neural disruptions caused by tumors. Experimental results on the BraTS2018 dataset demonstrate the effectiveness of the proposed methods.

In [34], Auto-Context Forests for brain tumor segmentation in multi-channel MRI images, enhancing generalization, compactness, and semantic understanding. Contributions include an efficient node-splitting criterion, faster training, and guided semantic bagging for improved performance. The proposed framework, a top performer in the MICCAI 2016 BRATS challenge, offers practicality, fast training, and robustness, with this paper detailing the challenge entry and discussing its results.

The challenging task of gliomas segmentation in brain tumors using deep learning and MRI modalities is addressed in [35]. The proposed hybrid convolutional neural network incorporates local and contextual information for accurate segmentation while mitigating overfitting with dropout regularization and batch normalization. A two-phase training procedure is employed to tackle data imbalance, resulting in improved performance on the BRATS 2013 dataset with higher scores

for dice, sensitivity, and specificity compared to state-of-the-art techniques. Additionally, pre-processing and post-processing steps enhance the segmentation accuracy by normalizing images and removing false positives.

The study in [36] focuses on detecting and classifying brain tumors from MRI images through six stages: Input Image, Pre-processing, Segmentation, Post Processing, Feature Extraction, and Classification. The initial phases involve reading the MRI image, pre-processing with image smoothing and enhancement techniques, and segmentation using the Pillar KMeans algorithm, which selects pillar pixels for effective segmentation. Experimental results demonstrate the algorithm's effectiveness in tumor segmentation, with post-processing operations applied to clearly locate the tumor in the brain.

Glioblastoma segmentation in medical image processing, highlighting limitations of current methods in capturing contextual information is explored in [37]. Leveraging the UNet architecture, the research employs a sophisticated training scheme with dynamic sampling, data augmentation, and class-sensitive loss, facilitating training on relatively small datasets. Qualitative comparison with state-of-the-art approaches demonstrates favorable performance of the proposed method, emphasizing its potential for improved glioblastoma segmentation.

The study in [38] introduces a novel 11-layer, three-dimensional Convolutional Neural Network (CNN) for brain lesion segmentation, addressing limitations of existing networks. To mitigate computational demands, an efficient dense training scheme is devised, integrating adjacent image patches for improved processing. A dual pathway architecture enables simultaneous processing of input images at multiple scales to incorporate local and contextual information. Post-processing employs a 3D fully connected Conditional Random Field to refine segmentation, yielding improved performance across three challenging lesion segmentation tasks in MRI patient data. The method demonstrates computational efficiency and achieves top-ranking performance on public benchmarks, facilitating adoption in research and clinical settings.

The study in [39] focuses on the detection and classification of brain tumors, emphasizing the urgency of early detection and treatment due to their significant impact on mortality. Utilizing neural networks, feature extraction via Gray Level Co-Occurrence Matrix (GLCM), and Principal Component Analysis (PCA) for image recognition and compression, the research aims to classify tumors as normal, benign, or malignant. K-means clustering is employed for segmentation, detecting tumor spread regions, and identifying defective cells. Simulation using MATLAB 2013 software demonstrates the effectiveness of the proposed method, with probabilistic neural networks (PNN) offering efficient classification accuracy.

Breast cancer remains a significant cause of mortality globally, particularly for women. Early detection is crucial for effective treatment. The study in [40] introduces a deep learning approach for breast cancer detection and classification in cytology images, employing transfer learning from pre-trained CNN architectures like GoogLeNet, VGGNet, and ResNet. By utilizing knowledge gained from one problem to another, the proposed framework achieves superior accuracy in detecting and classifying malignant and benign cells, surpassing other deep learning architectures in benchmark datasets.

In [41], improvements in semantic image segmentation using Deep Learning, focusing on atrous convolution and atrous spatial pyramid pooling (ASPP) techniques are discussed. Atrous convolution enables precise control over feature resolution and context incorporation without increasing parameters or computation. ASPP enhances segmentation robustness across multiple scales by probing convolutional features with filters at various sampling rates. Additionally, the study combines Deep Convolutional Neural Networks (DCNNs) with probabilistic graphical models to improve object boundary localization, achieving state-of-the-art performance on several datasets. The proposed “DeepLab” system achieves significant advancements in semantic segmentation tasks, with code publicly available for further research.

The study in [42] introduces a novel ensemble strategy for image denoising using multiple deep neural networks, addressing the challenge of high diversity in natural image patches and noise distributions. The approach divides the denoising

task into local subtasks based on patch complexity, employing separate networks for each subtask. At test time, the outputs of these networks are combined using a weighted mixture determined by the likelihood of each network for each noisy patch. Experimental results demonstrate significant performance improvements over single-network approaches, with reduced training samples and parameters, leading to decreased time complexity in both training and running.

A framework for supervised segmentation of gliomas from MRI scans, addressing challenges such as tumor location variability and intensity signature ambiguity is presented in [43]. It employs multiple modality intensity, geometry, and asymmetry feature sets to drive a random forest-based segmentation approach. The inclusion of asymmetry-related features, derived from optimal symmetric multimodal templates, demonstrates strong discriminative properties. Furthermore, probability maps generated from random forest models are used to refine the segmentation through a Markov random field regularization approach, achieving high performance as evidenced by its top-ranking performance in the MICCAI 2013 Multimodal Brain Tumor Segmentation challenge.

A framework for automatic brain tumor segmentation from MR images, incorporating simultaneous detection of edema is presented in [44]. Unlike other methods relying on contrast-enhanced images, this framework solely utilizes the T2 MR image channel, allowing for broader applicability. The segmentation process comprises three stages: abnormal region detection using a brain atlas, determination of intensity properties, and application of geometric and spatial constraints to identify tumor and edema regions. The method is validated on diverse real datasets, demonstrating its efficacy across various tumor characteristics.

A novel method for Glioblastoma (GBM) feature extraction using Gaussian mixture model (GMM) features from MRI images, including T1-WI, T2-WI, and FLAIR MR images is implemented in [45]. Multi thresholding segmentation with morphological operations is employed to detect pathological areas in the images. Evaluation using multi classifier techniques demonstrates that GMM features outperform principal component analysis (PCA) and wavelet-based features, achieving high accuracy in identifying GBM versus normal tissue across different

MRI modes. The results show promising potential for improving GBM heterogeneity characterization and facilitating early treatment.

An efficient brain tumor detection method utilizing Neural Networks (NN) and a previously developed brain tissue segmentation technique is implemented in [46]. It outlines the steps involved, including pre-processing, segmentation of pathological and normal tissues, feature extraction, and classification using NN. The proposed method is evaluated using Quality Rate (QR) and standard metrics such as sensitivity, specificity, and accuracy, demonstrating superior performance compared to other classification techniques like K-NN and Bayesian classification.

An automated system for brain tumor diagnosis and tumor region extraction, aiming to improve timely detection and diagnosis is presented in [47]. The system includes pre-processing for noise removal, texture feature extraction, and ensemble-based SVM classification achieving over 99% accuracy. It further employs a multi-step segmentation process, including skull removal, brain region extraction, and FCM clustering for accurate tumor region extraction from MR images, demonstrating promising results across datasets from different medical centers.

Various Principal Component Analysis (PCA) algorithms for dimension reduction in T1-weighted MRI images clustering for brain tumor segmentation are investigated in [48]. Five PCA algorithms are compared, including conventional PCA, PPCA, EM-PCA, GHA, and APEX, in combination with K-Means and Fuzzy C-Means clustering methods. Results suggest that PPCA yields the best outcomes, particularly when combined with K-Means, across different sizes of MRI images, indicating its efficacy in improving clustering performance for brain tumor segmentation.

An enhanced fully convolutional network for end-to-end brain tumor segmentation in MRI images, improving upon the U-Net architecture is introduced in [49]. Innovative features include up skip connections, inception modules, and a cascade training strategy, facilitating richer feature learning and sequential subregion segmentation. The proposed method outperforms U-Net, achieving higher accuracy

in tumor segmentation across different datasets, demonstrating its competitiveness with state-of-the-art approaches.

A novel brain tumor segmentation method combining fully convolutional neural networks (FCNNs) and Conditional Random Fields (CRFs) to achieve consistent segmentation results is studied in [50]. The method involves training FCNNs and CRFs using 2D image patches and slices, followed by fine-tuning with a voting-based fusion strategy. Evaluation on BRATS datasets demonstrates competitive performance, with the ability to segment brain images slice-by-slice more efficiently than patch-based methods.

A deep learning-based approach for automating brain tumor segmentation in MR images, aiming to improve accuracy in medical image analysis is proposed in [51]. By integrating Stationary Wavelet Transform (SWT) and a new Growing Convolutional Neural Network (GCNN), the method enhances segmentation efficiency compared to conventional systems. Experimental results demonstrate superior performance over Support Vector Machine (SVM) and Convolutional Neural Network (CNN) approaches, as evidenced by metrics such as accuracy, PSNR, and MSE.

The study in [52] introduces an automatic brain tumor segmentation method, combining the small kernels two-path convolutional neural network (SK-TPCNN) with random forests (RF). The SK-TPCNN structure enhances nonlinear mapping and mitigates overfitting by incorporating small and large convolutional kernels, increasing feature diversity. The learned features are then utilized by the RF classifier for joint optimization, effectively classifying MRI image voxels into normal brain tissues and tumor regions. The proposed method demonstrates improved performance in the Brain Tumor Segmentation Challenge (Brats) 2015 Training dataset.

In [53], an automated brain tumor segmentation method leveraging texture features and kernel sparse coding from FLAIR MRI scans. The process involves pre-processing MRIs to enhance contrast and correct intensity non-uniformity, followed by sparse coding on statistical eigenvectors. Kernel dictionary learning is then

applied to extract non-linear features, enabling the construction of adaptive dictionaries for healthy and pathological tissues. A kernel-clustering algorithm and linear discrimination method classify target pixels, with flood-fill operations enhancing segmentation quality. The approach showcases improved capacity and segmentation accuracy at low computational cost.

The study in [54] focuses on glioma segmentation from MRI images, crucial for clinical diagnostics and treatment planning due to the high mortality associated with these tumors. Automatic segmentation is necessary due to the large volume of MRI data, but variability among brain tumors poses a challenge. The proposed Deep Convolutional Symmetric Neural Network (DCSNN) integrates left-right asymmetry prior knowledge, achieving competitive segmentation results with an average Dice similarity coefficient of 0.852 on the BRATS 2015 database. Despite not being the top performer, DCSNN outperforms recent DCNN-based methods in segmentation efficiency, taking only about 10.8 seconds per patient case.

Urban scene classification using a fusion of hyperspectral and Pol-SAR data to provide comprehensive insights into complex urban scenes are reviewed in [55]. Existing fusion methods may lack in extracting sufficient information and integrating lower-dimensional data. To address this, an end-to-end convolutional neural network is proposed, featuring a novel two-stream architecture that separately processes each dataset before merging them in a balanced manner. Experimental results indicate the superior performance of this framework compared to other fusion methods, marking the first instance of a deep convolutional neural network effectively fusing hyperspectral and SAR data.

A novel approach for automatic image style recognition, crucial for various applications. Unlike traditional CNN methods focusing solely on object features, this approach incorporates texture features alongside object features is implemented in [56]. The proposed CNN architecture includes two pathways, one for objects and one for textures, jointly trained to capture complementary information. Experimental results, particularly with the VGG-19 model, demonstrate superior performance on benchmark datasets, surpassing previous state-of-the-art methods.

In [57], a novel technique for image compression using a deep wavelet autoencoder (DWA) in the context of brain imaging. Leveraging the feature reduction capability of autoencoders and the image decomposition property of wavelet transform, DWA aims to compress images efficiently for subsequent classification tasks using deep neural networks (DNN). Experimental results on a brain image dataset demonstrate the superiority of the proposed DWA-DNN classifier over existing methods like autoencoder-DNN or DNN alone, showcasing its potential for enhanced image processing in medical science.

The study in [58] introduces a method for automatic segmentation of MR brain images into tissue classes using a convolutional neural network (CNN). The CNN utilizes multiple patch and convolution kernel sizes to capture multi-scale information for accurate segmentation and spatial consistency. Not reliant on explicit features, the CNN learns relevant information from training data. Tested on various datasets, including images of preterm infants and adults, the method achieves high average Dice coefficients, demonstrating its robustness across different ages and acquisition protocols.

The significance of early detection and accurate segmentation of brain tumors using MRI scans due to their potential life-threatening nature is discussed in [59]. It introduces a novel deep learning algorithm, combining kernel-based CNN with M-SVM, for automatic and efficient tumor segmentation. The method involves pre-processing, feature extraction, image classification, and tumor segmentation steps, utilizing techniques like Laplacian of Gaussian filtering and Contrast Limited Adaptive Histogram Equalization. Experimental results indicate that the proposed approach achieves approximately 84% accuracy in brain tumor segmentation, outperforming existing algorithms.

The development of a diagnostic system for brain tumors using MRI images in DICOM format is given in [60]. This system accurately classifies tumors as benign or malignant, achieving a high classification accuracy of 98.9% based on experimental evaluation with brain tumor images. Brain tumors are highlighted as a life-threatening condition arising from abnormal cell growth in the brain.

A novel method for automatically dissecting brain tumors in MR images, comprising four stages: pre-processing, dissection, feature extraction and reduction, and classification is introduced in [61]. Pre-processing involves noise reduction using a Wiener filter. The dissection stage employs amended region recovering-based segmentation, while features are extracted using combined edge and texture-based methods. Principal Component Analysis (PCA) is then used for dimensionality reduction before classification using a kernel-based SVM. Evaluation metrics like similarity index (SI), overlap fraction (OF), and extra fraction (EF) show improved tumor detection compared to neural network-based classifiers.

The challenge of brain tumor detection and segmentation in medical image processing are proposed in [62]. A hybrid approach combining deep autoencoder and Bayesian fuzzy clustering for segmentation, followed by feature extraction using robust techniques like scattering transform and wavelet packet Sall is entropy, is proposed. Classification is achieved through a hybrid scheme of deep autoencoder and softmax regression. The method demonstrates high classification accuracy (98.5%) on the BRATS 2015 database, outperforming other state-of-the-art methods.

In [63], the importance of intrusion detection systems (IDS) in protecting wireless sensor networks (WSN) from security threats is proposed. It highlights the challenges faced by IDS due to irrelevant or redundant dataset dimensions, impacting detection speed and performance. To address this, the paper introduces feature selection using the self-adaptive differential evolution (SaDE) algorithm, which dynamically selects Candidate Solution Generation Strategies (CSGS) and optimizes control parameters. Experimental results on the KDDCUP99 dataset show SaDE's effectiveness compared to other algorithms, evaluated using the K-Nearest Neighbor (KNN) method.

The study in [64] discusses a deep learning-based approach for segmenting and recognizing brain tumors, particularly gliomas, from MRI scans. The method involves contrast enhancement, saliency map construction, feature extraction using a pre-trained CNN model, and texture analysis with dominant rotated LBP. Optimization through particle swarm optimization (PSO) is employed for feature selection and classification. Validation on BRATS2017 and BRATS2018 datasets

demonstrates high segmentation accuracy, with dice scores ranging from 79.94% to 93.7%, and classification accuracy exceeding 92% on BRATS2013, 2014, 2017, and 2018 datasets, showcasing superior performance in both segmentation and classification tasks for brain tumor analysis.

The extensive use of deep convolutional neural networks (CNNs) in brain MRI analysis, focusing on lesion segmentation, anatomical segmentation, and classification tasks is overviewed in [65]. It presents a comprehensive literature review detailing various CNN architectures, pre-processing techniques, data preparation methods, and post-processing strategies employed in this domain. The study aims to summarize the evolution of CNN architectures, discuss state-of-the-art strategies, analyses results from public datasets, and evaluate their strengths and limitations. Additionally, it serves as a detailed reference for current research activities in deep CNN-based brain MRI analysis and offers insights into future research directions in this field.

The study in [66] provides an overview of the challenges in automatic brain tumor segmentation due to factors like tumor diversity and the use of multiple imaging techniques. It emphasizes the importance of multimodal imaging, such as PET/CT and PET/MRI, in enhancing segmentation accuracy. The article discusses recent techniques for brain tumor segmentation using MRI, PET, CT, and multimodal imaging, outlining their principles, advantages, limitations, and future challenges.

The challenges faced by one-stage object detectors compared to two-stage detectors and proposes a novel solution called Focal Loss to address the issue of extreme foreground-background class imbalance during training are discussed in [67]. By reshaping the standard cross-entropy loss, Focal Loss focuses on hard examples, preventing easy negatives from overwhelming the detector during training. The proposed approach is evaluated through the design and training of a dense detector called Retina-Net, which achieves both speed and accuracy, surpassing existing state-of-the-art detectors.

A deep learning algorithm for scene categorization that incorporates both object attributes and spatial structures of scene images using two-pathway convolutional neural networks is introduced in [68]. Unlike traditional methods, each pathway focuses on a different aspect of images, allowing for more comprehensive information utilization. The algorithm addresses feature redundancy by adopting the $\ell_{2,1}$ norm during classifier training. Experimental results demonstrate the superior performance of the proposed method compared to conventional approaches, indicating its potential for broader applications.

The significance of noise removal in automatic speech recognition (ASR) systems and the increased demand for ASR in the Tamil language is discussed in [69]. It proposes a bidirectional recurrent neural network (BRNN) with a self-organizing map (SOM)-based classification scheme for Tamil speech recognition. The method involves pre-processing the input speech signal with a Savitzky–Golay filter, extracting Multivariate Autoregressive and perceptual linear predictive coefficients, and using SOM to select the appropriate feature vector length. Experimental results show that the proposed approach outperforms existing methods in terms of signal-to-noise ratio, classification accuracy, and mean square error.

The study in [70] introduces water wave optimization (WWO), a novel metaheuristic method inspired by shallow water wave theory, for solving global optimization problems. By mimicking the behavior of water waves such as propagation and breaking, WWO effectively explores high-dimensional solution spaces. With a simple algorithmic framework, small population size, and few control parameters, WWO demonstrates competitive performance compared to existing evolutionary algorithms across various benchmark problems and real-world applications like high-speed train scheduling in China.

Energy-saving targets in the industrial sector, particularly focusing on China's unique approach of setting mandatory "amount of energy saved" targets since 2006 are examined in [71]. Through case studies, it questions the reliability of reported data and highlights weaknesses in the enforcement and correlation of these targets compared to conventional volume and intensity targets. The study suggests replacing

"amount of energy saved" targets with "double-control" targets that combine volume and intensity targets for more effective energy conservation measures.

In [72], the growing interest in deep learning-based segmentation methods for brain MRI analysis, emphasizing their advantages over classical machine learning algorithms is discussed. It provides an overview of current deep learning architectures used for segmenting brain structures and lesions, evaluating their performance, speed, and characteristics. Additionally, the review offers insights into future trends and developments in this field.

Inspired by the swarming behavior of salps in oceans [73], the study offers two new optimization methods for solving single and multiple objective optimization problems: the Salp Swarm Algorithm (SSA) and the Multi-objective Salp Swarm Algorithm (MSSA). By experimenting with different mathematical functions, SSA successfully refines the initial random solutions and approaches the optimal solution. MSSA, on the other hand, provides great coverage and convergence estimates of Pareto optimum solutions. Real-world case studies, such as the design of maritime propellers and air foils, show how well SSA and MSSA work to solve complex, unknown search spaces in real-world issues.

1.3 Motivation

Brain tumor segmentation and classification is an important task for identifying irregularity in the brain, which results in rapid tumor development and it is the primary cause of death worldwide. Such a tumor decreases the brain tissue in size resulting in mass harm to the neurons in the brain. Thus, it is important to classify the tumor effectively and accurately. Different tumor classification methods are in practice; however, they limit due to various reasons like,

- Accuracy, efficiency, and consistency
- Using a high-quality image without noise and artifacts
- Removing variations of luminosity and contrast
- Achieving non-linear up sampling

The limitations of existing methods of brain tumor segmentation and classification need to be addressed by designing new methods which are better and efficient when compared to the existing methods.

1.4 Objectives

The objectives of the proposed work are,

- To design an automatic brain segmentation model based on deep belief network (DBN).
- To find an optimal way of finding the effective segments from the input MRI brain image.
- To model a new classification strategy based on deep learning classification approach in order to assure effective classification.
- To implement and enable the comparative analysis of the proposed method with respect to the existing methods of brain tumor segmentation and classification.

1.5 Organization of thesis

This chapter starts with the basics of digital image processing. What is a digital image. Smallest element of digital image is called as pixel. It gives idea about the MR image, how it is captured. Types of modalities. The types of tumors are explained in detail. Glioma is a tumor causing maximum deaths of patients. Early detection of tumor is needed to save the life of patient. All the current methods for detection of brain tumor are discussed with their limitations. Human by himself without help of machine cannot detect the tumor by looking at MRI. So, there is need of automatic method to detect the tumor. So, this chapter at the end defines the objectives for early and accurate detection of brain tumor.

In **Chapter 2**, the Seg Net and Salp Water Optimization-Driven Deep Belief Network (Seg+SWO+DBN) algorithm for brain tumor segmentation and classification from MRI images is implemented. The analysis of proposed method performed based on metrics like accuracy, sensitivity, specificity and Region of Convergence (ROC). The results are compared with existing methods like Fully Connected Neural Network combined with Conditional Random Fields (FCNN+CRF), Deep learning, Bayesian fuzzy and Deep Convolutional Neural Networks (DCNN).

In **Chapter 3**, the Hybrid Adam Sewing Training Optimization Enabled Deep Learning Technique (AdamSWO_DCNN) algorithm for brain tumor segmentation and classification from MRI images is implemented. The performance of proposed method is analyzed based on varying the training data and K- fold value. The results are compared with existing methods The results are compared with existing methods like Fully Connected Neural Network combined with Conditional Random Fields (FCNN+CRF), Deep learning, Bayesian fuzzy and Deep Convolutional Neural Networks (DCNN).

In **Chapter 4**, the Adaptive SalpSwarm Optimization (ASO-DRN) for brain tumor classification algorithm is implemented for brain tumor segmentation and classification from MRI images. The performance of proposed method is analyzed based on performance metrics like True Positive Rate (TPR) and True Negative Rate (TNR). The results are compared with existing methods.

In **Chapter 5**, the Adaptive Adam Salp Water Optimization with DBN and Alexnet (ASWO_DbneAlexnet) is implemented for brain tumor segmentation and classification from MRI images. The performance of proposed method is analyzed based on accuracy and precision. The results are compared with existing methods defining certain advantages of the proposed method.

In **Chapter 6**, the conclusion and future scope is discussed. It presents entire research study and exposes the different outputs which can be used by researchers studying neurological disorders and developing advanced diagnostic methods for clinical applications. Last but not least, the potential future work that might improve the system has been discussed.

CHAPTER

2

Robust and Adaptable SWO-based DBN for Brain Tumor segmentation and Classification

2.1 Introduction

Brain tumor classification in magnetic resonance imaging (MRI) images becomes very popular in treatment planning, early diagnosis, and outcome evaluation. It is very difficult for classifying and diagnosing tumors from several images. Thus, an automatic prediction system is necessary to classify brain tumors as malignant, core, edema, or benign. This chapter introduces the novel strategy based on Salp Water Optimization-based Deep Belief Network (SWO-based DBN) for the brain tumor classification. The SWO-based DBN technique can adapt to different types of brain tumors and imaging conditions, making it versatile for various clinical scenarios. Adaptability is a significant advantage of the SWO-based DBN technique in the context of brain tumor classification from MRI images. The proposed technique's adaptability enables it to handle variations in imaging conditions, ensuring robust performance across different MRI datasets and settings, also makes it suitable for various clinical scenarios, providing consistent and reliable performance under diverse conditions [73].

The major contribution of this chapter is:

- **Proposed SegNet for the brain tumor segmentation:** The proposed SegNet is employed for segmenting each region, which is modified through SWO. SegNet is effective as it stores only max-pooling indices of feature maps, and the decoder network is employed for achieving better performance.
- **Proposed SWO-based DBN for brain tumor classification:** The SWO-based DBN is employed for training DBN for brain tumor detection that categories into edema, malignant, core, and benign. Here, SWO-based DBN is designed by integrating SSA and WWO.

The chapter is arranged as follows: section 2.2 elaborates the challenges faced, which are considered as the inspiration for developing the proposed technique. The proposed SWO-based DBN classifier is portrayed in section 2.3. The outcomes of the proposed strategy with other methods are depicted in section 2.4 and section 2.5 present the conclusion.

2.2 Challenges

The issues encountered by the prevailing approaches are detailed as follows:

- (i) Clinical settings may present unique challenges, such as limited availability of data, variations in patient demographics, or changes in imaging technology over time. The SWO-based DBN technique's adaptability makes it suitable for various clinical scenarios, providing consistent and reliable performance under diverse conditions [74].
- (ii) Brain imaging segmentation is complicated in segmentation because of its imbalanced data available in dataset, as majority of the pixels in MR image belongs to the healthy voxels.
- (iii) Variations in imaging conditions refer to differences in how MRI scans are performed, which can impact the quality and appearance of the images. These variations may include, magnetic field strength, MRI machines can have different magnetic field strengths, such as 1.5 Tesla (T) or 3T.
- (iv) Higher field strengths generally result in better image quality and higher resolution. Sequence Parameters, MRI scans can be performed using various imaging sequences, such as T1-weighted, T2-weighted, or FLAIR (Fluid-Attenuated Inversion Recovery). Each sequence highlights different tissue properties and can affect the appearance of brain tumors [77].
- (v) The spatial resolution of MRI images, determined by factors such as voxel size and slice thickness, can vary between scans. Higher resolution images provide more detailed information but may require longer scan times. Contrast agents may be administered to enhance the visibility of certain structures or abnormalities in MRI images. Variations in contrast agent administration protocols can affect the appearance of brain tumors and surrounding tissues [78].

- (vi) Differences in MRI scanner hardware and software configurations, such as coil types, gradient strengths, and reconstruction algorithms, can influence image quality and characteristics.

Segmentation of Gliomas using computer-aided diagnosis is highly demanding due to its unbalanced shape as well as the subtle boundaries of the tumor with the neighboring area [79].

2.3 Proposed Salp Water Optimization-based Deep Belief Network for brain tumor segmentation and classification

The main aim is to create an efficient technique for brain tumor segmentation and classification using the proposed SWO-based DBN. The proposed tumor segmentation method involves three different steps, like segmentation, feature extraction, along with brain tumor classification. Here, the input image is passed to the pre-processing module to get rid of artifacts and noise present in the image. The obtained image is forwarded to the segmentation module. In the segmentation phase, the input brain image is segmented with the help of SegNet that is customized based on the introduced optimization algorithm named SWO. The segmented tumor result is passed to the feature extraction module, wherein CNN features are mined with the CNN classifier. The feature extracted from a convolutional layer of the deep CNN classifier is specified as the CNN features.

The extracted CNN features are subjected to the classifier, wherein the brain tumor classification process is carried out with the DBN classifier [80] that effectively classifies the tumor as benign, malignant, core, and edema. However, the DBN classifier is tuned with the introduced optimization algorithm called SWO, which is designed by integrating the SSA [73] with the WWO [70], respectively. Figure 2.1 illustrates the structural representation of developed SegNet+SWO-based DBN for segmentation and categorization of brain tumor.

Initially, random selection of the image is done so as to execute the classification process on the images available in the dataset. Assume a database K containing s number of images be expressed by,

$$K = \{X_1, X_2, \dots, X_r, \dots, X_s\} \quad (2.1)$$

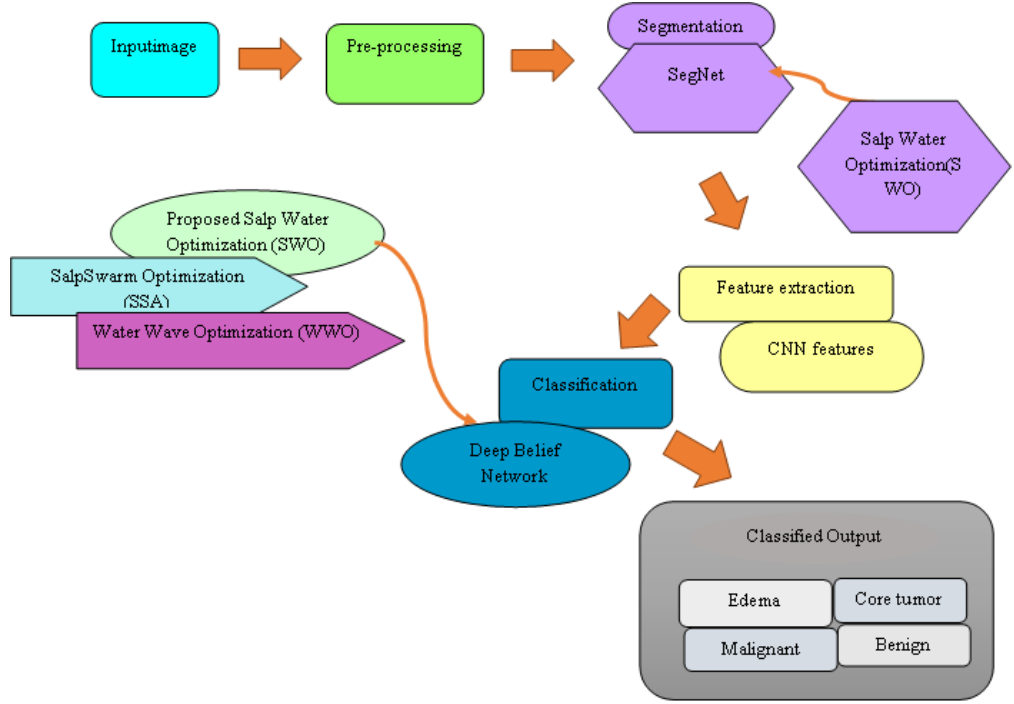


Figure 2.1: Schematic representation of the devised SegNet+SWO-based DBN model for tumor segmentation and classification

Here X_s represents the overall images, and X_r denotes r^{th} image that is chosen as the input in pre-processing the brain tumor segmentation and classification mechanism.

2.3.1 Pre-processing

The initial step is the pre-processing of the input image, which is the very important phase in analysis of the medical images. Here, the input image X_r is subjected to the pre-processing module, which facilitates the smooth processing of the input image and makes the image apt for further processing. Additionally, pre-processing is executed for elimination of the artifacts and noise that exists in the image. The pre-processing is regarded as the image enhancement module that has the ability for improving image contrast. The pre-processing is performed using RGB to grey conversion, skull strip removal, and histogram equalization. RGB to grey conversion method converts the color image into greyscale. The removal of non-brain structure and unwanted portions present in the image are isolated using skull stripping, and image contrast is improved using histogram equalization. The output of the pre-processor is represented as, X_r^* .

2.3.2 Segmentation of pre-processed image with SegNet

Segmentation is the process of separating the pre-processed image into different segments, such as pixels and image objects. The pre-processed image X_r^* is fed as input of the segmentation module, wherein SegNet [81] is utilized in the segmentation process. Here, SegNet is trained by the proposed SWO to find the tumorous regions considering each segment.

(a) SegNet

SegNet [81] is the encoder network where the related decoder network follows the pixel-wise classification layer. This encoder network containing 13 convolutional layers where the training process is performed from the weights for the detection purpose. In addition, the fully connected layers are rejected to obtain high-resolution feature maps at the deepest encoder output. Thus, the SegNet encoder network diminishes the count of parameters at the output of the deepest encoder. The SegNet employs the maximal pooling indices to up-sample and convolves the trainable decoder filter bank without learning feature maps. SegNet is the decoder to up-sample the input feature maps with low resolution. In addition, the decoder performs the pooling indices to evaluate the max-pooling step of the related encoder for achieving non-linear upsampling. Thus, up-sample maps are spread out and convolved with the trainable filters for creating the dense feature maps.

(b) Training of SegNet with the proposed Salp Water Optimization

The introduced SWO is utilized to train the SegNet to segment the tumorous region of the brain effectively for further processing. The segmented result is denoted as R . The algorithmic procedures of the introduced SWO algorithm are given in the following subsections.

Step 1: Initialization:

In the primary step, the population of salp is randomly initialized with the number of solutions, and is represented by,

$$I = \{I_1, I_2, \dots, I_l, \dots, I_w\} \quad (2.2)$$

Here, w denotes the overall count of solutions in population, and I_l refers to l^{th} the solution.

Step 2: Fitness function:

The solution, which is optimal is found by estimating the fitness to classify brain tumors from the input image. Furthermore, it is calculated corresponding to lowest error value, and the best solution is found by considering the solution with minimal error. The value of fitness is computed by using the subsequent equation,

$$MSE = \frac{1}{K} [\sum_{O=1}^K U_{target} - O_u] \quad (2.3)$$

Here, κ denotes the count of training samples, U_{target} represent the target output and O_u denote the estimated output of the classifier.

Step 3: Solution update with the introduced SWO algorithm:

The weights are determined in this step using the developed SWO for tuning DBN and then the solution is updated using weights which account the minimal error value. The following expression gives the update equation [73] of follower SSA algorithm,

$$B_e^l(x+1) = \frac{1}{2} (B_e^l(x) + B_e^{l-1}(x)) \quad (2.4)$$

The WWO is employed to enhance the performance, and for addressing the optimization problems of the algorithm. According to WWO [70], the update equation of breaking is given by,

$$B_e^l(x+1) = B_e^l(x) + \text{Gaussian}(0,1)\mu P_e \quad (2.5)$$

$$B_e^l(x) = B_e^l(x+1) - \text{Gaussian}(0,1)\mu P_e \quad (2.6)$$

Substitute equation (2.6) in equation (2.4), the solution becomes,

$$B_e^l(x+1) = \frac{1}{2} (B_e^l(x+1) - \text{Gaussian}(0,1)\mu P_e + B_e^{l-1}(x)) \quad (2.7)$$

$$B_e^l(x+1) - \frac{1}{2} B_e^l(x+1) = \frac{1}{2} [B_e^{l-1}(x) - \text{Gaussian}(0,1)\mu P_e] \quad (2.8)$$

$$\frac{1}{2} B_e^l(x+1) = \frac{1}{2} [B_e^{l-1}(x) - \text{Gaussian}(0,1) \mu P_e] \quad (2.9)$$

Therefore, the weight update among layers of MLP is carried out with the location update of developed SWO as,

$$B_e^l(x+1) = B_e^{l-1}(x) - \text{Gaussian}(0,1) \mu P_e \quad (2.10)$$

where, the term μ signifies the breaking coefficient, and the term P_e refers to the length of e^{th} dimension of search space.

Algorithm 2.1: Pseudocode of proposed SWO for brain tumor classification

| |
|--|
| Input: Salp population (initial set of candidate solutions) |
| Output: Best solution (optimized solution for brain tumor classification) |
| Procedure |
| Begin |
| Initialize the salp population with random positions in the search space. |
| Calculate the fitness function for each salp (search agent) to evaluate the quality of the solution. |
| While stopping condition is not met (e.g., maximum iterations or acceptable solution): |
| For each salp in the population: |
| If the salp is a follower: |
| Update its position using the follower equation (Equation 2.17). |
| End If |
| End For |
| Adjust the salp positions to ensure they are within the lower and upper variable bounds. |
| Re-check the feasibility of solutions to maintain valid candidate solutions. |
| $x = x + 1$ |
| The variable 'x' in this context represents the position of a salp in the search space, which is updated iteratively to minimize or maximize the fitness function. |
| End While |
| Return the optimal solution (the best-performing salp). |
| End Procedure |

Step 4: Feasibility re-evaluation:

The feasibility is recomputed depending on the fitness value, therefore if new solution generated is found to be better when compared to the prior one, the new solution replaces the old one.

Step 5: Termination:

The procedure is kept reiterated until the finest solution is attained while classifying tumor. Algorithm 2.1 depicts pseudo-code of the introduced technique.

2.3.3 Feature extraction with CNN features

Once segmentation is performed, features are extracted for acquiring the necessary features based on the CNN features, which certifies effective recognition of brain tumor. The segmented image R is forwarded to the feature extraction phase for performing the effective mining of feature. The following subsections explains the feature extraction process used in this work.

(a) CNN features:

CNN refers to a multi-layered network that is utilized in detection of the intricate feature that are present in the pre-processed image. CNN architecture comprises convolutional (Conv) layers, pooling (POOL) layers, as well as Fully Connected (FC) layers, and every layer has its own function. The initial layer is the convolution layer that is made use of in extraction of vital features existing in the pre-processed image and produces the relationship among the image features and the pixel values. The pre-processed image T taken as input and the convolutional layer extracts the CNN features. Thus, the CNN features refer to the features mined from the preliminary convolutional layer and are expressed by f_1 with dimension $[1 \times 256]$. Figure 2.2 portrays the CNN feature mined using the convolutional layer.

Thus, the feature vector attained in the feature extraction phase can be represented by,

$$D = \{ D_m ; 1 < m < p \} \quad (2.11)$$

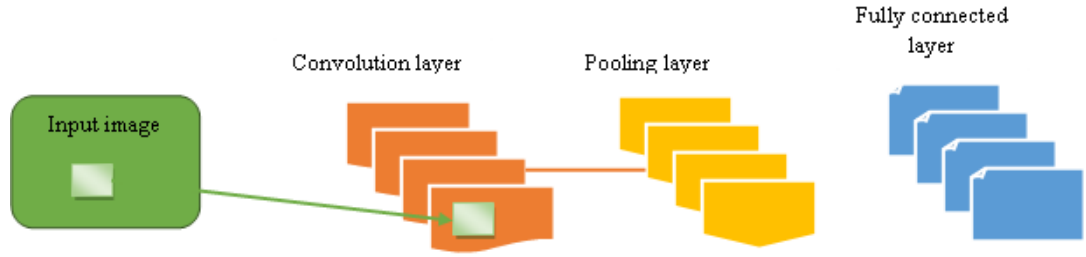


Figure 2.2: CNN feature extraction

2.3.4 Brain tumor classification with the developed Salp Water Optimization-based Deep Belief Network

The brain tumor classification with the developed SWO-based DBN is presented in this section, and the detection is performed with the help of a feature vector containing mined features. The extracted features are applied to DBN [82] for classification, and the training is done through SWO. The main intention of the introduced SWO is to categorize the regions of the tumor in the input image using the extracted features. The developed SWO is the integration of WWO in SSA. The SSA [73] is inspired by the dynamic foraging behavior of squirrels and it plays an efficient role in locomotion, which is said to be gliding. The squirrel's behavior is mathematically formulated by considering food search features. However, the global best solutions are achieved by the SSA with improved convergence.

SSA is highly consistent and precise and it delivers efficient solution for real-time problems. Meanwhile, WWO [70] is motivated by the waves which adapted three wave-enabled operators with refraction, propagation, and breaking for enhancing the high-dimensional solution space of the optimization issue. Thus, the method attains the trade-off among exploration and exploitation. Additionally, the technique boosts up the convergence speed in addition to maximization of the solution, and achieved enhanced balance among the exploration and exploitation. Therefore, the integration of WWO and SSA is made to maximize the general performance of the algorithm. The structure of DBN and algorithmic procedure of the developed SWO are given as follows.

(a) Structure of Deep Belief Network

The feature vector D attained from the feature extraction step are forwarded to classifier for achieving the brain tumor classification. The DBN [83] is the major

portion of the Deep Neural Network (DNN) containing several different layers, like Multilayer Perceptron's (MLPs) and Restricted Boltzmann Machines (RBMs). In addition, the RBMs are comprised of hidden as well as visible units that are interconnected with weights. However, MLPs are feed-forward networks, which consists of input, hidden, as well as output layers. In this case, networks with several layers are utilized to tackle any difficulties and hence, make the brain tumor segmentation and the classification effective. DBN avoids overfitting and improves model performance by enhancing the model generalization. Also, DBN has the advantage of being a generative model which generates samples depending on the features learned by the model through training. The DBN architecture is depicted in Figure 2.3.

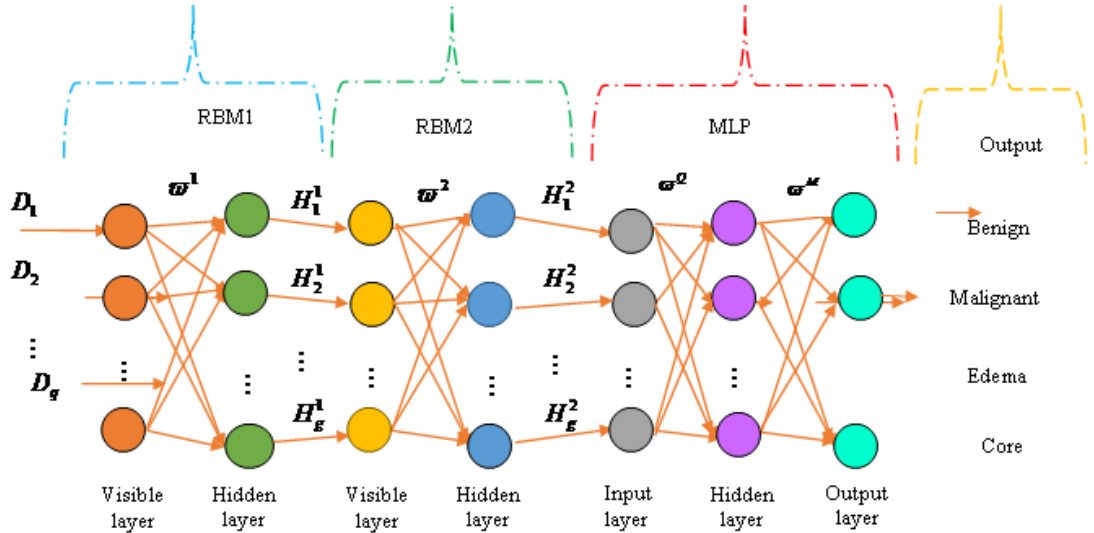


Figure 2.3: DBN classifier architecture

The features generated with the CNN features are given as input to the visible layer, and the hidden layer of RBM-1 is expressed by,

$$D^1 = \{D_1^1, D_2^1, \dots, D_b^1, \dots, D_q^1\}; \quad 1 \leq b \leq q \quad (2.12)$$

$$H^1 = \{H_1^1, H_2^1, \dots, H_m^1, \dots, H_g^1\}; \quad 1 \leq m \leq g \quad (2.13)$$

where, the b^{th} visible neuron of RBM-1 is denoted by D_b^1 , number of hidden neurons is represented as g , the term H_m^1 refers to m^{th} hidden neuron. Here, the visible and the hidden layer comprises of neurons wherein every neuron poses bias. If Y and Z

indicates the biases in the hidden and the visible layer, then the RBM-1-layer biases are expressed as,

$$Y^1 = \{Y_1^1, Y_2^1, \dots, Y_b^1, \dots, Y_q^1\} \quad (2.14)$$

$$Z^1 = \{Z_1^1, Z_2^1, \dots, Z_m^1, \dots, Z_g^1\} \quad (2.15)$$

where, the term Y_b^1 signifies the bias of b^{th} visible neurons, and Z_m^1 signify the bias of m^{th} hidden neurons. The weight vector for RBM-1 is characterized as,

$$\varpi^1 = \{\varpi_{b,m}^1\}; 1 \leq b \leq q; 1 \leq m \leq g \quad (2.16)$$

where the weight among b^{th} visible neurons and m^{th} hidden neurons are represented $\varpi_{b,m}^1$. The bias and weights connected to every visible neuron is utilized to evaluate the hidden layer output from RBM-1, which is expressed by,

$$J_m^1 = \lambda \left[Z_m^1 + \sum_{\varpi} (D_b^m)^1 \varpi_{b,m}^1 \right] \quad (2.17)$$

where the term λ represents activation function. Consequently, the output achieved from the RBM-1 is given by,

$$J^1 = \{J_m^1\}; 1 \leq m \leq g \quad (2.18)$$

Then, the RBM-1 output is subjected as input to the RBM-2 visible layer. Moreover, RBM-2-layer input is represented by D^2 . Likewise, the RBM-2 hidden layer is represented by H^2 . The RBM-2 weight vector is denoted as ϖ^2 , and m^{th} hidden neuron output is expressed as H_m^2 , and bias connected to m^{th} hidden neuron is Z_m^2 . Hence, the result generated by the hidden layer is denoted by H^2 .

The output of the RBM-2 hidden layers is fed to the input MLP layer, given by,

$$G = \{G_1, G_2, \dots, G_m, \dots, G_c\} = \{J_m^2\}; 1 \leq m \leq g \quad (2.19)$$

Here, m represents the total count of neurons in the input layer. The hidden layer MLP can be represented by the following expression,

$$A = \{A_1, A_2, \dots, A_S, \dots, A_E\}; 1 \leq S \leq E \quad (2.20)$$

Here, E represents the overall hidden neurons. Consider d_s be bias of the hidden neuron S , with $s = 1, 2, \dots, E$. MLPs output layer is expressed by,

$$B = \{B_1, B_2, \dots, B_L, \dots, B_C\}; 1 \leq L \leq C \quad (2.21)$$

where C represents overall neurons existing in output layer. Here, the MLP took two weight vectors; the weight vector available connecting the input and the hidden layer, and remaining among hidden, and the output layer. Consider ϖ^β be weight vector among the input layer and the hidden layer, expressed as,

$$\varpi^\beta = \{\varpi_{mS}^\alpha\}; 1 \leq m \leq g; 1 \leq S \leq E \quad (2.22)$$

where ϖ_{mS}^α reference to the weight among neurons m and hidden neurons S . The hidden layer output is represented by,

$$A_m = \left[\sum_{m=1}^g \varpi_{m,S}^\beta * A_S \right] \beta_S \quad (2.23)$$

where the term A_S refers to S input layer of MLP. ϖ^ρ represent the weights among hidden as well as output layer, and is given by the following,

$$\varpi^\chi = \{\varpi_{SL}^\chi\}; 1 \leq S \leq E; 1 \leq L \leq C \quad (2.24)$$

Hence, the output vector is estimated with the weights ϖ^χ and the following equation gives the output of the hidden layer,

$$O_u = \sum_{S=1}^E \varpi_{SL}^\chi * A_m \quad (2.25)$$

where the ϖ_{SL}^χ reference to weight between hidden neuron S as well as output neuron L and the output of the hidden layer is represented by A_m .

(b) Training of DBN using Salp Water Optimization

The tuning of DBN [30] is done based on the introduced SWO algorithm for determining the optimal weights to tune DBN classifier used in the classification of

the brain tumor. The optimal weights are introduced based on SWO algorithm to tune DBN for deriving optimal outputs while classifying brain tumor. The brain tumor classification considers the introduced SWO-enabled DBN for input image classification and deals with a new input image that is arrived from distributed sources. A brief explanation about the tuning process of the devised SWO is given in section 2.3.2.

(c) The hyperparameters used in the network for training are:

- Batch Size: The batch sizes used were 100, 200, 300, and 400.
- Hidden Neurons: Hidden neuron counts of 50, 100, 150, and 200 were tested.

2.4 Results and discussion

The results of the created SegNet+ SWO-based DBN classifier utilized for classifying brain tumor is elaborated and discussed in detail in this section. The dataset used in the proposed method is, multimodal brain tumor segmentation challenge, i.e. BRATS 2018 dataset [82]. In this dataset, every patient's image is collected from four modalities, which include T1C, T1, FLAIR, and T2. Here, every modality consists of 130 to 176 brain slices, which is considered for the analysis. Totally, 10 sets of images are employed for the analysis, from that FLAIR images are considered for brain tumor segmentation and classification. By following a similar annotation protocol, all the imaging datasets are segmented manually with one to four raters. Annotations have the peritumoral edema (ED - label 2), GD-enhancing tumor (ET - label 4), and the necrotic and non-enhancing tumor core (NCR/NET - label 1). BRATS 2020 dataset [83] uses MRI images on segmentation for brain tumor classification. It focuses on the overall survival prediction of the patient and evaluates an algorithmic uncertainty in the segmentation of tumors.

2.4.1 Evaluation metrics

The performance of the developed SegNet +SWO-based DBN is evaluated using three metrics, like specificity, accuracy, and sensitivity.

(a) Accuracy: The accuracy is defined to measure the closeness degree of an estimated value related to their raw value in optimal brain tumor classification, and it is expressed by [62],

$$Accuracy = \frac{T_p + T_n}{T_p + T_n + K_p + K_n} \quad (2.26)$$

where T_p refer to true positive, K_p refer to false positive, T_n indicates true negative, and K_n represents false negative, respectively.

(b) Sensitivity: It is utilized to measure the ratio of positives that are identified correctly by the classifier, and is expressed by [62],

$$Sensitivity = \frac{T_p}{T_p + K_n} \quad (2.27)$$

(c) Specificity: It is defined as the ratio of negatives that are identified correctly by the classifier and is illustrated as [62],

$$Specificity = \frac{T_n}{T_n + K_p} \quad (2.28)$$

(d) Receiver Operating Characteristics (ROC) curve: ROC is the graphical representation of the relationship existing between true positive rate (TPR) and false positive rate (FPR), and it is the measure that pictures the performance of the system.

2.4.2 Simulation results

Figure 2.4 illustrates the experimental outputs of the proposed SegNet+ SWO-based DBN. Figure 2.4 (a) represents the input image taken from BRATS 2018 dataset. Here, the set of images are said to be cases. From the set of cases, four images are available, and are taken as the input image for brain tumor segmentation and classification, and Figure 2.4 (b) depicts ground truth image. Figure 2.4 (c) shows the segmented output image using SegNet.

Figure 2.5 shows the experimental outputs of the proposed SegNet+ SWO-based DBN using BRATS 2020 dataset [83]. Figure 2.5 (a) represents the input image taken from BRATS 2020 dataset. Here, the set of images are said to be cases. From the set of cases, four images are available, and are taken as the input image for brain tumor segmentation and classification, and figure 2.5 (b) reveals the ground truth image. Figure 2.5 (c) depicts the segmented output image using SegNet.

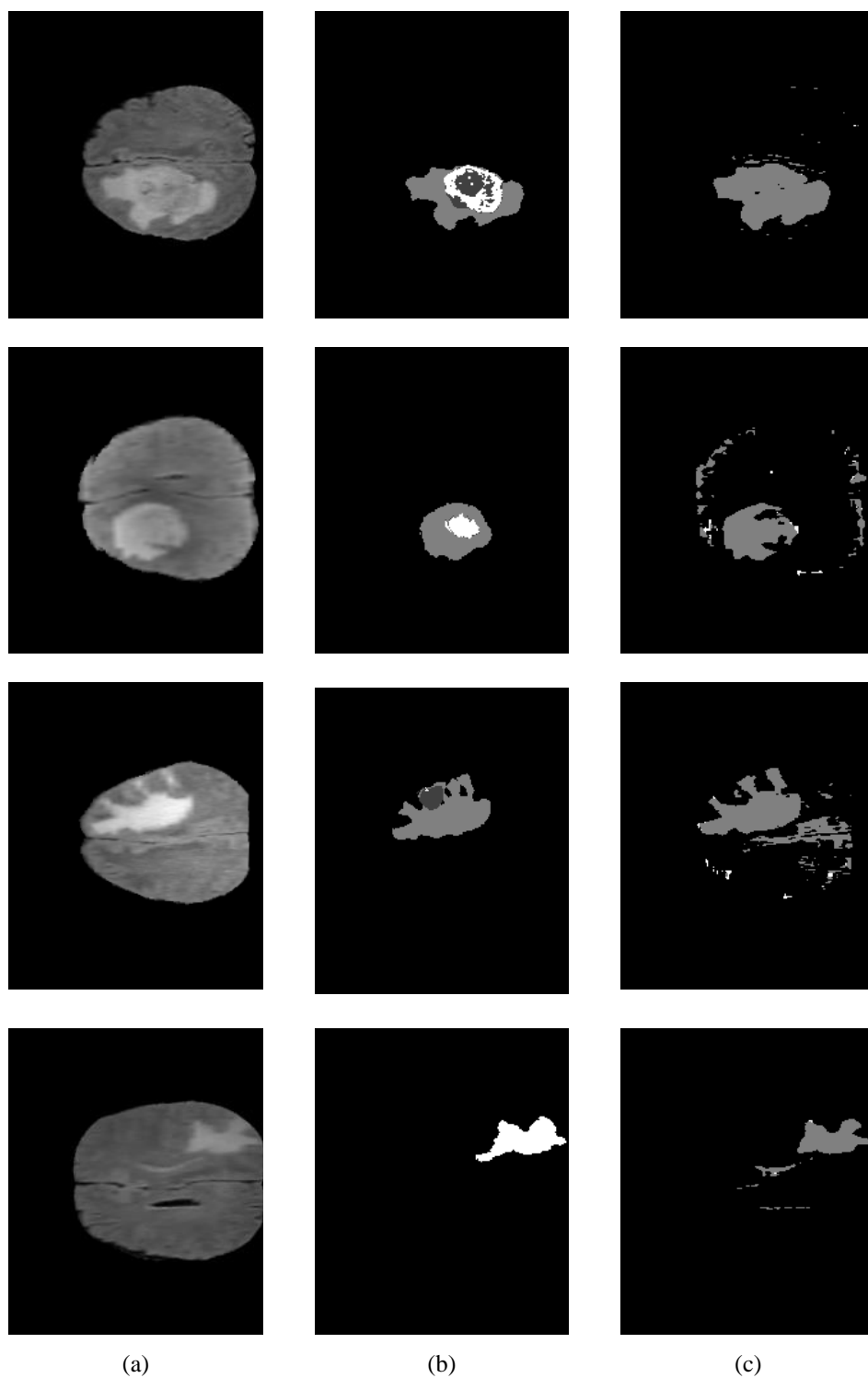


Figure 2.4: Experimental results using BRATS dataset 2018, (a) input image, (b) ground truth image, and (c) segmented output image

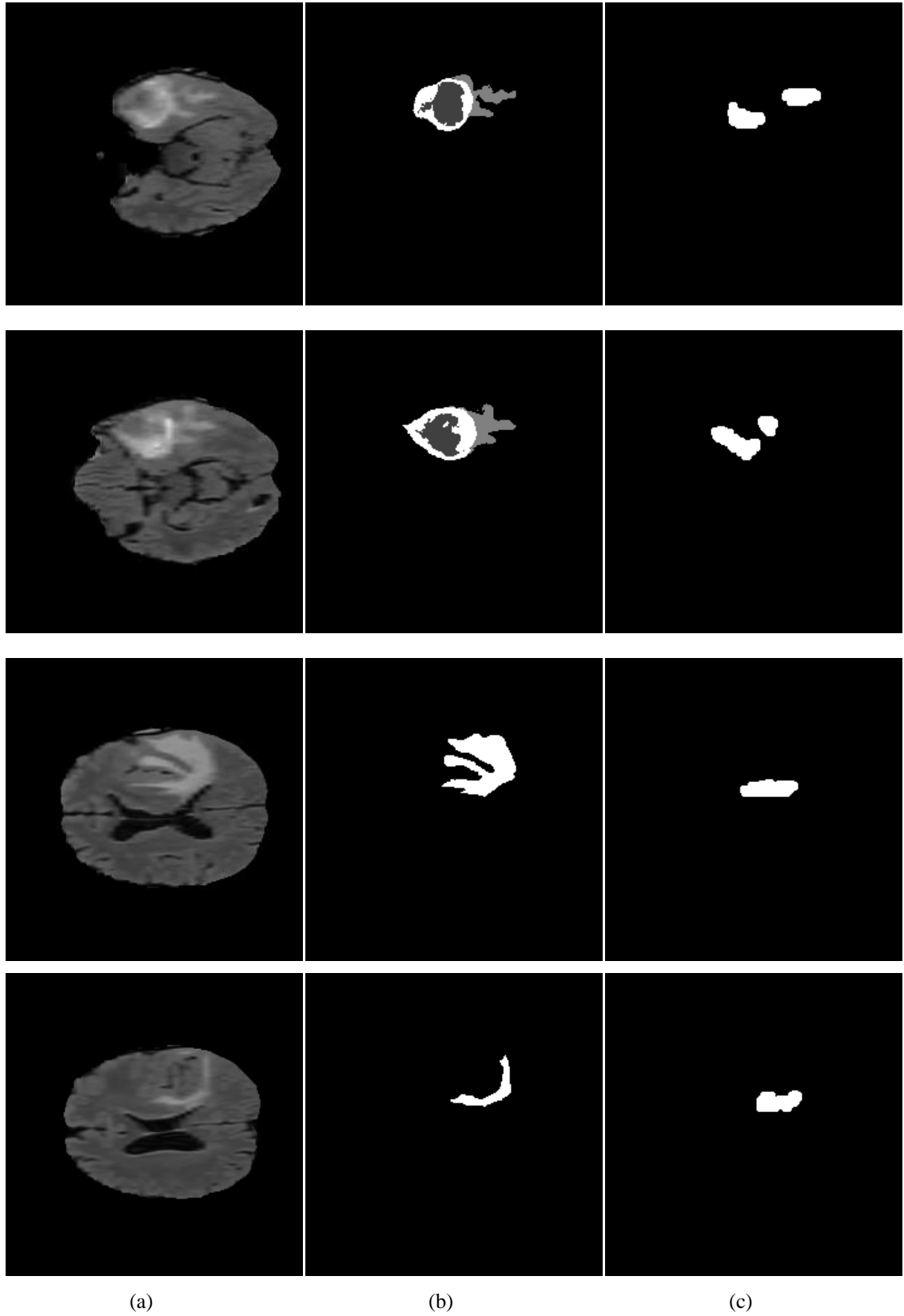


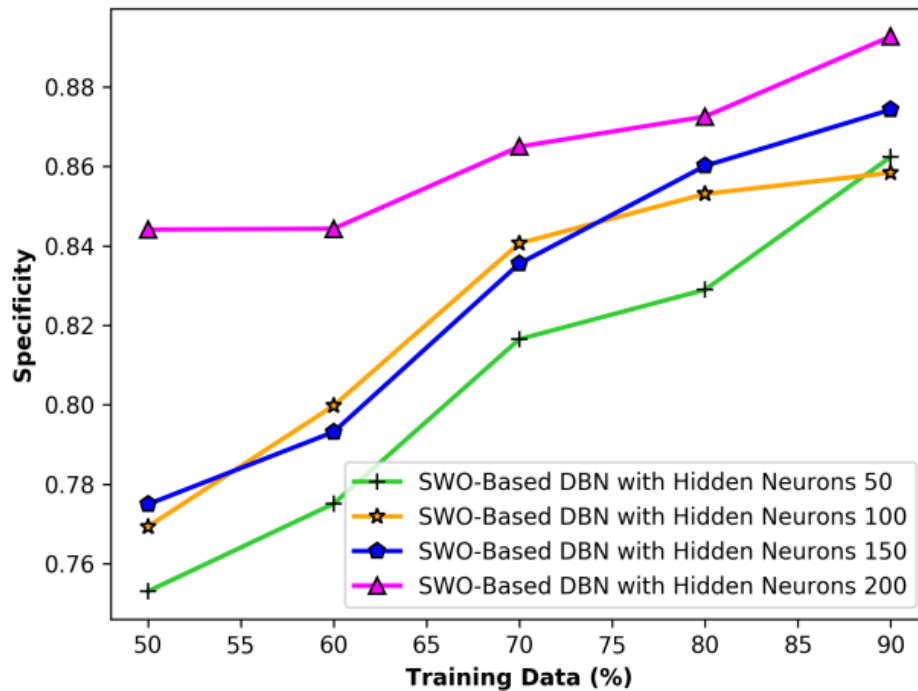
Figure 2.5: Experimental results using BRATS dataset 2018, (a) input image, (b) ground truth image, and (c) segmented output image

2.4.3 Performance analysis using dataset 2018

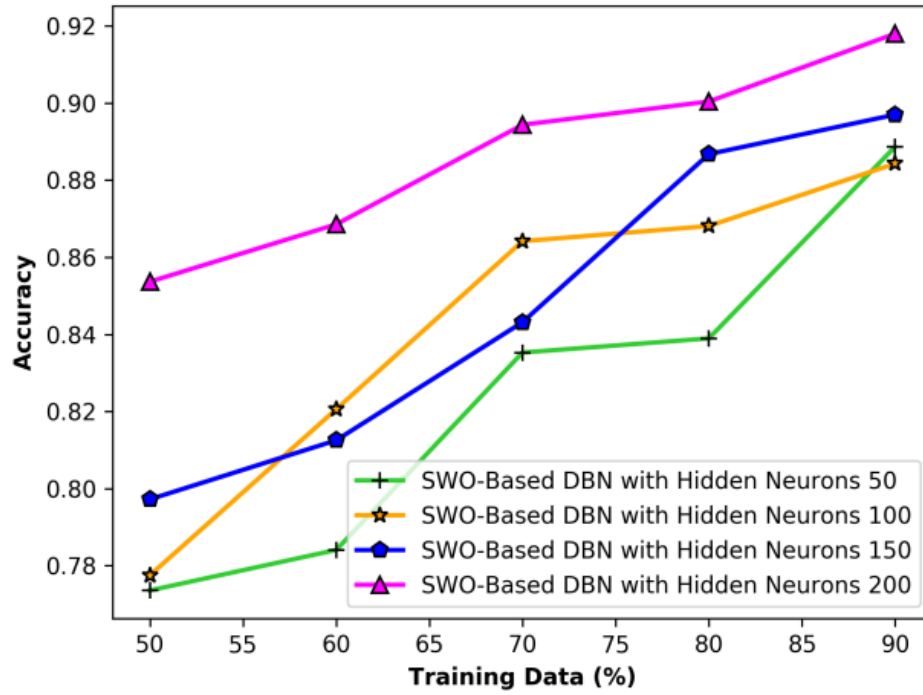
This section presents the analysis of the developed model using the BRATS 2018 dataset, analyzed through varying the number of hidden neurons, and batch size. The analysis is done based on metrics.

a) Analysis using hidden neurons

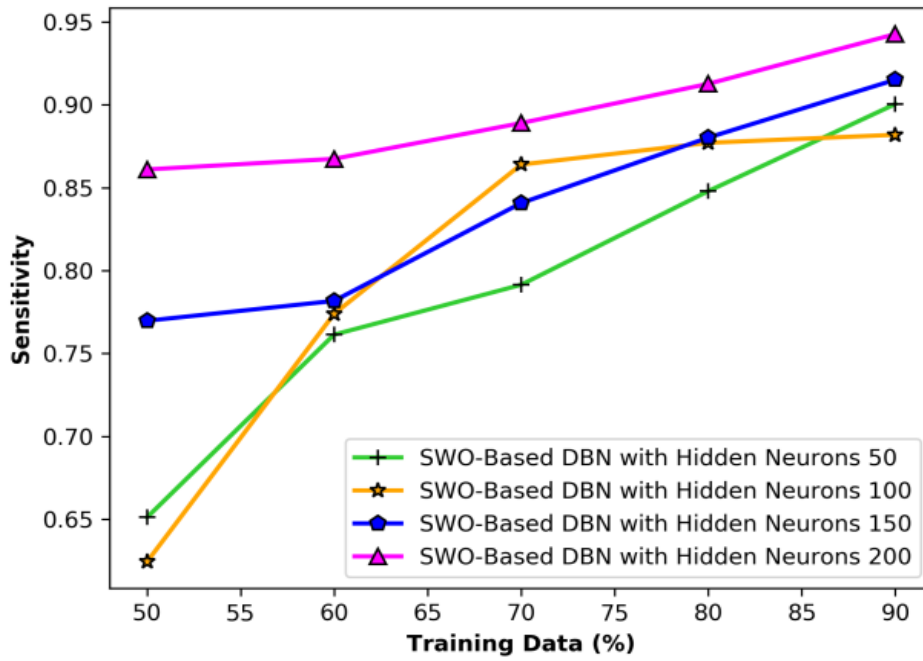
The analysis of the developed model with different hidden neurons is depicted in Figure 2.6. The analysis concerning specificity metric by varying the training data percentage is shown in Figure 2.6 (a). When training data = 90%, specificity values of proposed model with hidden neurons 50, 100, 150, and 200 are 0.862, 0.858, 0.874, and 0.892. Figure 2.6 (b) portrays the performance analysis of accuracy. When training data=90%, the accuracy value measured by SegNet+SWO-based DBN with hidden neuron 50 is 0.888, SegNet+ SWO-based DBN with hidden neuron 100 is 0.884, SegNet+ SWO-based DBN with hidden neuron150 is 0.896, and SegNet +SWO-based DBN with hidden neuron 200 is 0.917. The analysis based on sensitivity metrics with different training data percentages is shown in Figure 2.6 (c). When 90% of training data is considered, the sensitivity values of the proposed model with hidden neurons 50, 100, 150, and 200 are 0.900, 0.881, 0.915, and 0.942.



(a)



(b)

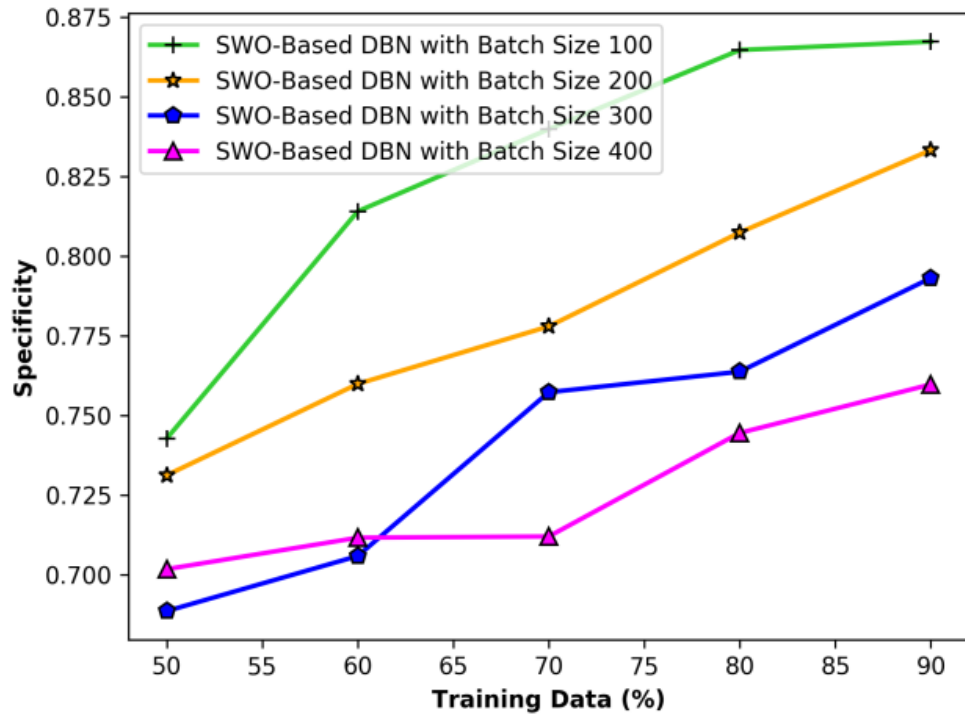


(c)

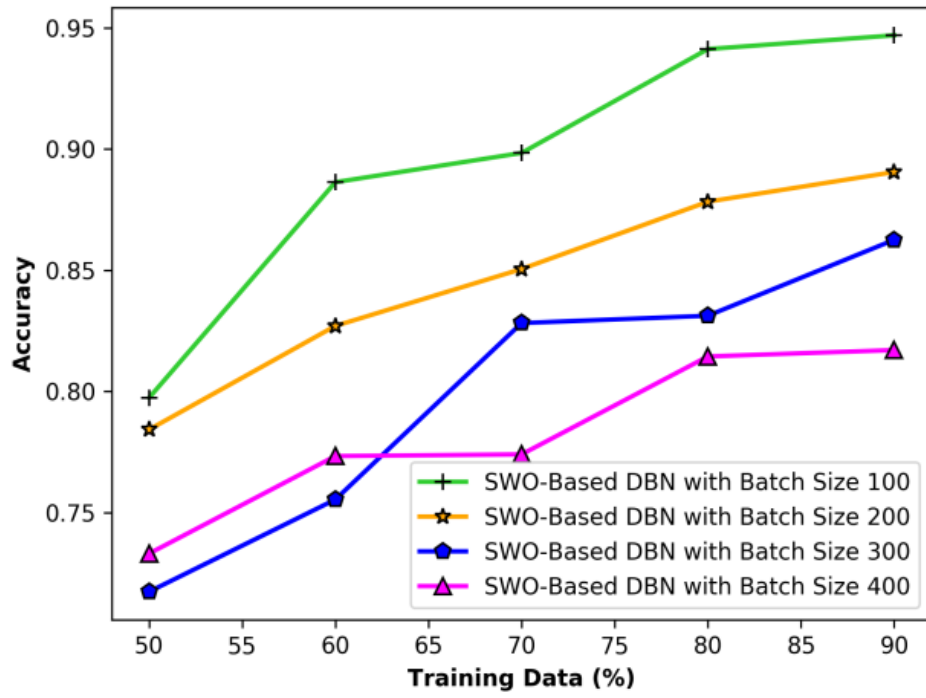
Figure 2.6: Performance analysis with hidden neurons (a) specificity, (b) accuracy, (c) sensitivity

(b) Analysis using a batch size

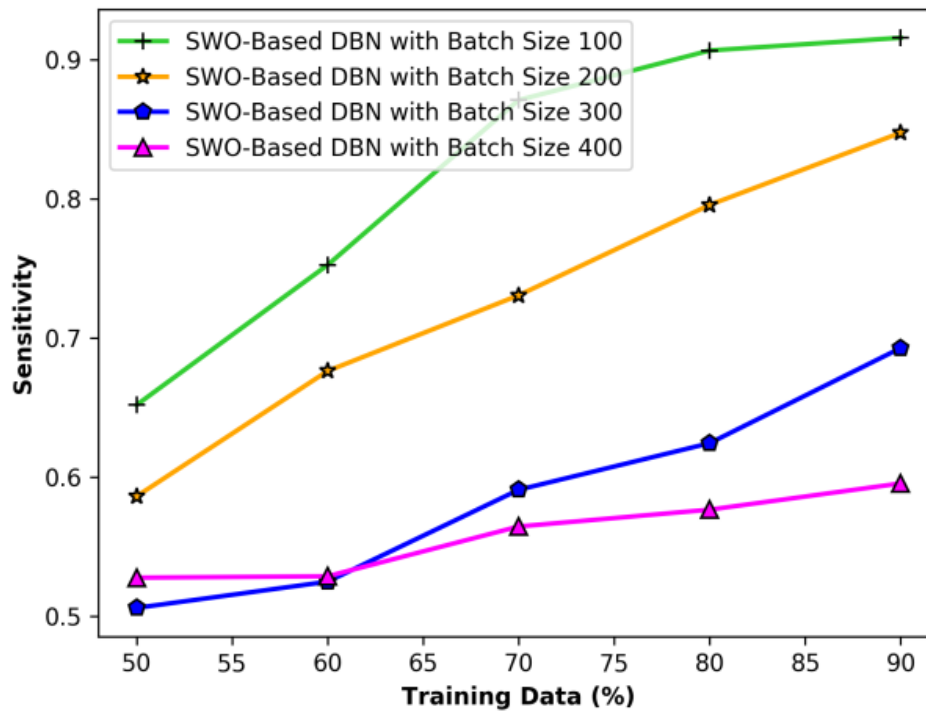
The analysis of the developed model with the different batch sizes is depicted in Figure 2.7. The analysis for specificity metric with different training data percentages is illustrated in Figure 2.7 (a). When training data = 90%, the specificity values of proposed model with batch sizes 100, 200, 300, and 400 are 0.867, 0.833, 0.793, and 0.759. Figure 2.7(b) portrays the performance analysis of accuracy. When training data=90%, the accuracy value measured by SegNet +SWO-based DBN with batch size 100 is 0.946, SegNet +SWO-based DBN with batch size 200 is 0.890, SegNet +SWO-based DBN with batch size 300 is 0.862, and SegNet +SWO-based DBN with batch size 400 is 0.817. The analysis based on sensitivity metrics with different training data percentages is depicted in figure 2.7 (c). When 90% of training data is considered, the sensitivity values of the proposed model with batch sizes 100, 200, 300, and 400 are 0.915, 0.847, 0.692, and 0.595.



(a)



(b)



(c)

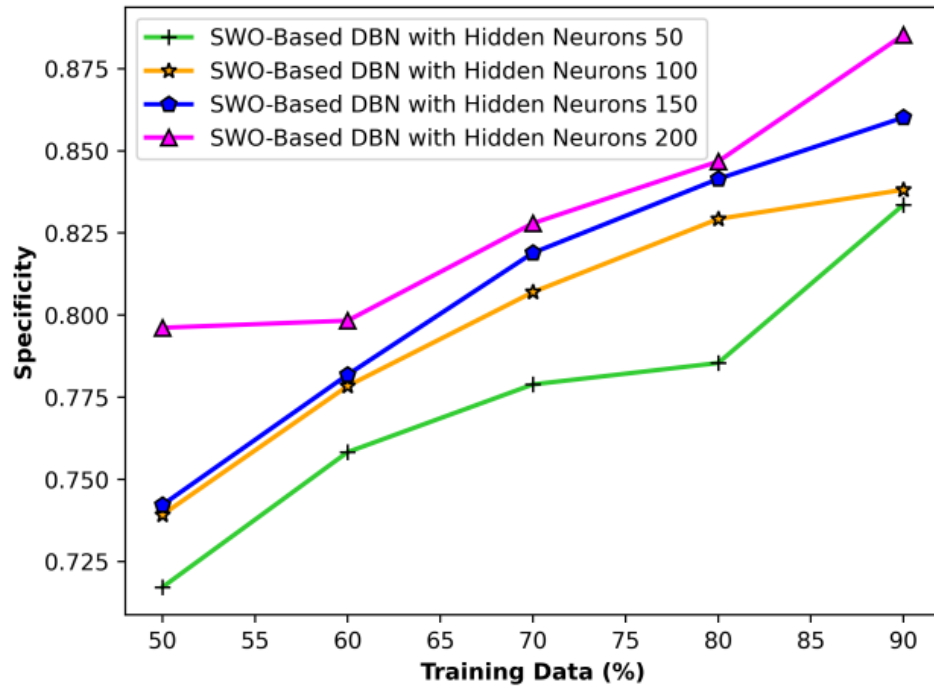
Figure 2.7: Performance analysis with batch size (a) specificity, (b) accuracy, (c) sensitivity

2.4.4 Performance analysis using BRATS 2020 dataset [83]

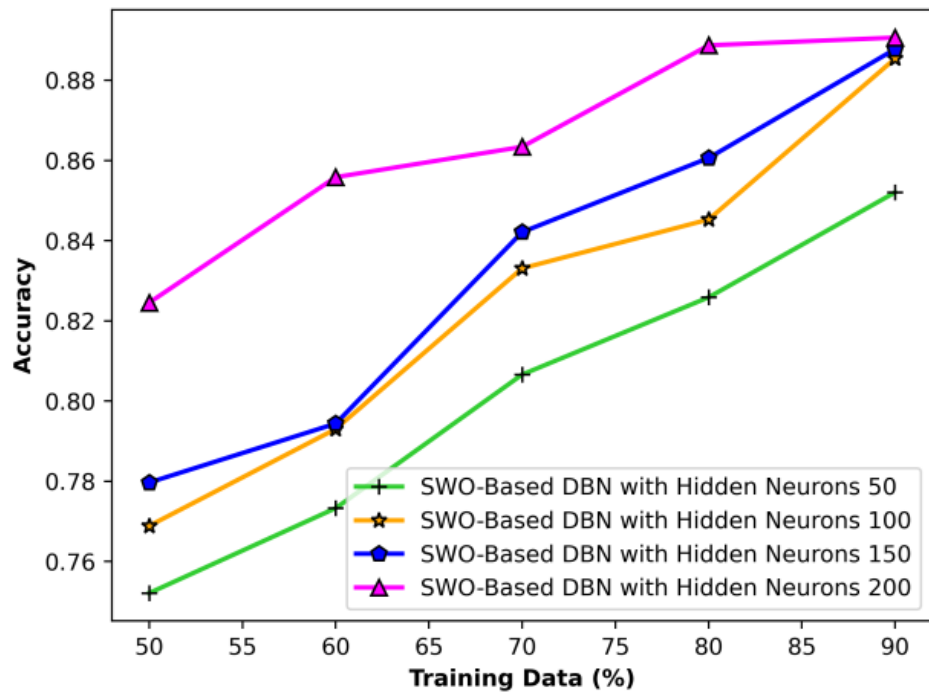
This section presents the analysis of the developed model using the dataset 2020 by changing the number of hidden neurons, and batch size. The analysis is done based on metrics.

(a) Analysis using hidden neurons

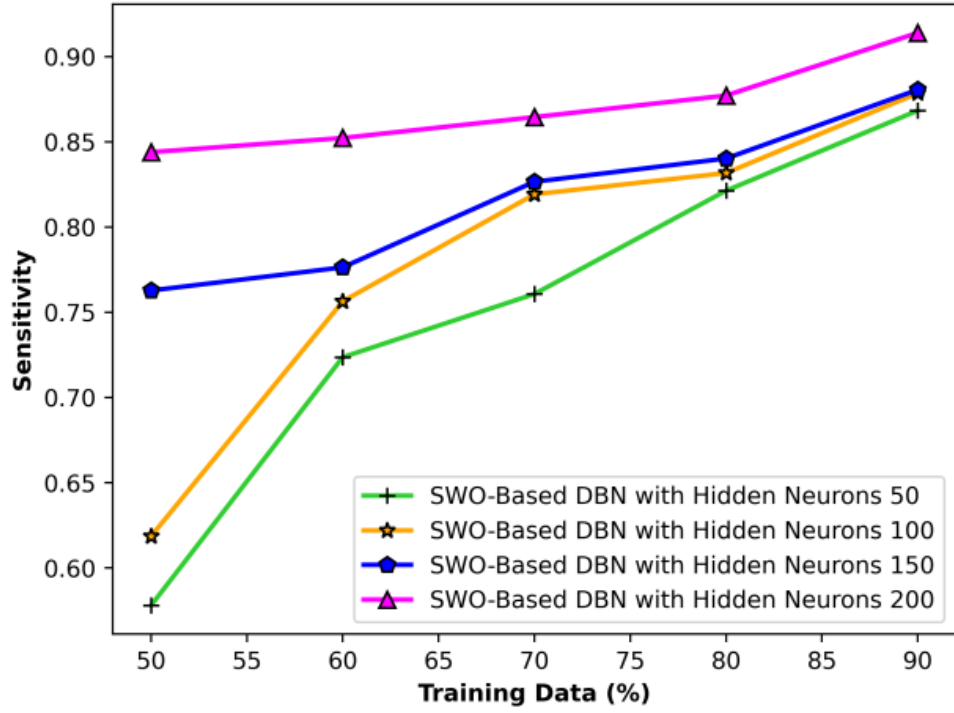
The analysis of the developed model using BRATS dataset 2020 with different hidden neurons is depicted in Figure 2.8. The analysis for specificity by varying the training data percentage is shown in revealed Figure 2.8 (a). When training data=90%, specificity values of proposed model with hidden neurons 50, 100, 150, and 200 are 0.833, 0.838, 0.860, and 0.885. Figure 2.8 (b) portrays the performance analysis of accuracy. When training data=90%, the accuracy value measured by SegNet + SWO-based DBN with hidden neuron 50 is 0.852, SegNet+ SWO-based DBN with hidden neuron 100 is 0.885, SegNet+ SWO-based DBN with hidden neuron 150 is 0.887, and SegNet +SWO-based DBN with hidden neuron 200 is 0.890. The analysis based on sensitivity metrics with different training data percentages is shown in Figure 2.8 (c). When 90% of training data is considered, the sensitivity values of the proposed model with hidden neurons 50, 100, 150, and 200 are 0.868, 0.878, 0.880, and 0.913.



(a)



(b)

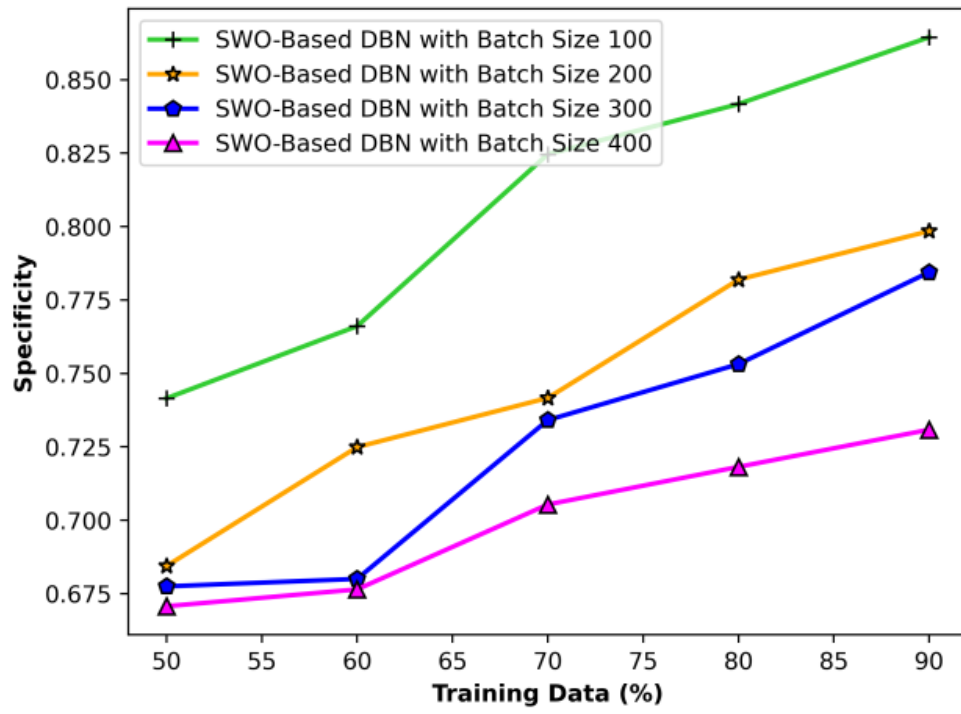


(c)

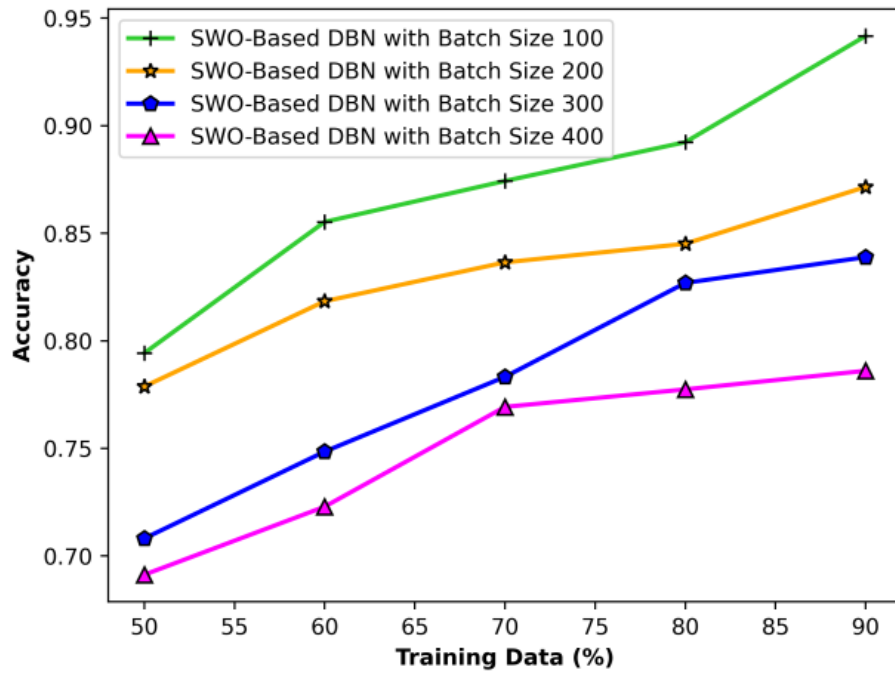
Figure 2.8: Performance analysis with hidden neurons (a) specificity, (b) accuracy, (c) sensitivity

(b) Analysis using a batch size

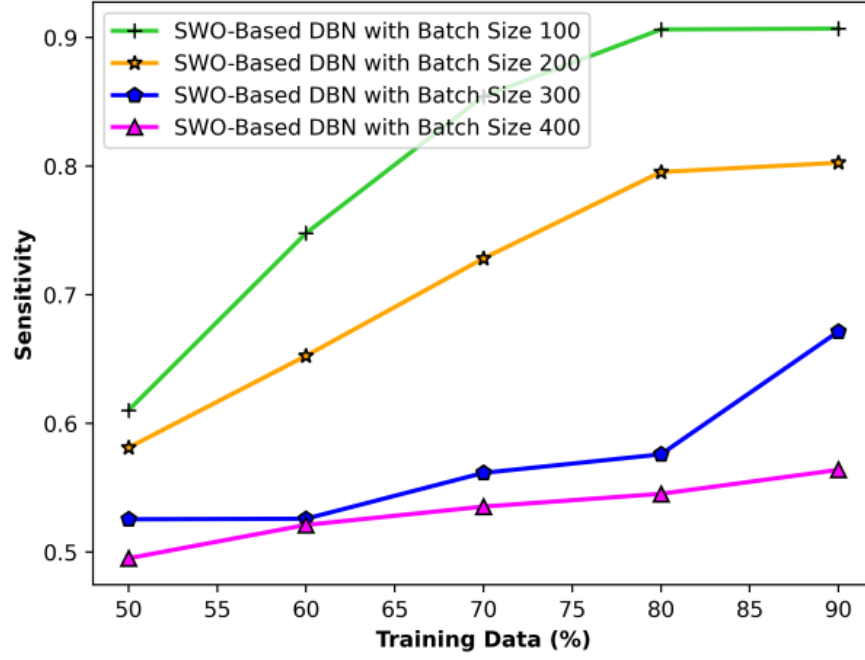
The analysis of the developed model using the BRATS 2020 dataset with different batch sizes is shown in Figure 2.9. The analysis for specificity metric with different training data percentages is illustrated in Figure 2.9 (a). When training data=90%, the specificity values of proposed model with batch sizes 100, 200, 300, and 400 are 0.864, 0.798, 0.784, and 0.730. Figure 2.9 (b) portrays the performance analysis of accuracy. When training data=90%, the accuracy value measured by SegNet +SWO-based DBN with batch size 100 is 0.941, SegNet +SWO-based DBN with batch size 200 is 0.871, SegNet +SWO-based DBN with batch size 300 is 0.838, and SegNet +SWO-based DBN with batch size 400 is 0.786. The analysis based on sensitivity metrics with different training data percentages is depicted in Figure 2.9 (c). When 90% of training data is considered, the sensitivity values of the proposed model with batch sizes 100, 200, 300, and 400 are 0.906, 0.802, 0.671, and 0.563.



(a)



(b)



(c)

Figure 2.9: Performance analysis with batch size (a) specificity, (b) accuracy, (c) sensitivity

2.4.5 Comparative methods

The performance of the developed approach is evaluated by comparing the developed with existing methods, such as FCNN+CRF+DBN [50], Deep learning+DBN [51], Bayesian fuzzy+ DBN [62], and Deep CNN+DBN [54], respectively.

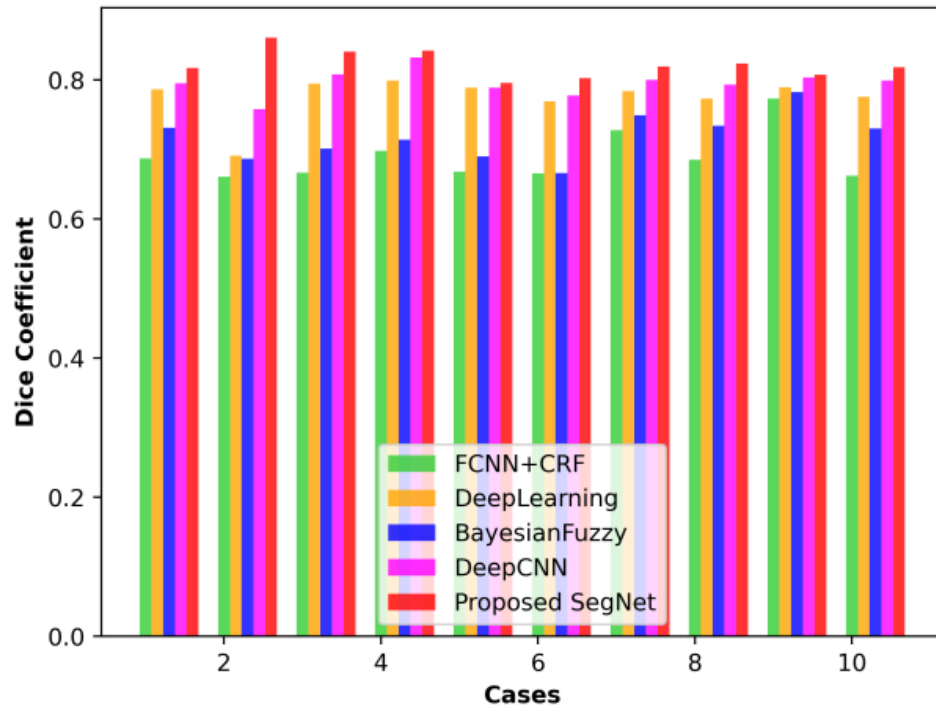
2.4.6 Comparative analysis using dataset 2018

This section describes the comparative analysis of the developed SegNet +SWO-based DBN approach based on performance metrics with different training data percentages using dataset 2018 [82].

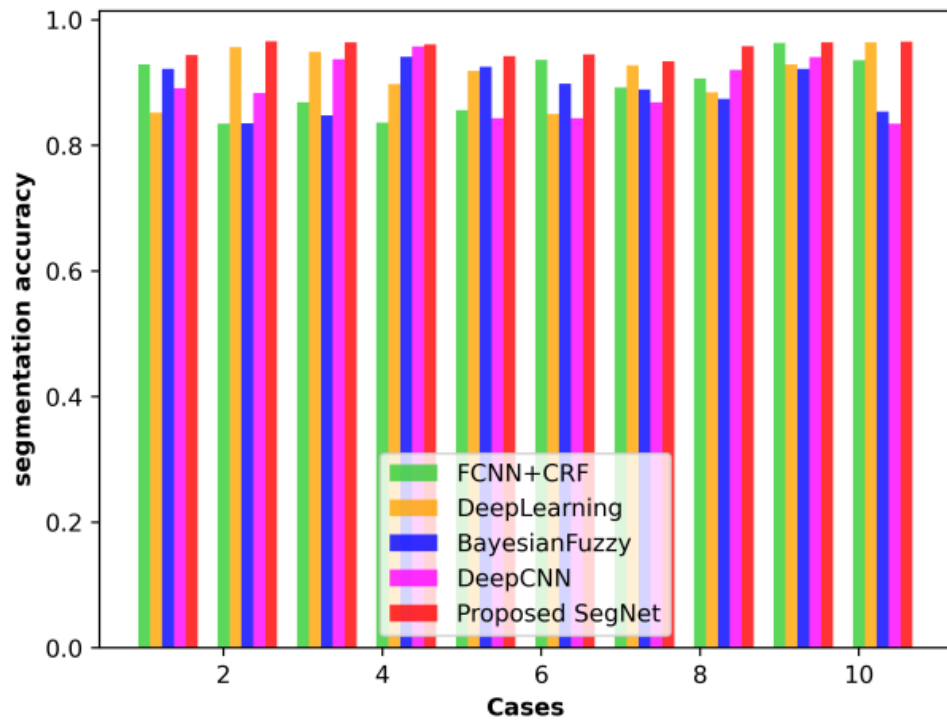
(a) Analysis using segmentation

The analysis of methods using segmentation accuracy parameter is deliberated in Figure 2.10. In Figure 2.10 (a) the Dice coefficient for various cases is revealed. Here, the cases denote the total number of images. When image = 2, the Dice coefficient of methods computed by FCNN+CRF, Deep learning, Bayesian fuzzy, Deep CNN, and proposed SegNet are 0.660, 0.690, 0.686, 0.758, and 0.860. Figure 2.10 (b) shows the segmentation accuracy of the method using dataset 2018. When image = 2, the segmentation accuracy of methods computed by FCNN+CRF, Deep

learning, Bayesian fuzzy, Deep CNN, and proposed SegNet are 0.834, 0.956, 0.835, 0.883, and 0.965.



(a)



(b)

Figure 2.10: Analysis of methods for Dataset 2018 using (a) dice coefficient, (b) segmentation accuracy

The segmentation accuracy in a tabular form using the BRATS 2018 dataset for the proposed method and existing methods are given in below Table 2.1.

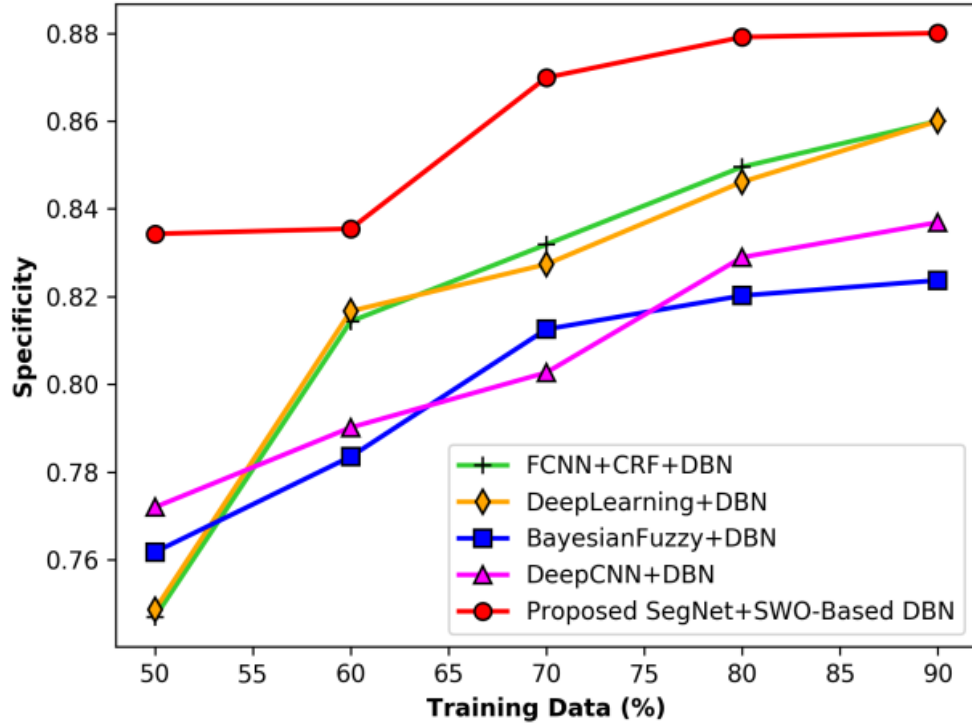
Table 2.1 Segmentation accuracy using the proposed method and existing methods for BRATS 2018 dataset

| | FCNN+ CRF [50] | Deep Learning [51] | Bayesian Fuzzy [62] | DeepCNN [54] | Proposed SegNet |
|----------------|---------------------------|-------------------------------|--------------------------------|-------------------------|----------------------------|
| Image 1 | 0.928 | 0.852 | 0.921 | 0.891 | 0.944 |
| Image 2 | 0.834 | 0.956 | 0.835 | 0.883 | 0.965 |
| Image 3 | 0.868 | 0.948 | 0.847 | 0.937 | 0.964 |
| Image 4 | 0.836 | 0.897 | 0.941 | 0.957 | 0.960 |
| Image 5 | 0.856 | 0.925 | 0.918 | 0.843 | 0.942 |
| Image 6 | 0.936 | 0.849 | 0.898 | 0.843 | 0.945 |
| Image 7 | 0.892 | 0.927 | 0.889 | 0.868 | 0.934 |
| Image 8 | 0.906 | 0.884 | 0.874 | 0.920 | 0.958 |
| Image 9 | 0.963 | 0.929 | 0.921 | 0.940 | 0.964 |
| Image 10 | 0.935 | 0.964 | 0.853 | 0.834 | 0.965 |
| Image 11 | 0.781 | 0.857 | 0.829 | 0.865 | 0.872 |
| Image 12 | 0.797 | 0.857 | 0.818 | 0.874 | 0.915 |
| Methods | FCNN+ CRF [50] | Deep Learning [51] | Bayesian Fuzzy [62] | DeepCNN [54] | Proposed SegNet |
| Image 13 | 0.759 | 0.864 | 0.842 | 0.897 | 0.923 |
| Image 14 | 0.761 | 0.851 | 0.833 | 0.887 | 0.918 |
| Image 15 | 0.753 | 0.805 | 0.797 | 0.842 | 0.869 |

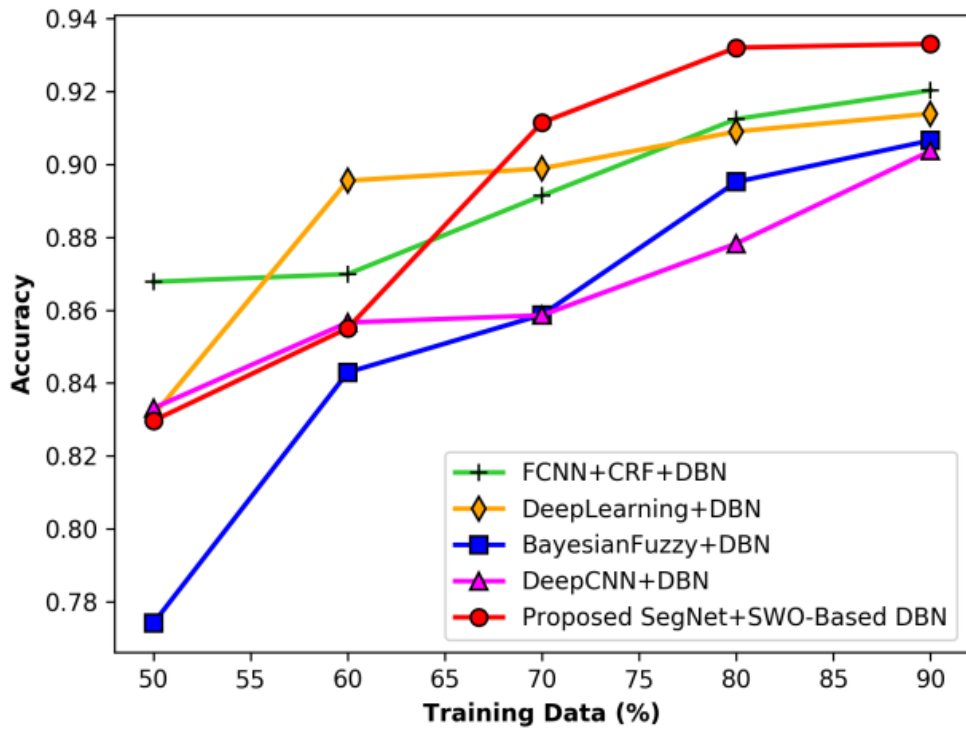
(b) Analysis using training data

Figure 2.11 illustrates the analysis of methods with different training data considering specificity, accuracy, and sensitivity parameters. The analysis of methods using specificity parameter is deliberated in Figure 2.11 (a). When training data=90%, the specificity of methods measured by FCNN+CRF+DBN, Deep learning+ DBN, Bayesian fuzzy + DBN, Deep CNN+DBN, and proposed SegNet +SWO-based DBN are 0.86, 0.86, 0.823, 0.836, and 0.880. The analysis of methods based on accuracy is deliberated in Figure 2.11 (b). When training data=90%, the accuracy of methods measured by FCNN+CRF+DBN, Deep learning+ DBN, Bayesian fuzzy+ DBN, Deep CNN+DBN, and proposed SegNet +SWO-based DBN are 0.920, 0.913, 0.906, 0.903, and 0.933. The analysis of methods using sensitivity

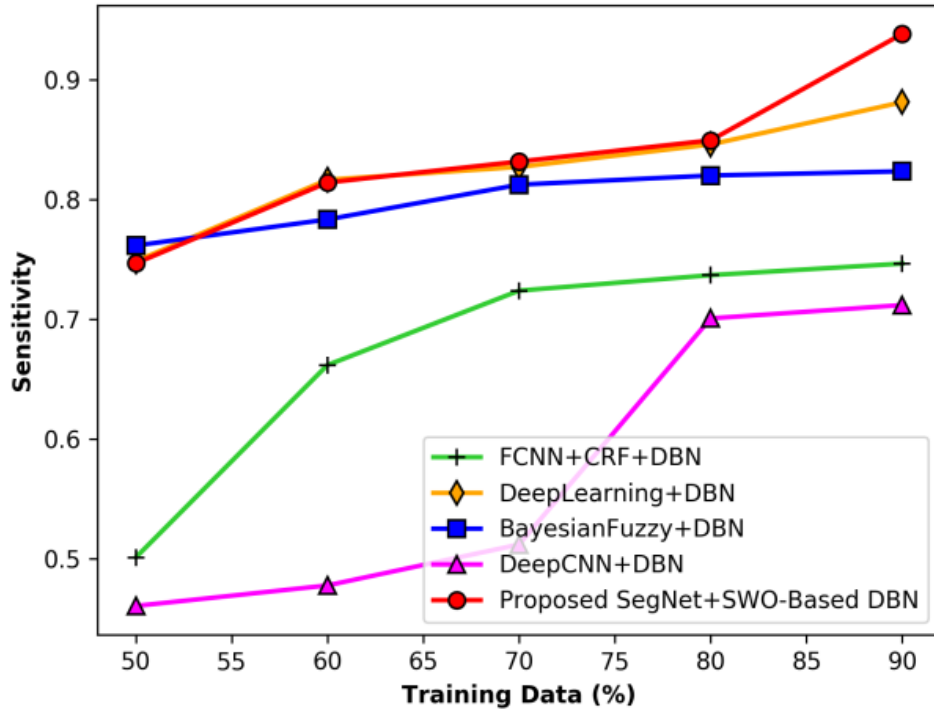
parameters is deliberated in Figure 2.11 (c). When training data=90%, the sensitivity of methods measured by FCNN+CRF+DBN, Deep learning+ DBN, Bayesian fuzzy+ DBN, Deep CNN+DBN, and proposed SegNet +SWO-based DBN are 0.746, 0.881, 0.823, 0.712, and 0.938. Figure 2.11 (d) illustrates the ROC of developed SegNet +SWO-based DBN for brain tumor segmentation and classification. For a minimal of 0.1 as FPR, the TPR obtained by the methods, FCNN+CRF+DBN, Deep learning+ DBN, Bayesian fuzzy+ DBN, Deep CNN+DBN, and proposed SegNet +SWO-based DBN is 0.453, 0.575, 0.764, 0.767, and 0.776, respectively.



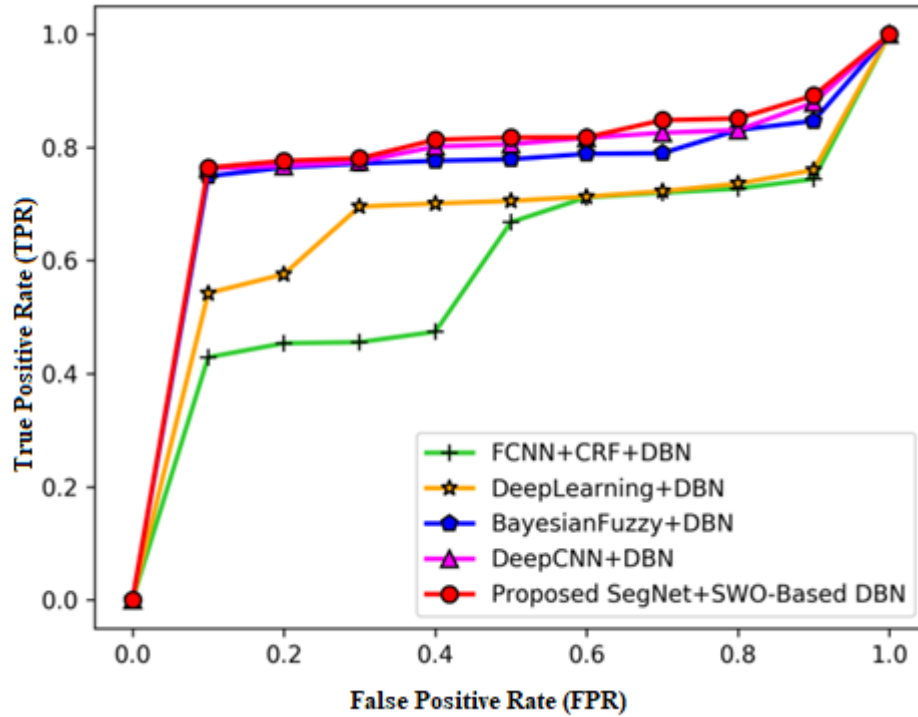
(a)



(b)



(c)



(d)

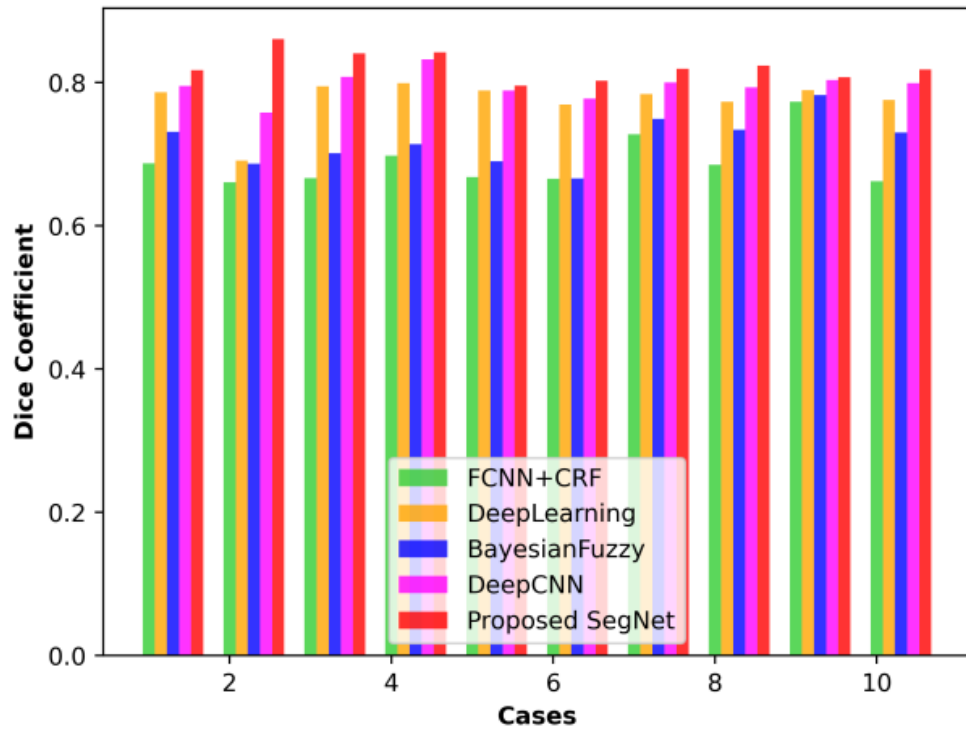
Figure 2.11: Analysis of methods considering training data (a) specificity, (b) accuracy, (c) sensitivity, and (d) ROC (FPR vs TPR)

2.4.7 Comparative analysis using dataset 2020 [83]

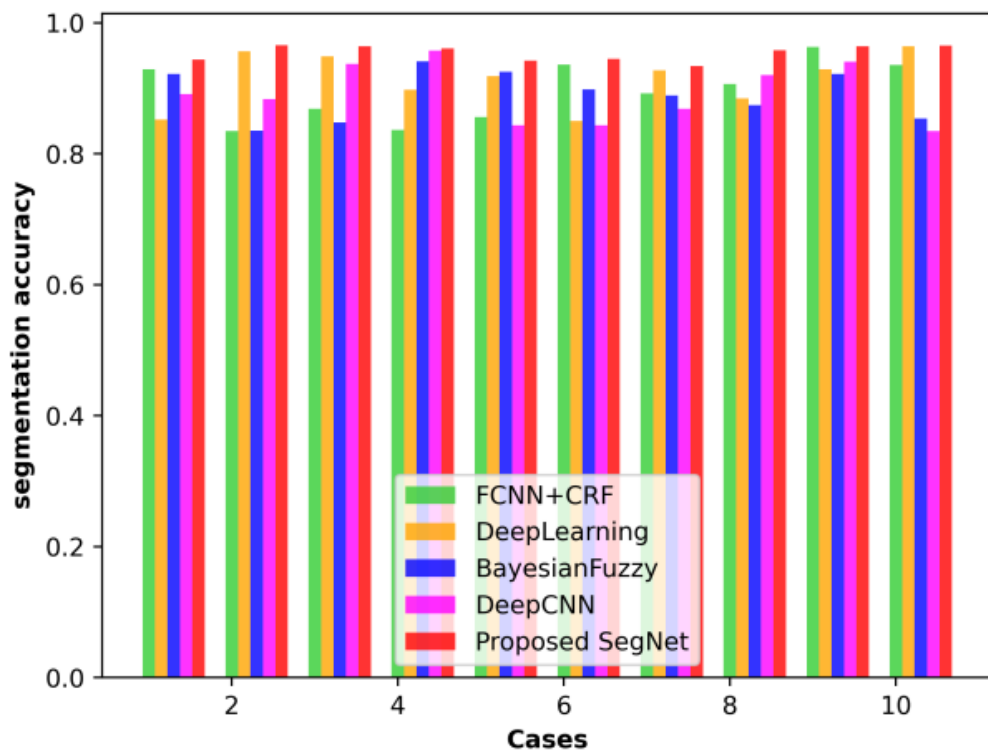
This section shows the comparative analysis of the developed SegNet +SWO-based DBN approach using dataset 2020 based on performance metrics with different training data percentages.

(a) Analysis using segmentation

The analysis of methods for dataset 2020 using segmentation is deliberated in Figure 2.12. In Figure 2.12 (a) the Dice coefficient for different images is revealed. When image = 2, the Dice coefficient of methods computed by FCNN+CRF, Deep learning, Bayesian fuzzy, Deep CNN, and proposed SegNet are 0.658, 0.764, 0.695, 0.792, and 0.857. Figure 2.12 (b) shows the segmentation accuracy of the method using dataset 2020. When image = 2, the segmentation accuracy of methods computed by FCNN+CRF, Deep learning, Bayesian fuzzy, Deep CNN, and proposed SegNet are 0.857, 0.926, 0.858, 0.926, and 0.958.



(a)



(b)

Figure 2.12: Analysis of methods for Dataset 2020 using (a) dice coefficient, (b) Segmentation accuracy

The segmentation accuracy in a tabular form using the BRATS 2020 dataset for the proposed method and existing methods are given in below Table 2.2.

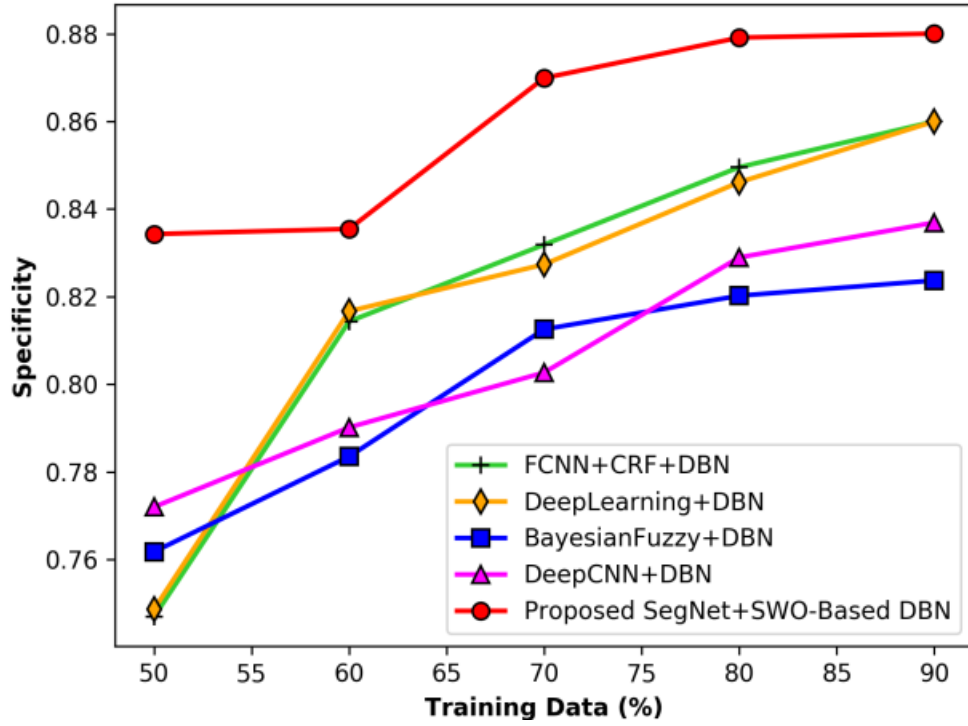
Table 2.2: Segmentation accuracy using the proposed method and existing methods for BRATS 2020 dataset

| | FCNN+ CRF [50] | Deep Learning [51] | Bayesian Fuzzy [62] | Deep CNN [54] | Proposed SegNet |
|----------|---------------------------|-------------------------------|--------------------------------|--------------------------|----------------------------|
| Image 1 | 0.812 | 0.866 | 0.815 | 0.881 | 0.936 |
| Image 2 | 0.857 | 0.926 | 0.858 | 0.926 | 0.958 |
| Image 3 | 0.818 | 0.850 | 0.850 | 0.895 | 0.946 |
| Image 4 | 0.804 | 0.876 | 0.820 | 0.917 | 0.952 |
| Image 5 | 0.828 | 0.872 | 0.838 | 0.946 | 0.957 |
| Image 6 | 0.865 | 0.901 | 0.884 | 0.908 | 0.930 |
| Image 7 | 0.814 | 0.929 | 0.824 | 0.945 | 0.954 |
| Image 8 | 0.803 | 0.862 | 0.848 | 0.947 | 0.952 |
| Image 9 | 0.804 | 0.852 | 0.827 | 0.853 | 0.915 |
| Image 10 | 0.824 | 0.871 | 0.850 | 0.916 | 0.925 |
| Image 11 | 0.828 | 0.849 | 0.845 | 0.872 | 0.873 |
| | FCNN+ CRF [50] | Deep Learning [51] | Bayesian Fuzzy [62] | Deep CNN [54] | Proposed SegNet |
| Image 12 | 0.808 | 0.840 | 0.813 | 0.847 | 0.876 |
| Image 13 | 0.801 | 0.824 | 0.810 | 0.870 | 0.874 |
| Image 14 | 0.891 | 0.913 | 0.899 | 0.915 | 0.949 |
| Image 15 | 0.820 | 0.850 | 0.825 | 0.934 | 0.959 |

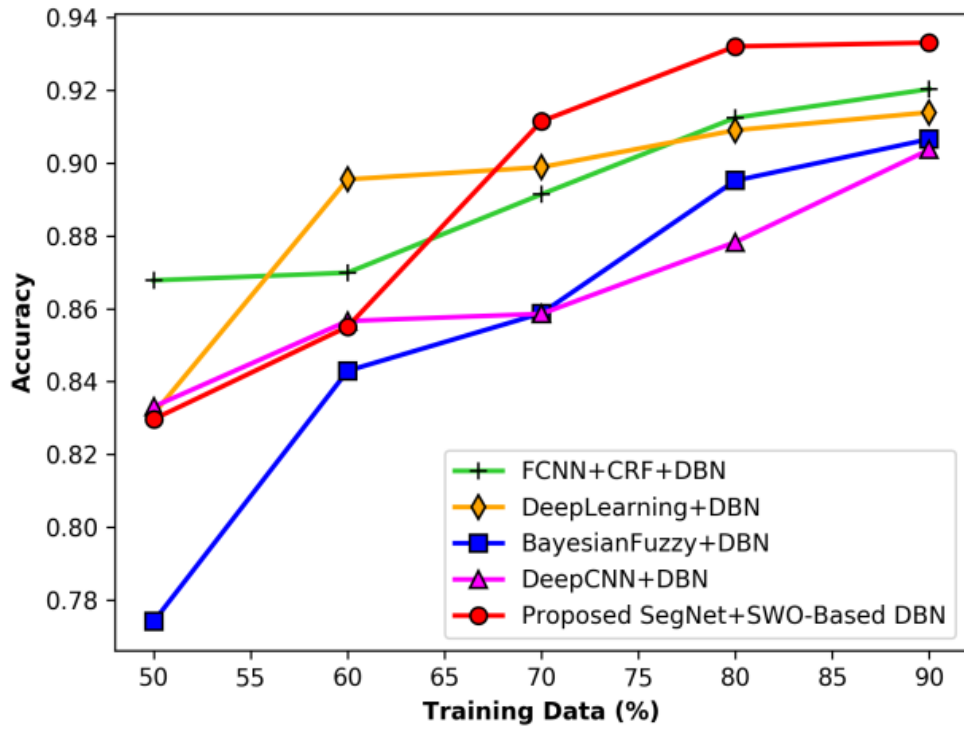
(b) Analysis using training data

Figure 2.13 illustrates the analysis of methods using dataset 2020 with different training data considering specificity, accuracy, and sensitivity parameters. The analysis of methods using specificity parameter is deliberated in Figure 2.13 (a). When training data = 90%, the specificity of methods measured by FCNN+CRF+DBN, Deep learning+ DBN, Bayesian fuzzy+DBN, Deep CNN+DBN, and proposed SegNet +SWO-based DBN are 0.816, 0.824, 0.820, 0.845, and 0.853. The analysis of methods based on accuracy is deliberated in Figure 2.13 (b). When training data=90%, the accuracy of methods measured by FCNN+CRF+DBN, Deep learning+ DBN, Bayesian fuzzy+ DBN, Deep CNN+DBN, and proposed SegNet +SWO-based DBN are 0.875, 0.886, 0.882, 0.901, and 0.921. The analysis of

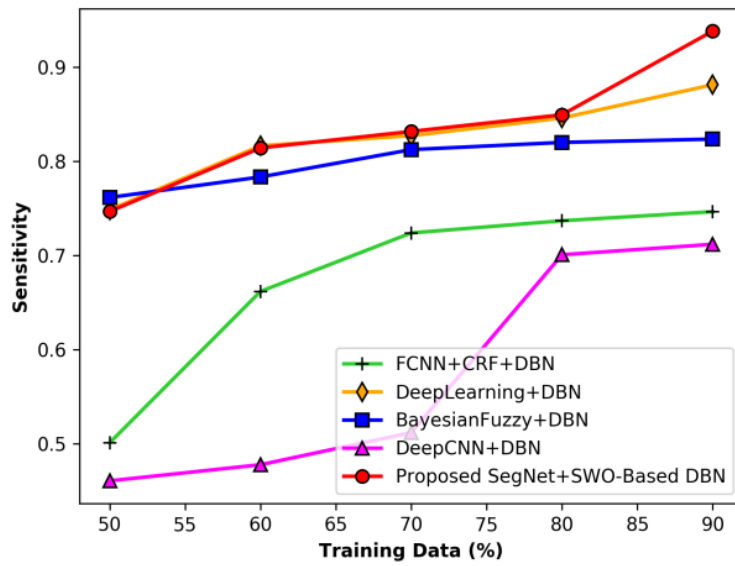
methods using sensitivity parameters is deliberated in Figure 2.13 (c). When training data = 90%, the sensitivity of methods measured by FCNN+CRF+DBN, Deep learning+ DBN, Bayesian fuzzy+ DBN, Deep CNN+DBN, and proposed SegNet +SWO-based DBN are 0.675, 0.809, 0.720, 0.880, and 0.928. Figure 2.13 (d) illustrates the ROC of developed SegNet +SWO-based DBN for brain tumor segmentation and classification. For a minimal of 0.1 as FPR, the TPR obtained by the methods, FCNN+CRF+DBN, Deep learning+ DBN, Bayesian fuzzy+ DBN, Deep CNN+DBN, and proposed SegNet +SWO-based DBN is 0.421, 0.544, 0.730, 0.735, and 0.744, respectively.



(a)



(b)



(c)

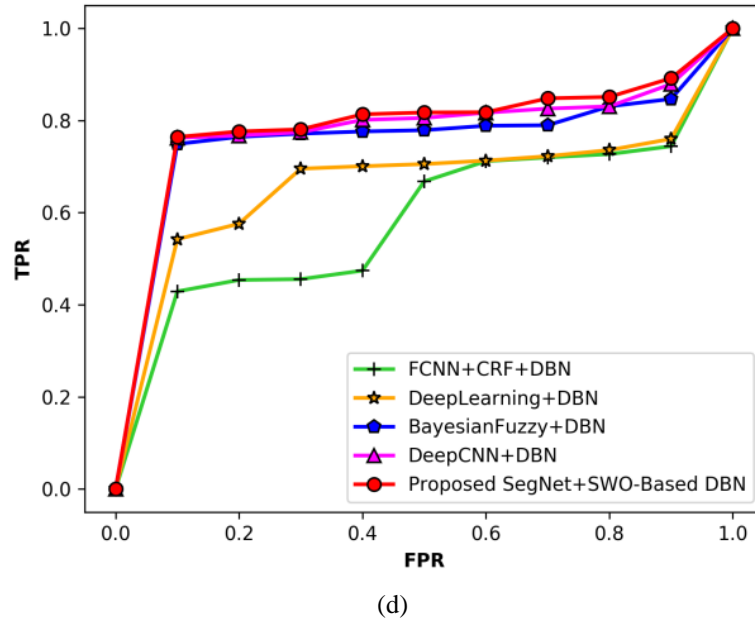


Figure 2.13: Analysis of methods using dataset 2020 considering training data (a) specificity, (b) accuracy, (c) sensitivity, and (d) ROC

2.4.8 Comparative discussion

Table 2.3 illustrates the comparative discussion using segmentation accuracy and dice coefficient parameters by varying the images. The maximal segmentation accuracy attained by the developed SegNet with the value of 0.965 and dice coefficient of 0.804, whereas the specificity of existing FCNN+CRF+DBN, Deep learning+ DBN, Bayesian fuzzy+ DBN, and Deep CNN+DBN is 0.935, 0.964, 0.853, and 0.834 for segmentation accuracy and 0.557, 0.640, 0.613, and 0.761 for dice coefficient.

| Dataset | Variation | Metrics | FCNN + CRF [50] | Deep learning [51] | Bayesian fuzzy [62] | Deep CNN [54] | Proposed SegNet |
|-----------------|-----------|--------------------------|-----------------------|--------------------------|---------------------------|------------------|--------------------|
| Dataset 2018 | Images | Segmentation accuracy | 0.935 | 0.964 | 0.853 | 0.834 | 0.965 |
| | | Dice coefficient | 0.557 | 0.640 | 0.613 | 0.761 | 0.804 |
| Dataset 2020 | Images | Segmentation accuracy | 0.815 | 0.876 | 0.860 | 0.906 | 0.957 |
| | | Dice coefficient | 0.684 | 0.709 | 0.702 | 0.761 | 0.711 |

Table 2.3: Comparative discussion for segmentation

Table 2.4 elaborates the analysis of maximum performance attained by the methods by varying the training data percentage considering performance metrics. The maximal specificity attained by the developed SegNet +SWO-based DBN with the value of 0.880, whereas the specificity of existing FCNN+CRF+DBN, Deep learning+ DBN, Bayesian fuzzy+ DBN, and Deep CNN+ DBN are 0.86, 0.86, 0.823, and 0.836. The maximal accuracy computed by proposed SegNet +SWO-based DBN with a value of 0.933, whereas the accuracy of existing FCNN+CRF+DBN, Deep learning+ DBN, Bayesian fuzzy+ DBN, and Deep CNN+DBN is 0.920, 0.913, 0.906, and 0.903. In addition, the maximal sensitivity value measured by SegNet +SWO-based DBN is 0.938, whereas the existing FCNN+CRF+DBN, Deep learning+ DBN, Bayesian fuzzy+ DBN, and Deep CNN + DBN are 0.746, 0.881, 0.823, and 0.712, for dataset 2018. By using dataset 2020, the specificity of the developed SegNet +SWO-based DBN is about 0.853, whereas the specificity of existing FCNN+CRF+DBN, Deep learning+ DBN, Bayesian fuzzy+ DBN, and Deep CNN+ DBN are 0.816, 0.824, 0.820, and 0.845. The maximum sensitivity and accuracy of the developed SegNet +SWO-based DBN is 0.928 and 0.921, whereas for the existing FCNN+CRF+DBN, Deep learning+ DBN, Bayesian fuzzy+ DBN, and Deep CNN+DBN the accuracy and sensitivity is about 0.875, 0.886, 0.882, 0.901 and 0.675, 0.809, 0.720, 0.880 respectively.

Table 2.4: Comparative discussion based on training data percentage

| Datasets | Variation | Metrics | FCNN+ CRF [50] | Deep Learning +DBN [51] | Bayesian fuzzy [62] | Deep CNN [54] | Proposed SegNet + SWO |
|-----------------|-----------------------------|-------------|----------------------|-------------------------------|---------------------------|---------------------|-----------------------------|
| Dataset 2018 | Training data percentage | Specificity | 0.860 | 0.860 | 0.823 | 0.836 | 0.880 |
| | | Accuracy | 0.920 | 0.913 | 0.906 | 0.903 | 0.933 |
| | | Sensitivity | 0.746 | 0.881 | 0.823 | 0.712 | 0.938 |
| Dataset 2020 | Training data percentage | Specificity | 0.816 | 0.824 | 0.820 | 0.845 | 0.853 |
| | | Accuracy | 0.875 | 0.886 | 0.882 | 0.901 | 0.921 |
| | | Sensitivity | 0.675 | 0.809 | 0.720 | 0.880 | 0.928 |

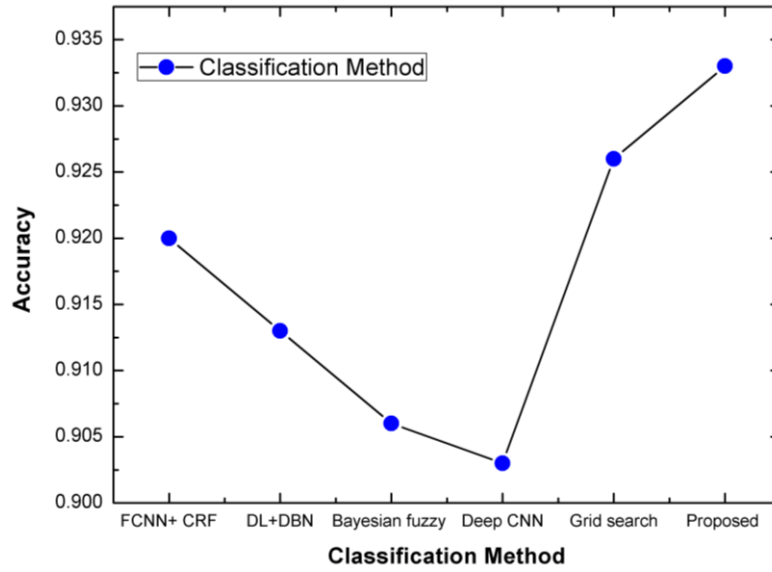


Figure 2.14: Comparative plot of classification accuracy of different methods

Table 2.5 gives the analysis of performance attained by the methods. The maximal accuracy computed by proposed SegNet +SWO-based DBN with a value of 0.933, whereas the accuracy of existing FCNN+CRF+DBN, Deep learning+ DBN, Bayesian fuzzy+ DBN, Deep CNN+DBN and grid search is 0.920, 0.913, 0.906, 0.903 and 0.926. Thus, the implemented method outperformance all other classification methods specifically the grid search algorithm [153]. The same is drawn in Figure 2.14.

Table 2.5: Comparative discussion of classification accuracy

| Metrics | FCNN+ CRF [50] | Deep Learning +DBN [51] | Bayesian fuzzy [62] | Deep CNN [54] | Grid search [153] | Proposed SegNet + SWO |
|----------|----------------------|-------------------------------|---------------------------|---------------------|-------------------------|-----------------------------|
| Accuracy | 0.920 | 0.913 | 0.906 | 0.903 | 0.926 | 0.933 |

2.5. Summary

The brain tumor classification is performed using DBN, which aims at improving the detection performance. The classical methods of automatic brain tumor classification using the DNN reveal poor performance with the presence of unwanted data, which is tackled based on the developed brain tumor classification method. In the proposed method, SWO trains the classifier, deriving optimal weights. Here, pre-processing is initially done by the input image to remove the artifacts and noise contained in the image. In addition, the SegNet is introduced for the

segmentation for generating the segments based on the pre-processed image. Here, the SegNet is modified using the proposed SWO. Once the segmentation is done, the feature extraction is carried out using CNN features. Finally, the extracted features are induced by DBN for determining the core, edema, benign, and malignant regions. The training of DBN is performed by the proposed SWO algorithm, which is newly designed by combining WWO and SSA.

The performance of the technique heavily relies on the quality and quantity of the training data, and its effectiveness may vary when applied to datasets with different characteristics or from diverse populations. Data dependency is a critical factor to consider when evaluating the effectiveness of the SWO-based DBN technique for brain tumor classification. The accuracy and reliability of the training data significantly influence the performance of the technique. High-quality data, free from errors or inconsistencies in tumor annotations, allows the model to learn meaningful patterns and features, leading to more accurate classification results.

Data availability statement

The data underlying this article are available in BRATS 2018 dataset and BraTS 2020 dataset at “<https://www.med.upenn.edu/sbia/brats2018/data.html>”, and <https://www.med.upenn.edu/cbica/brats2020/>.

CHAPTER

3

Enhanced Brain Tumor Recognition with Adam-based Techniques for Clinical Diagnosis

3.1 Introduction

A brain tumor (BT) is a growth of tissue that is organized by a gradual accumulation of anomalous cells and it is significant to segment and classify the BT from the magnetic resonance imaging (MRI) for treatment. Generally, the brain contains billions of active cells that makes the classification process difficult. Globally, 150 kinds of BT exist from which the benign and malignant are important. Benign cancer produces within the brain, whereas the malignant cancer that produces the outer side of brain [84]. Furthermore, the grading of BT helps to improve the lifespan of people. The manual detection of BT is complex and inaccurate, hence, to address the problem of manual detection, automated computerized techniques have been introduced [85]. Based on the machine learning and deep learning techniques, the researcher does not require advice from surgical experts to detect the tumor [86]. Recently, the deep neural network has been modelled to segment and classify the BT from the image [87]. Another technique used for classifying BT is a fully automated Convolutional neural network (CNN) model for making accurate and quick decision by the researcher. Moreover, the researchers have been introduced the automated and efficient BT classification system based on the machine learning approaches. Though, attaining high accuracy is the main challenge in classifying the brain image due to the vagueness [88].

This level of accuracy is crucial for accurately identifying and localizing tumor boundaries [89], which is essential for treatment planning and monitoring disease progression. Accurate segmentation and classification of brain tumors enable clinicians to precisely identify the location, size, and characteristics of the tumor [90]. This information is essential for determining the most appropriate treatment

approach, whether it involves surgery, radiation therapy, chemotherapy, or a combination of modalities [91].

This chapter invents the novel BT segmentation and classification techniques using Adam Sewing Training Based Optimization with the UNet++ (AdamSTBO+UNet++) and Adam Salp Water Wave Optimization with the Deep Convolutional Neural Network (AdamSWO-DCNN) algorithm. AdamSTBO+UNet++ performs the segmentation task, and AdamSWO-DCNN performs the classification task.

The key contributions in this chapter are,

- **Proposed AdamSTBO_UNet++ for BT segmentation:** The BT segmentation in this chapter is formulated by UNet++ and its weight is optimally tuned by the Adam STBO algorithm, which is the incorporation of Adam optimizer with the STBO algorithm.
- **Proposed AdamSWO_DCNN for BT classification:** The BT classification is carried out by the DCNN in which its weight is trained by the AdamSWO algorithm, which is formulated by the combination of Adam optimizer with the SWO algorithm. In addition, SWO is formed by the integration of SalpSwarm Algorithm (SSA) and Water Wave Optimization (WWO).

This chapter is organized as follows: The challenges are explained in section 3.2, AdamSTBO_UNet++ and AdamSWO_DCNN is exhibited in section 3.3, the graphical result obtained by the experimentation is provided in section 3.4 and the final findings and summary is given in section 3.5.

3.2 Challenges

The problems which are solved by the AdamSWO_DCNN for BT segmentation and classification is explained below,

- (i) The main challenge of DCNN in is to utilize the excess layers or regularization strategies with small image dataset for performing the BT classification.
- (ii) The accurate segmentation of BT from the large amount of MRI is challenging and time consuming. Moreover, the spatial and structural changeability among

BT to segment the MRI image is challenging.

- (iii) Reducing computation time in segmentation tasks, especially those involving deep learning techniques, is indeed a common challenge.
- (iv) Despite the introduction of Bayesian fuzzy clustering for BT segmentation, its prolonged training time posed a hurdle. Despite attempts to enhance accuracy through the utilization of multiple classifiers, this challenge persists for the proposed method.

3.3 Proposed Adam SWO-DCNN for BT segmentation and classification

This chapter introduces the novel BT classification technique for classifying the MRI image into the four types of tumors, such as edema, core tumor, benign and malignant. In this chapter, BT is segmented and classified by the deep learning model with the optimization technique. For that, the input image is collected from the dataset and the available image noise is cleaned by the bilateral filter [92]. After that, BT is segmented using U-Net++ [93], which is trained by the AdamSTBO that is formed by the integration of Adam optimizer together with the STBO algorithm [94]. After the segmentation, the significant features, such as CNN [95], Local optimal oriented pattern (LOOP) [96], Local gradient pattern (LGP), pyramid histogram of oriented gradients (PHOG) [97] and Gray-level co-occurrence matrix (GLCM) [98] are extracted. Finally, the BT classification is carried out using DCNN [99], which is trained by AdamSWO. In addition, the AdamSWO is the assimilation of Adam optimizer and SWO. Besides, the process flow diagram of AdamSWO for BT classification is given in Figure 3.1.

3.3.1 Image acquisition

Let us assume the MRI image dataset B , which contains the y number of input images, and is formulated as,

$$B = \{B_1, B_2, \dots, B_k, \dots, B_y\} \quad (3.1)$$

Here, y is the total number of input images and B_k specifies the k^{th} input images.

3.3.2 Image pre-processing

The pre-processing is performed simultaneously after acquiring the input image from the dataset since the acquired image may contains some noises. In order to filter this, the bilateral filtering [92] is applied to the input image B_k to eliminate the noise from the gathered image. The bilateral filtering is a non-linear filter, which processes the local image information, such as spatial position information and pixel value information for cleaning the image. Besides, it preserves the edges of an image by substituting the weighted mean of nearest pixel value on the place of noise pixel. This is expressed as [92],

$$B_f = \frac{1}{U_p} \sum_{k \in \Xi} U_k(u, k) U_m(u, k) B_k \quad (3.2)$$

where, B_f specifies the filtered image, B_k specifies the input of bilateral filter, Ξ indicates the neighborhood pixel, U_p specifies the normalization coefficient and the spatial and range kernel is denoted as U_k and U_m .

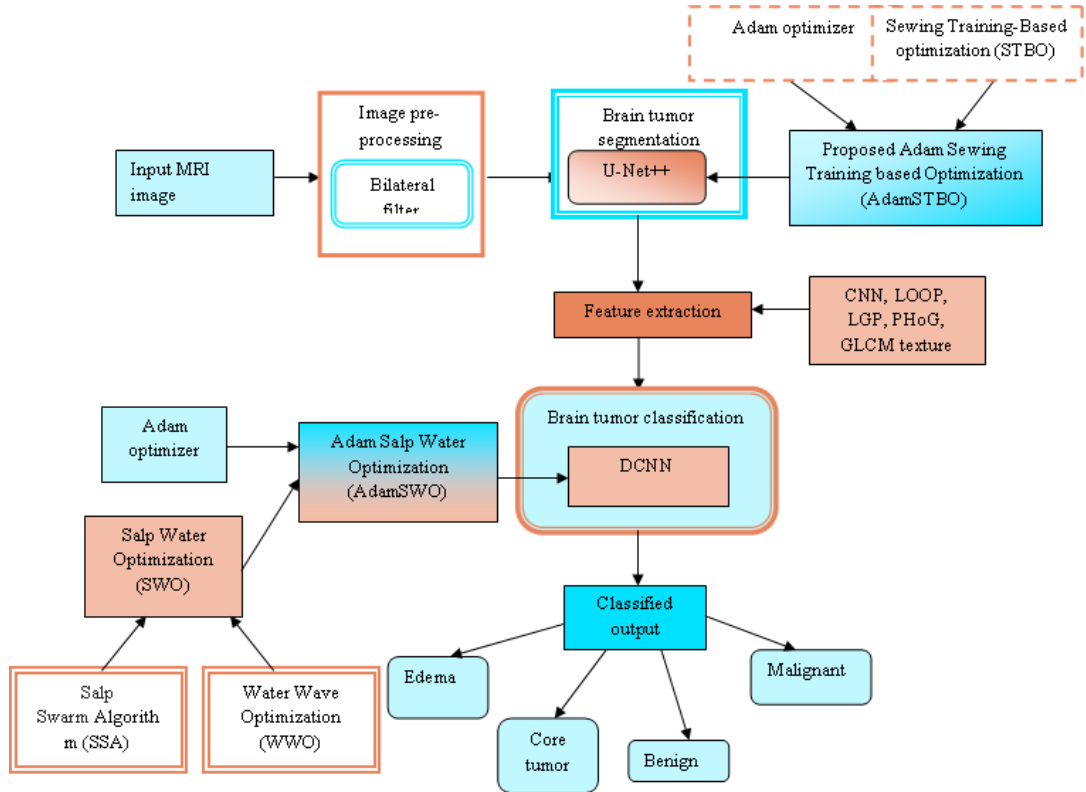


Figure 3.1: Block diagram of Adam SWO-DCNN for BT classification

3.3.3 BT segmentation using UNet++

The processing step after the pre-processing is BT segmentation, wherein the BT segmentation is completed by the UNet++ model. UNet model is the improved version of UNet++ model that considers the input B_f for BT segmentation. The segmentation using UNet++ model affords the improved accuracy rate than the other existing segmentation methods since the other methods reduced the image quality while processing.

(a) Design of UNet++

UNet++ is the segmentation network d in this chapter in which its function is to segment the BT from the pre-processed image. It is similar to the UNet but the UNet++ model provides the changes in skip connections between encoder and decoder. Here, the feature map of encoder part is similar to the feature map of decoder part and these two parts are linked through the skip connections. Thus, the skip connections are responsible for maintaining the information between both sides by consolidating the feature maps of encoder before joining them to the decoder's feature map.

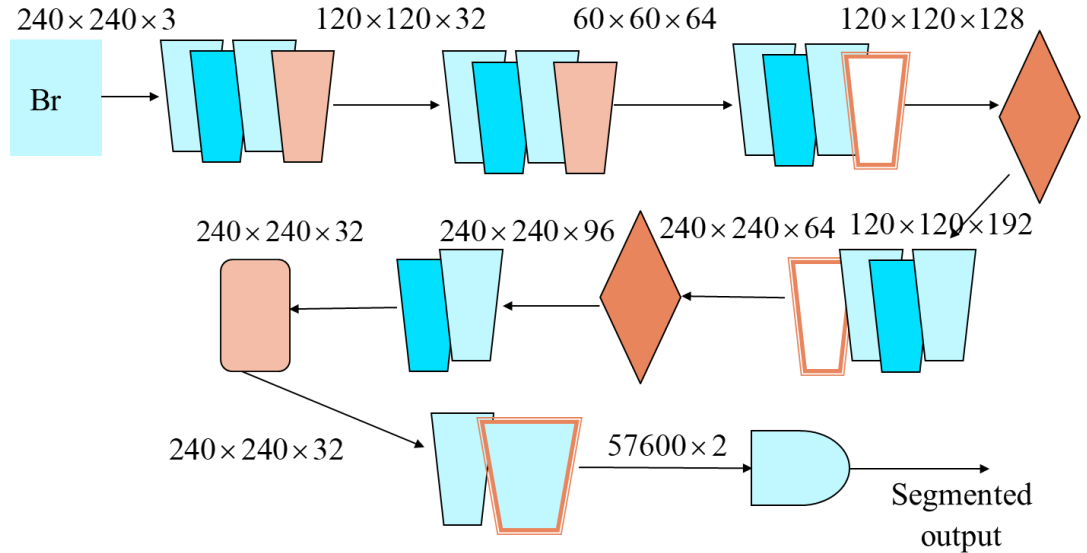


Figure 3.2: Structure of UNet++

In addition, the UNet++ model has to handle and receive the feature map of dissimilar scale in the decoder part. Besides, the feature map of encoder and feature map of decoder part is interlinked with one other through the skip connections.

Figure 3.2 shows the design of UNet++ model that produces the segmented output as Q_s . In Figure 3.2, pale bluish box characterizes the conv layer, dark bluish box states the dropout layer, pale orange colored box states the max pooling layer, orange bordered box shows the upsampling layer, an orange rhombus box denotes the concatenation layer, orange colored rectangle box shows the seg feat layer, blue filled orange bordered box shows the reshape layer and blue colored semi-circle states the activation layer.

(b) Training of UNet++ using AdamSTBO algorithm

This chapter proposes the novel AdamSTBO algorithm for training the weight of UNet++. In this chapter, the UNet++ model considers the segmented output Q_s as an input for BT segmentation in order to improve the classification process. Furthermore, the weight constraints of UNet++ model is tuned by introducing the AdamSTBO algorithm, and the AdamSTBO algorithm is formed by applying Adam Optimizer with the updated location of STBO [94]. Adam optimizer is a gradient dependent optimization scheme in which its best position is track educing stochastic objective function. Also, this method is computationally efficient, easy to execute and consider small memory space. Additionally, the hyper-parameters in this method require less tuning. In STBO, the mathematical modelling is designed in three phases, such as training instructor (TI) selection, training phase for sewing and practicing phase. In the training instructor selection phase, the trainee selects the training instructor based on their experience and sewing skills. In the training phase, the trainee copies the sewing strategies of trainer, and in the practicing phase, the new tailor practicing and improving the sewing skills based on the instruction of trainer. In order to design the new AdamSTBO algorithm, the Adam and AdamSTBO concept has to be combined. The algorithmic processes of AdamSTBO algorithm are explained as below.

(c) Initialization

The initialization step initializes the population members of AdamSTBO, such as training instructors and beginner tailors. In this method, the population members are represented in matrix form, which is given as,

$$M = \begin{bmatrix} M_1 \\ M_q \\ M_V \end{bmatrix}_{V \times y} = \begin{bmatrix} M_{1,1} & \cdots & M_{1,r} & \cdots & M_{1,y} \\ \vdots & \ddots & \vdots & \ddots & \vdots \\ M_{q,1} & \cdots & M_{q,r} & \cdots & M_{q,y} \\ \vdots & \ddots & \vdots & \ddots & \vdots \\ M_{V,1} & \cdots & M_{V,r} & \cdots & M_{V,y} \end{bmatrix}_{V \times y} \quad (3.3)$$

Here, the population matrix is labelled as M , M_q denotes the q^{th} member of STBO, V specifies the population members of STBO and the problem variable count is indicates as y . Moreover, all population members are arbitrarily initialized by,

$$M_{q,r} = K_r + g \cdot (R_r - K_r); \quad q = 1, 2, \dots, V, r = 1, 2, \dots, y \quad (3.4)$$

Here, $M_{q,r}$ specifies the r^{th} variable computed by q^{th} member of STBO, g specifies the random number, upper and lower bounds are signified as K_r and R_r .

(d) Fitness computation

The fitness function is computed to predict the best solution. In this section, the fitness function is evaluated using Mean squared Error (MSE) in which its minimum value is used as the final solution for BT segmentation. Thus, the expression becomes,

$$P_{fit} = \frac{1}{t} \sum^t (Q_s^* - Q_s)^2 \quad (3.5)$$

Here, Q_s^* specifies the expected output, Q_s shows the classified output of UNet++ and t denotes the total sample count.

(e) Training phase

This phase is the modelling of training phase which involves two steps. For performing the training phase, the training instructors are initially selected by the trainee, and then they gather the sewing intelligence of training instructors. Here, the training instructor is selected based on the best objective function. Thus, the expression for selecting the probable training instructor is given by [62],

$$PTN_q = \left\{ M_s \mid P_{fit,s} < P_{fit,s}, s \in \{1, 2, \dots, V\} \right\} \cup \{ M_{best} \} \quad (3.6)$$

Here, the probable training instructor at q^{th} member in STBO is given by PTN_q . In this phase, the new location of population members in the first phase is portrayed as,

$$M_{q,r}^{S1} = M_{q,r} + g_{q,r} (TN_{q,r} - N_{q,r} M_{q,r}) \quad (3.7)$$

The above equation can be modified into,

$$M_{q,r}(w+1) = M_{q,r}(w) + g_{q,r} (TN_{q,r} - N_{q,r} M_{q,r}(w)) \quad (3.8)$$

$$M_{q,r}(w+1) = M_{q,r}(w) + g_{q,r} . TN_{q,r} - g_{q,r} . N_{q,r} . M_{q,r}(w) \quad (3.9)$$

$$M_{q,r}(w+1) = M_{q,r}(w) [1 - g_{q,r} . N_{q,r}] + g_{q,r} . TN_{q,r} \quad (3.10)$$

Here, $M_{q,r}^{S1}$ denotes the population member at first phase. In order to progress the effectiveness of training phase, the Adam algorithm is applied with the present position of STBO algorithm. From Adam,

$$M_r^q(w) = M_r^{q-1}(w-1) - \beta b^{\wedge}(w) / \sqrt{E^{\wedge}(1) + \varepsilon} \quad (3.11)$$

Substituting equation (3.11) in equation (3.10),

$$M_{q,r}(w+1) = \left(M_r^{q-1}(w-1) - \beta b^{\wedge}(w) / \sqrt{E^{\wedge}(1) + \varepsilon} \right) [1 - g_{q,r} . N_{q,r}] + g_{q,r} . TN_{q,r} \quad (3.12)$$

Here, $M_{q,r}(w+1)$ denotes the position of q^{th} solution in r^{th} dimension at iteration $w+1$, $M_{q,r}(w-1)$ specifies the position of q^{th} solution in r^{th} dimension at iteration $w-1$, β specifies the parameter, $g_{q,r}$ denotes the random number between (0, 1), selected instructor is specified as TN and $N_{q,r}$ is indicated as random number values between (1, 2).

This is the conclusive updated equation of AdamSTBO algorithm. After updating every position using equation (3.12), the new position is validated based on objective function, and optimal position is decided using the below formula,

$$M_q = \begin{cases} M_{q,r} (w+1), & P_{fit,q}^{S1} < P_{fit,q} \\ M_q, & Else \end{cases} \quad (3.13)$$

Equation (3.12) is the final updated expression for AdamSTBO algorithm.

(f) Duplicating instructor skills

In this phase, the STBO members mimics the sewing characteristics of instructor in order to update the position. Thus, the new position of STBO members are formulated as,

$$M_{q,r}^{S2} = \begin{cases} TN_{q,r} & r \in SD_q \\ M_{q,r} & Else \end{cases} \quad (3.14)$$

Here, M_r^{P2} denotes the random location of r^{th} member in STBO and $M_{q,r}^{S2}$ signifies the new locality of population member at second phase. After updating the position using equation (3.14), the old position is replaced by the new position based on objective function, and optimal position is decided using the below formula,

$$M_q = \begin{cases} M_q^{S2}, & P_{fit,q}^{S2} < P_{fit,q} \\ M_q, & Else \end{cases} \quad (3.15)$$

Here, $P_{fit,q}^{S2}$ is the objective function of M_q^{S2} .

(g) Practicing phase

In the practicing phase, the solution is updated based on simulating the beginner tailoring practices for improving the sewing skills. In order to calculate the new position, the new location encloses by each member is initially determined and the new position replaces the old position based on,

$$M_q = \begin{cases} M_q^{S3}, & P_{fit,q}^{S3} < P_{fit,q} \\ M_q, & Else \end{cases} \quad (3.16)$$

Here, M_q^{S3} is the computed new position based on older position and $P_{fit,q}^{S3}$ is the objective function.

(h) Re-evaluate feasibility

The feasibility of each solution is evaluated after completing each iteration. Thus, the new position replaces the older position if the computed new position is better than the older one.

(i) Termination

All the above-mentioned processes are repetitive till the best solution is determined. The pseudocode of AdamSTBO is explained in Algorithm 3.1.

Algorithm 3.1: Pseudocode of AdamSTBO

| |
|--|
| Input: Population size, problem dimensions, upper and lower bounds |
| Output: Optimal solution |
| Initialization: |
| Initialize the population matrix 'M' with random values within the bounds. |
| Compute the fitness of each member using the Mean Squared Error (MSE). |
| Training phase: |
| Select the training instructor and compute the new position |
| Duplicating Instructor Skills: |
| Update the Optimiser (STBO) member's position using equation (3.12) and (3.13) |
| Perform the instructor skill duplication by mimicking the sewing characteristics |
| Compute the SD_q |
| Evaluate the new position of optimiser by using equation (3.14) |
| Renew the location of optimiser member by using objective function equation (3.15) |
| Practicing Phase: |
| Update the salutation based on simulating the beginner tailoring practices. |
| Renew the location of q^{th} member using equation (3.16) |
| End |
| Re-evaluate Feasibility: Replace old positions with new ones if they improve the fitness. |
| Termination: |
| Repeat above steps until the stopping condition (e.g., max iterations or convergence) is met |
| Return the best solution. |
| End |

Here, the introduced AdamSTBO is developed by the integration of Adam optimizer and STBO algorithm. Thus, the AdamSTBO algorithm helps to improve the segmentation accuracy of UNet++ for BT segmentation.

3.3.4 Feature extraction

After the BT segmentation using UNet++, the feature extraction is carried out to excavate the significant features, such as CNN, LOOP, LGP, PHoG [97] and GLCM features [98]. In addition, the GLCM features include ASM, IDM, entropy and correlation. The extracted features obtained from this phase helps to increase the effectiveness of BT classification using DCNN. Each of these features obtained from segmented image Q_s are explained in this part is explained below.

(a) Convolutional neural network (CNN) features

The CNN feature is extracted from the convolutional (conv) layer of CNN. The CNN model comprises of three layers involving conv layer, pooling layer and fully connected (FC) layer. Thus, the structure of CNN is explained in Figure 3.3. Thus, the CNN feature obtained from the CNN is signified as z_1 .

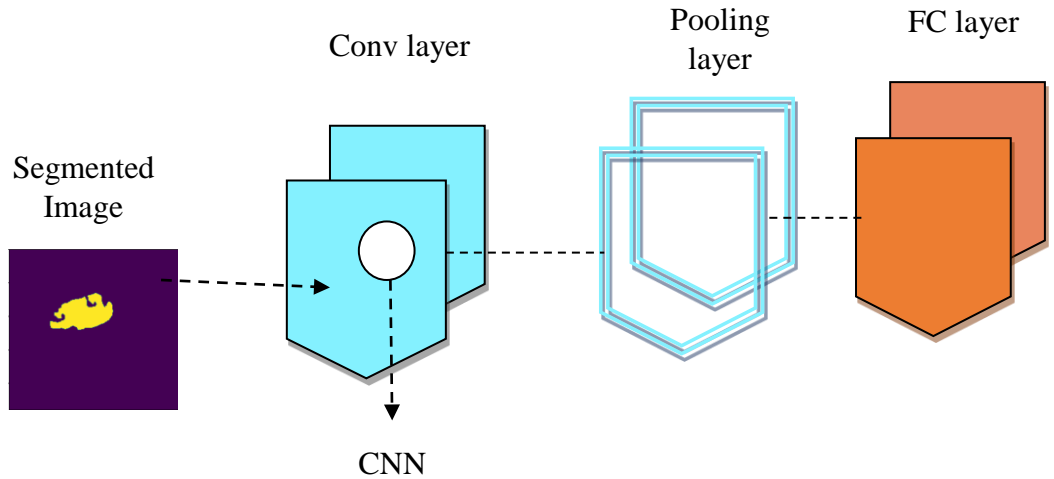


Figure 3.3: Extracted CNN feature from CNN

(b) Local optimal oriented pattern (LOOP)

The second feature is the LOOP feature, which is formulated by the amalgamation of Local Directional Pattern (LDP) and Local Binary Pattern (LBP)

feature that sustains the quality of available information. Thus, the expression for LOOP feature is denoted as [92],

$$z_2 = LOOP(w_x, y_x) = \sum a(c_n - c_x).2^{v_n} \quad (3.17)$$

Here, c_n and c_x be the intensity values of pixels and the LOOP feature is specified as z_2 .

(c) Local gradient pattern (LGP)

LGP is a tiny feature vector, which is extracted from each pixel of segmented image Q_s . LGP feature produces the constant patterns regardless of local intensity discrepancies along the edges. In order to calculate the LGP operator, the eight neighbor's gradient values of specified pixels are computed. The average values of these gradient values are used to generate the LGP feature, which is specified as z_3 .

(d) PHOG feature

PHOG feature is a descriptor, which is computed based on the histogram of gradient orientation (HOG) feature that represents the image into the pyramid shaped structure. For calculating the PHOG feature, the HOG feature is initially computed for every grid at each pyramid level. Based on these features, the final feature is obtained by combining it, and the feature is notified as z_4 .

(e) Gray-level co-occurrence matrix (GLCM) feature

GLCM is a statistical method to analyze the texture of spatial relationship among the pixels. In this chapter, the GLCM method computes the texture features, like ASM, IDM, entropy and correlation. Hence, each of these features are explained below.

(i) Angular Second Moment (ASM)

The ASM feature is computed using the below expression [62],

$$b_1 = \sum_{v=0}^{L-1} \sum_{w=0}^{L-1} (M(v, w))^2 \quad (3.18)$$

Here, $M(v, w)$ specifies the input image.

(ii) Inverse Difference Moment (IDM)

The standard equation for computing IDM is given below [62],

$$b_2 = \sum_{v=0}^{L-1} \sum_{j=0}^{L-1} \frac{1}{1+(v-w)} M(v, w) \quad (3.19)$$

(iii) Entropy

The expression for computing entropy is given by [62],

$$b_3 = - \sum_{v=0}^{L-1} \sum_{w=0}^{L-1} P(v, w) \times \log(v, w) \quad (3.20)$$

(iv) Correlation

The standard formula for computing the correlation is denoted as [62],

$$b_4 = \sum_{v=0}^{L-1} \sum_{w=0}^{L-1} \frac{\{v \times w\} \times M(v, w) - \{\chi_e \times \chi_f\}}{\Omega_e \times \Omega_f} \quad (3.21)$$

Here, Ω_e and Ω_f are the standard deviation of input image

Hence, the final texture feature obtained using the GLCM method is given by, $z_5 = \{b_1, b_2, b_3, b_4\}$. In addition, the final feature vector obtained from the feature extraction is denoted as $z = \{z_1, z_2, z_3, z_4, z_5\}$. Thus, the final feature vector used for BT classification is obtained by combining all the extracted features CNN, LOOP, LGP, PHoG and GLCM features.

3.3.5 BT classification using AdamSWO-DCNN

The final step in this research is the BT classification, wherein the processing is carried out by the Adam SWO-DCNN. In this step, the BT classification is initially done by the DCNN that considers the extracted feature z as the input of DCNN, and it provides the classified output as edema, core tumor, benign and malignant. Moreover, the weight of DCNN is optimized by the AdamSWO, which is modelled by the amalgamation of Adam Optimizer with the SWO algorithm. Furthermore, SWO algorithm is formed by combining SSA and WWO. The DCNN model provides the better result with various detection and classification systems.

Furthermore, the accuracy rate and speed of processing achieved by the DCNN is relatively higher than the other classifiers. Here, DCNN classifies the BT into the following section explains the design of DCNN, and its schematic model is given in Figure 3.4.

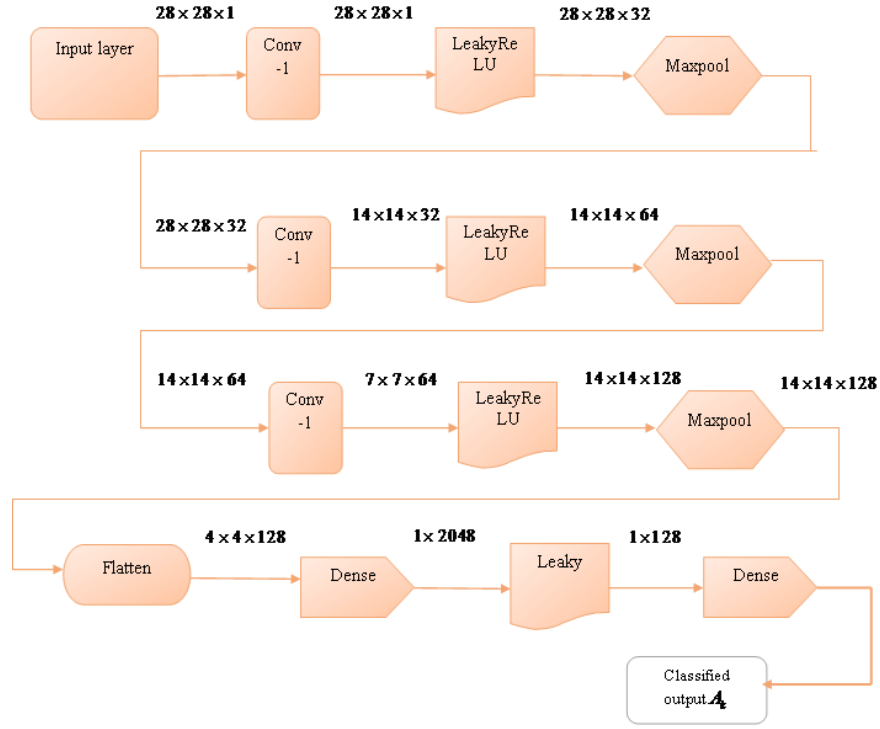


Figure 3.4: Structure of DCNN

(a) Design of DCNN

DCNN generally comprises of three basic layers, such as conv layer, pool layer and FC layer, where each layer perform the separate processes, such as feature extraction, sampling and BT classification. In DCNN, the increasing count of conv layer aids to progress the classification accuracy. In order to perform the classification, the extracted CNN feature from CNN layer is directly applied to the FC layer such that the classified outcome is obtained.

(i) Conv layer

The most important layer in DCNN is conv layer that encloses the multiple consecutive layers. Here, the obtained feature from one layer is applied to the input of next layer. In the input is passed to the conv layer, which is the extracted feature,

and its outcome is passed to the pool layer in order to perform the sampling process. The expression for conv layer is denoted as [92],

$$\left(P_h^a\right)_{n,v} = \left(S_h^a\right)_{n,v} + \sum_{w=1}^{H_1^{h-1}} \sum_{l=-\varepsilon_1^h}^{\varepsilon_1^h} \sum_{t=-\varepsilon_2^h}^{\varepsilon_2^h} \left(W_{a,w}^h\right)_{l,t} * \left(P_h^{a-1}\right)_{n+l,v+t} \quad (3.22)$$

Here, * depicts the conv operator, $\left(P_h^a\right)_{n,v}$ denotes the feature map of conv layer, $\left(P_h^{a-1}\right)_{n+l,v+t}$ indicates the feature map of preceding conv layer, $W_{a,w}^h$ shows the kernel function and S_h^a is the bias of conv layer.

(ii) Activation function

The activation function in DCNN determines the output like yes or no.

(iii) Rectified Linear Unit (ReLU)

It acts as an activation function that eliminates the negative values to make the classification process as simple and effective. Thus, the output got from the ReLu layer is expressed as,

$$P_h^a = \text{fun}\left(P_w^{a-1}\right) \quad (3.23)$$

Here, $\text{fun}()$ specifies the activation function of conv layer.

(iv) Pooling layer

For further simplifying the computation process, the DCNN introduces the pooling layer that reduces the input dimensions by integrating the outcome of various layers. The pooling layer perform as a sampling layer, and the feature map resolution is reduced to improve the invariance of features to the misrepresentations obtainable in the input image.

(v) FC layer

The extracted features are presented to the FC layer that produces the classified result using the below formula [92],

$$Q_h^a = \varpi\left(Y_h^a\right) \text{ with } Y_h^a = \sum_{w=1}^{H_1^{h-1}} \sum_{l=-\varepsilon_1^h}^{\varepsilon_1^h} \sum_{t=-\varepsilon_2^h}^{\varepsilon_2^h} \left(W_{a,w}^h\right)_{l,t} * \left(P_h^{a-1}\right)_{n+l,v+t} \quad (3.24)$$

Here, $(W_{a,w}^h)_{l,t}$ denotes the weight metric in FC layer and the classified output get from the DCNN is specified as A_k . In addition, the weight of DCNN is tuned by the AdamSWO algorithm.

(b) Training of DCNN using AdamSWO

The introduced AdamSWO in this research is used to train the weight of DCNN in order to attain the efficient BT classification. Hence, the AdamSWO is modelled by the incorporation of Adam Optimizer with the SWO algorithm. In addition, the SWO is generated by combining the merits of SSA and WWO. SSA is modelled based on the swarming characteristics of salps while foraging and moving on the ocean. The advantage of SSA is that it provides an efficient optimization solution with better coverage and convergence rate. Likewise, WWO is a nature inspired optimization approach in which its mathematical expression is derived based on the phenomena of water waves including refraction, breaking and propagation for searching the solution in high dimensional search space. Besides, the computational complexity of this approach while updating the optimal position is less.

Adam optimizer is a gradient dependent optimization approach in which its best position is determined based on the stochastic objective function. Besides, this method is computationally efficient, easy to implement and consume less memory space. Furthermore, the hyper-parameters in this model require less tuning. Thus, the hybrid optimization is derived by combining the advantages of Adam optimizer, SSA and WWO. Furthermore, the algorithmic processes of AdamSWO are explained as below.

(i) Initialization

The first step is to initialize the number of salps, which are arbitrarily initialized for attaining the best solutions, and is given by,

$$M = \{M_1, M_2, \dots, M_d, \dots, M_u\} \quad (3.25)$$

Here, M_d denotes the d^{th} salp and u is the total number of salps.

(ii) Fitness computation

The fitness computation is done to evaluate the optimal solution for BT segmentation and classification using mean squared Error. Here, the least value of fitness is selected as the final solution, and is denoted as,

$$Z = \frac{1}{m} \sum_{c=1}^m (A_k^* - A_k)^2 \quad (3.26)$$

Here, m is the total sample count, A_k is the classified outcome of DCNN and A_k^* is the expected outcome of classifier.

(iii) Solution update based on AdamSWO

In this step, the weight of DCNN is computed to upgrade its weights using AdamSWO and the location update is done using MSE. In order to achieve this, the swarming characteristics of salps and natural aspects of water waves are initially combined to get SWO, and is then modified using Adam optimizer. Thus, the final updated expression for SWO is given by,

$$M_r^q(w+1) = M_r^{q-1}(w) - \text{Gaussian}(0,1)\alpha C_r \quad (3.27)$$

Here, $M_r^{q-1}(w)$ indicates the position of $(q-1)^{th}$ follower in r^{th} dimension at iteration w , $M_r^q(w+1)$ indicates the location of r^{th} follower in q^{th} dimension at iteration $w+1$, α specifies the breaking coefficient and C_r shows the span of r^{th} dimension in the search space.

For further improving the update location of SWO, the Adam algorithm is introduced. From Adam,

$$M_r^q(w+1) = M_r^{q-1}(w) - \beta b^{\wedge}(w) / \sqrt{E^{\wedge}(1) + \varepsilon} \quad (3.28)$$

From equation (3.27), adding $M_r^q(w)$ on both sides,

$$M_r^q(w+1) + M_r^q(w) = M_r^{q-1}(w) - \text{Gaussian}(0,1)\alpha C_r + M_r^q(w) \quad (3.29)$$

Applying equation (3.28) in equation (3.29), then the equation becomes,

$$M_r^q(w+1) = M_r^{q-1}(w) - \text{Gaussian}(0,1)\alpha C_r + M_r^{q-1}(w) - \beta b^\wedge(w) / \sqrt{E^\wedge(1)} + \varepsilon - M_r^q(w) \quad (3.30)$$

Here, $b^\wedge(w)$ specifies the exponential moving average of gradient, $E^\wedge(1)$ is the squared gradient. This is the final equation used for updating the location of salps using AdamSWO.

(iv) Re-evaluate feasibility

After every iteration, the determined solution is renewed using the fitness function. Then, the new position is selected to be updated if the old solution is weaker than the new one.

(v) Termination

Every step explained above are performed repeatedly till the best solution is determined for BT classification. The pseudocode of AdamSWO is explained in Algorithm 3.2.

Algorithm 3.2: Pseudocode of AdamSWO

| |
|---|
| Input: Salp's population $M = \{M_1, M_2, \dots, M_d, \dots, M_u\}$ |
| Output: Optimal solution |
| Start |
| Initiate the population of salp |
| Calculate the fitness function for entire salp |
| For every salp M^q |
| If ($q = 1$) |
| Renew the expression of follower salp by equation (3.30) |
| end |
| end |
| Amends the salps based on the lower and bounds |
| end |
| Re-compute the feasibility of solutions |
| $w = w + 1$ |
| end for |

end while

Optimal solution is achieved

End

3.4 Results and discussion

The result achieved by the experimentation of AdamSWO-DCNN for BT segmentation and classification is explained below. The dataset used for the proposed Adam SWO-DCNN is BRATS 2018 dataset [82] in which its stored data is gathered from four modalities, like T1, T1C, T2 and fluid-attenuated inversion recovery (FLAIR). Every modality in this dataset comprises 130 to 176 brain slices, which are used for the assessment. Here, 10 image sets from the FLAIR modality is used for the BT segmentation and classification.

3.4.1 Performance metrics

The performance metrics used for assessing the effectiveness of Adam SWO-DCNN is accuracy, positive predictive value (PPV), negative predictive value (NPV), true positive rate (TPR), true negative rate (TNR) and dice coefficient.

(i) Accuracy: Accuracy is the measure used to determine the effectiveness of classified output, which is specified as [62],

$$h_1 = \frac{h_p + h_n}{h_p + h_n + l_p + l_n}$$

(3.31)

Here, h_p and h_n are the true positive and true negative, l_p and l_n are the false positive and false negative.

(ii) Positive predictive value (PPV): It is the proportion of truly identified positive results to the total number of positive results, which is given by [62],

$$h_2 = \frac{h_p}{h_p + l_p}$$

(3.32)

(iii) Negative predictive value (NPV): It is the proportion of truly identified negative results to the total number of negative results, which is given by [62],

$$h_3 = \frac{h_n}{h_n + l_n}$$

(3.33)

(iv) True positive rate (TPR): It is the ratio of correctly classified positive results from the classified of positive class, which is given by [62],

$$h_4 = \frac{h_p}{h_p + l_n}$$

(3.34)

(v) True negative rate (TNR): It is the ratio of correctly classified negative results from the classified of negative class, which is given by [62],

$$h_1 = \frac{h_n}{h_n + l_p}$$

(3.35)

3.4.2 Experimental result

The experimental result of AdamSWO-DCNN for BT segmentation and classification at different stage of processing is explained in Figure 3.5. The input image used for experimentation is given in Figure 3.5 (a), pre-processed image based on bilateral filtering is exposed in Figure 3.5 (b), segmentation output obtained from UNet++ is exposed in Figure 3.5 (c), extracted LGP feature is shown in Figure 3.5 (d) and the LOOP feature is shown in Figure 3.5 (e).

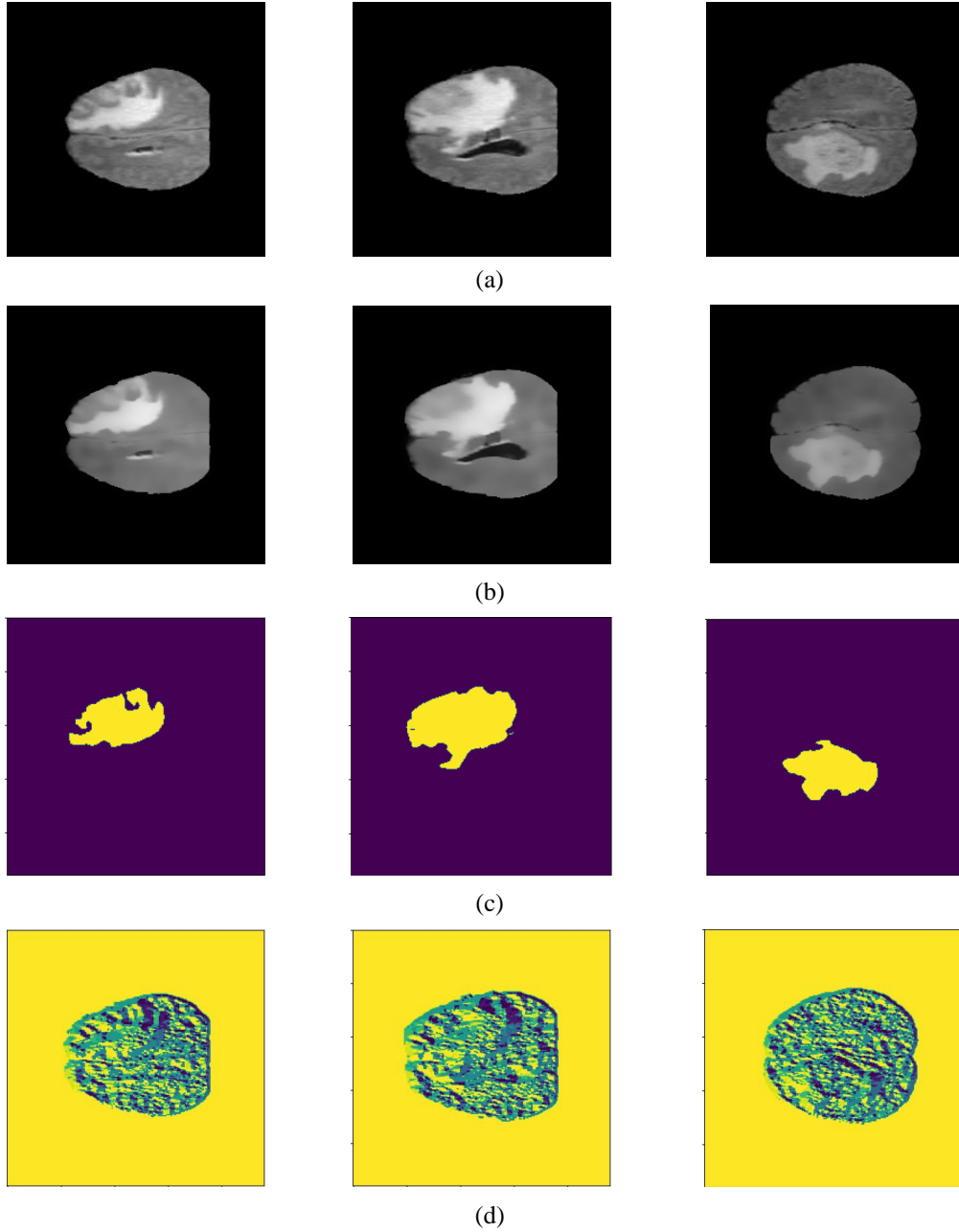
3.4.3 Competitive analysis

The competitive techniques used for assessing the efficacy of AdamSWO-DCNN are FCNN+CRF [50], Deep learning [51], Bayesian fuzzy [62] and DeepCNN [54]. The analysis of evaluating the AdamSWO-DCNN is done based on accuracy, PPV, NPV, TPR TNR and dice coefficient in accordance with the training set and k-value.

(a) Analysis based on training data

Figure 3.6 (a) illustrates the accuracy graph of AdamSWO-DCNN. When the training data is 90%, then the AdamSWO-DCNN attained the accuracy of 92.8%, and the FCNN+CRF, Deep learning, Bayesian fuzzy and DeepCNN got the accuracy

of 89.3%, 92%, 91.5% and 89.8%. The NPV graph of AdamSWO-DCNN is exposed in Figure 3.6 (b). The NPV value of AdamSWO-DCNN and FCNN+CRF, Deep learning, Bayesian fuzzy and DeepCNN techniques are 91.8%, and 89%, 91.2%, 91.1% and 89.5 % for the training set of 90%. The PPV graph for the AdamSWO-DCNN is given in Figure 3.6 (c).



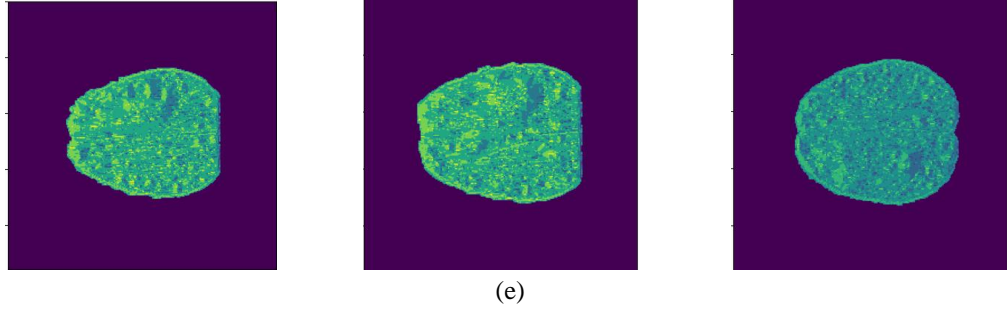
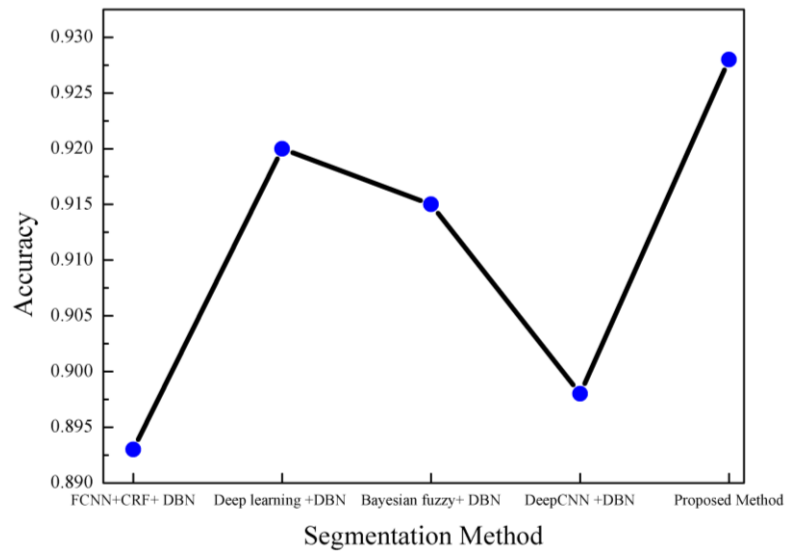
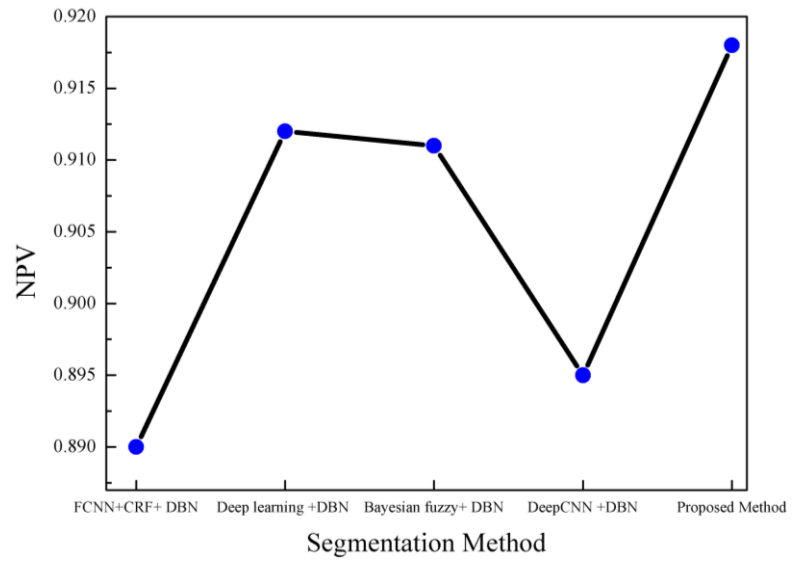


Figure 3.5: Experimental result of AdamSWO-DCNN a) Input images, b) Pre-processed images, c) Segmented images, d) LGP feature, e) Loop feature

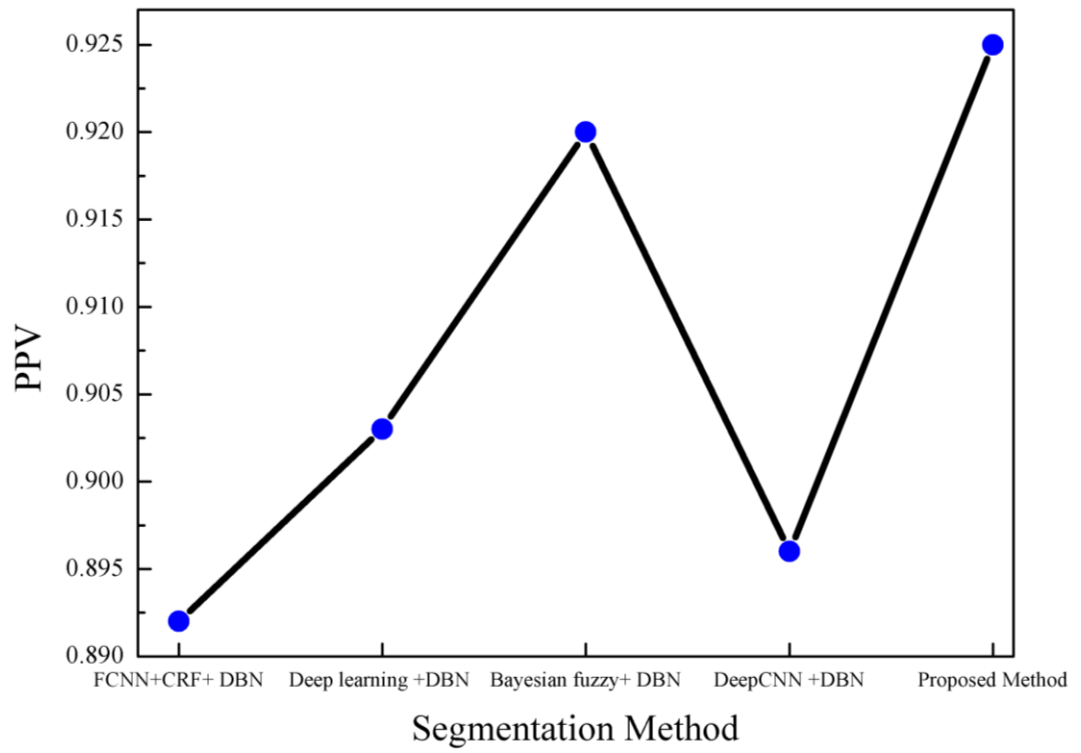
The PPV value achieved by the AdamSWO-DCNN is 92.5%, likewise, the PPV of traditional BT segmentation schemes are 89.2%, 90.3%, 92% and 89.6% for the training set value of 90%. The TNR graph of AdamSWO-DCNN with respect to the varying training set value is given in Figure 3.6 (d). As the value of training set is 90%, the AdamSWO-DCNN got the TNR of 92.9%, whereas the competitive methods used for the analysis attained the TNR of 89.6%, 92.0%, 90.7% and 92.5%. The TPR graph of AdamSWO-DCNN with respect to the varying training set value is given in Figure 3.6 (e). When the training set value is 90%, then the TPR achieved by the AdamSWO-DCNN and competitive methods are 92.9%, 88.2%, 89% 92.1% and 90.8%.



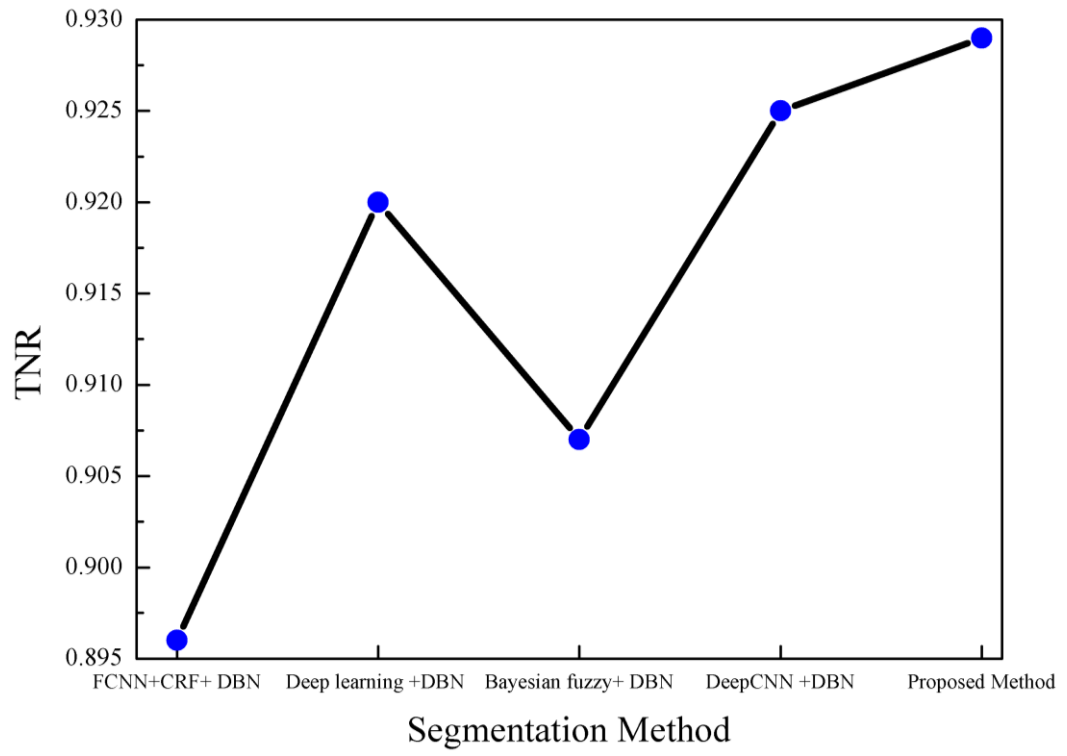
(a)



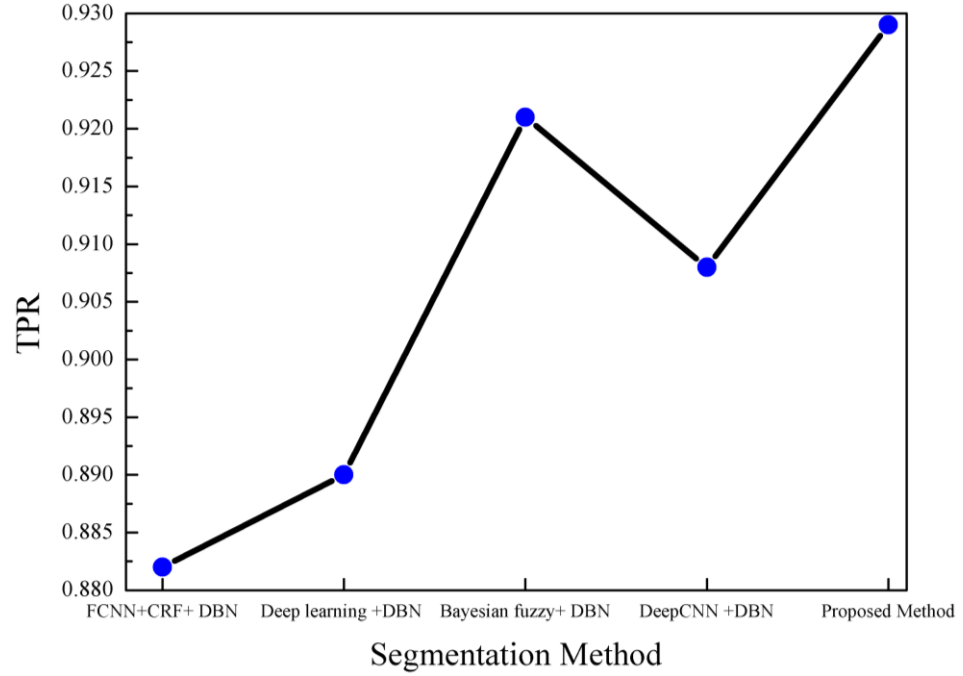
(b)



(c)



(d)

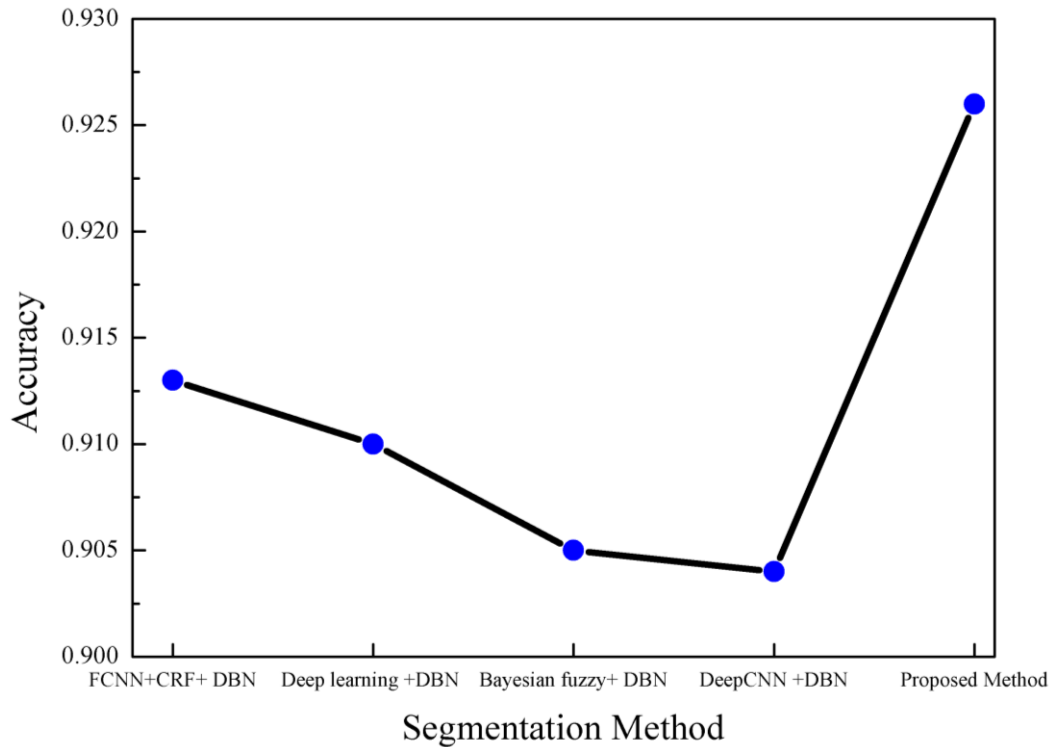


(e)

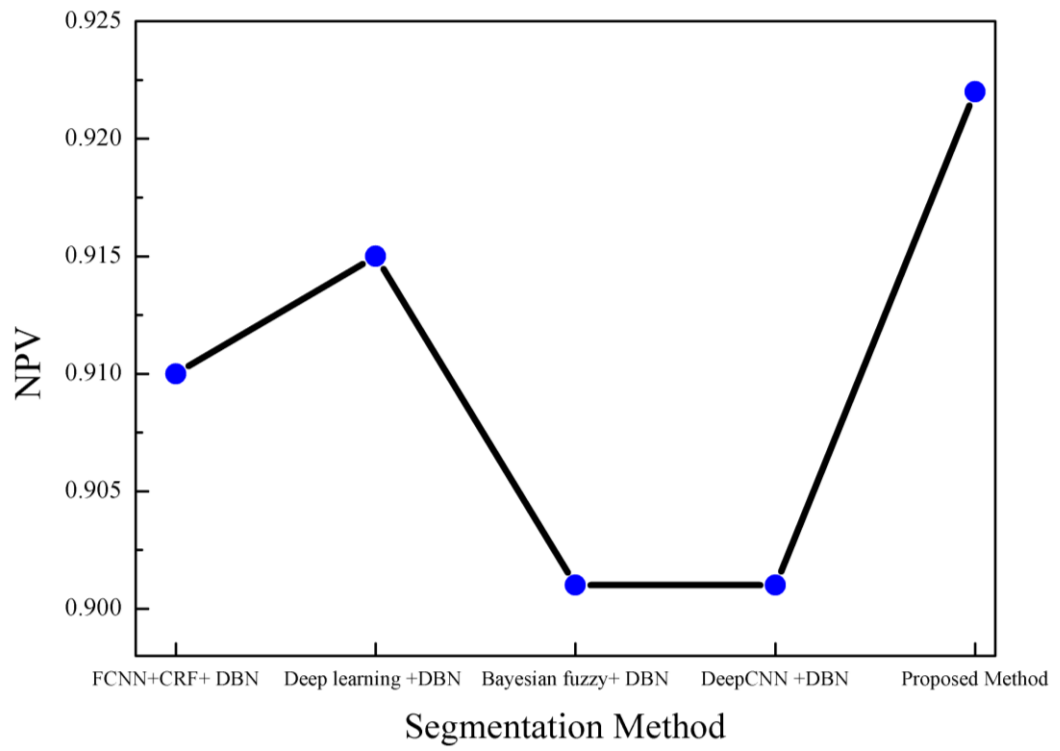
Figure 3.6: Analysis of evaluation metrics with respect to training data (a) Accuracy, (b) NPV, (c) PPV, (d) TNR, (e) TPR

(b) Analysis based on K-value

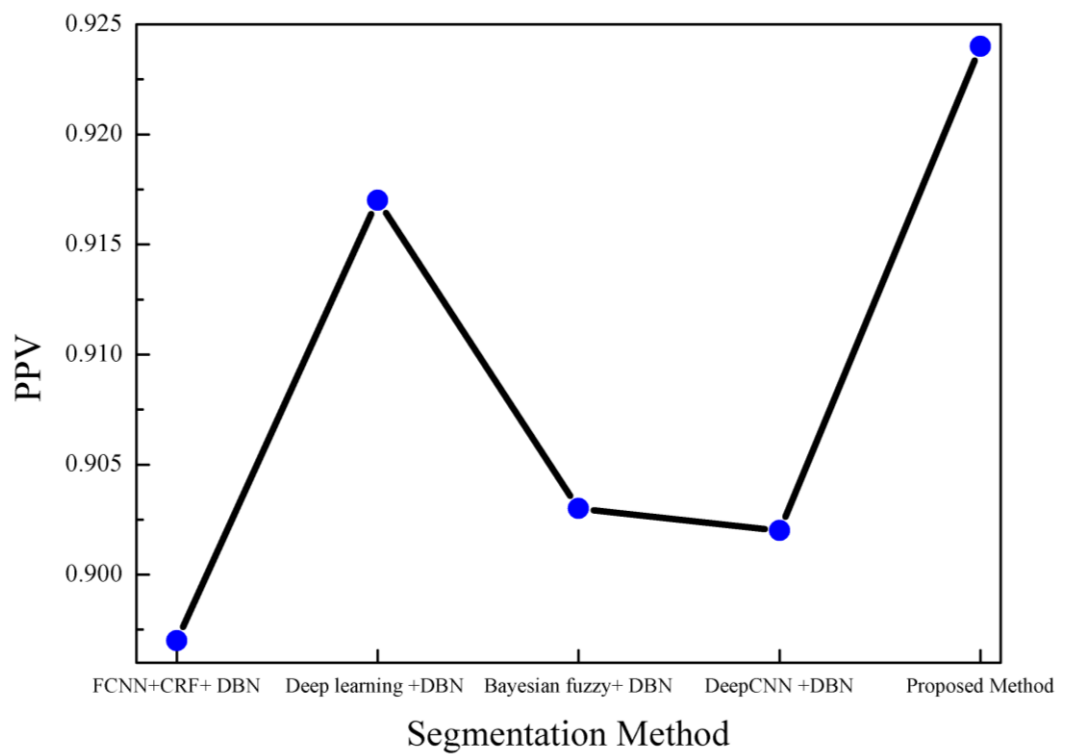
Figure 3.7 (a) shows the accuracy graph of AdamSWO-DCNN. When the k-value is 9, then the AdamSWO-DCNN attained the accuracy of 92.6%, and the FCNN+CRF [50], Deep learning [51], Bayesian fuzzy [62] and DeepCNN [54] got the accuracy of 91.3%, 91%, 90.5% and 90.4%. The NPV graph of AdamSWO-DCNN is shown in Figure 3.7 (b). When the k-value is 9, then the NPV achieved by the AdamSWO-DCNN and competitive methods are 92.2%, 91%, 91.5%, 90.1% and 90.1%. The PPV graph of AdamSWO-DCNN is exposed in Figure 3.7 (c). The PPV value of AdamSWO-DCNN and FCNN+CRF, Deep learning, Bayesian fuzzy, DeepCNN and techniques are 0.924, 0.897 0.917 0.903 and 0.902 respectively. Figure 3.7 (d) illustrates the TNR graph of AdamSWO-DCNN. When the k-value is 9, then the AdamSWO-DCNN attained the TNR of 92.8%, and the FCNN+CRF, Deep learning, Bayesian fuzzy and DeepCNN got 87.1%, 89.3%, 90.2% and 89.6%. The TPR graph for the AdamSWO-DCNN is given in Figure 3.7 (e). The TPR value achieved by the AdamSWO-DCNN is 92.9%, likewise, the TPR of traditional BT segmentation schemes are 91.6%, 89.7%, 91.1% and 89.4% for the k- value of 9.



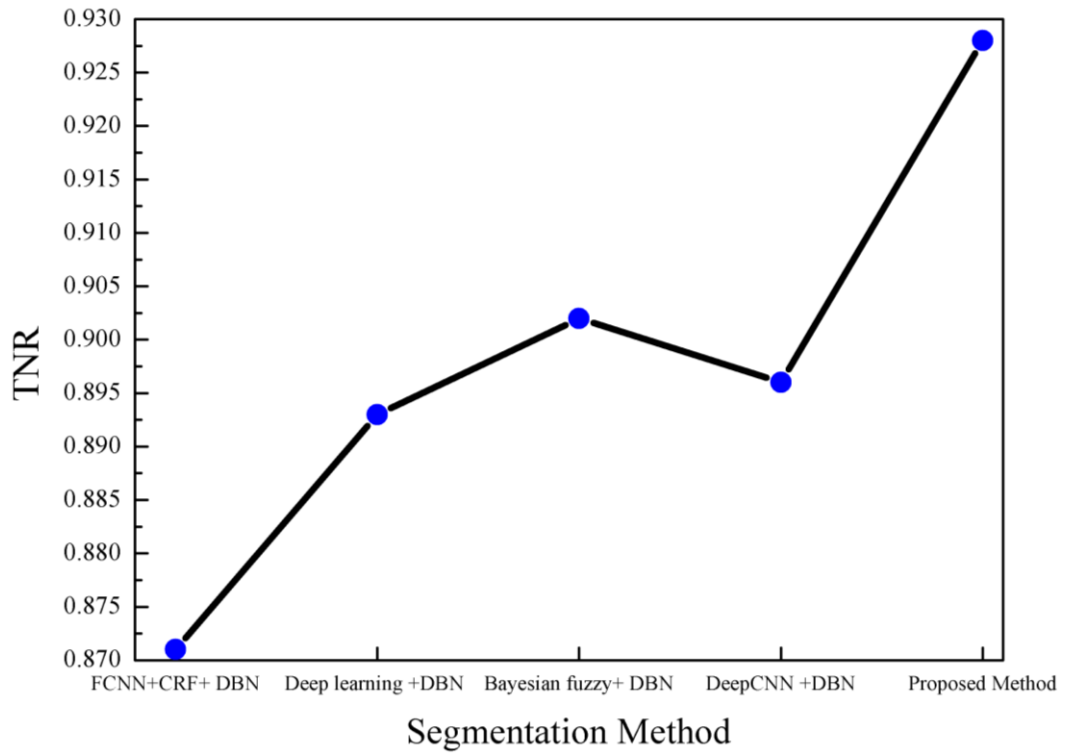
(a)



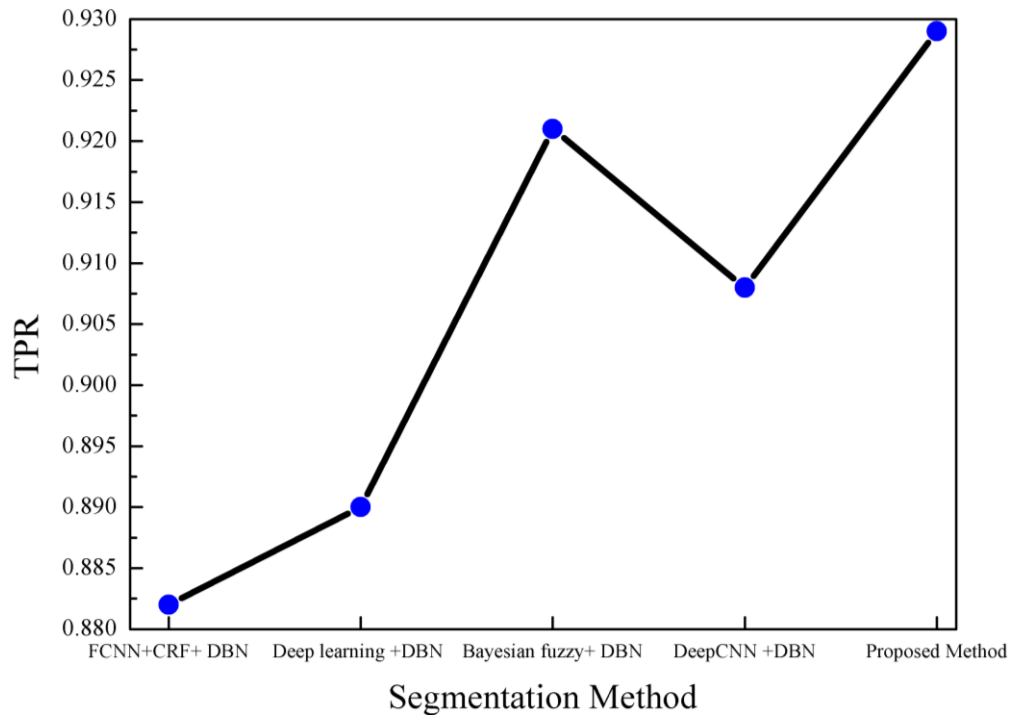
(b)



(c)



(d)



(e)

Figure 3.7: Analysis of evaluation metrics with respect to k-value a) Accuracy, (b) NPV, (c) PPV, (d) TNR, (e) TPR

3.4.4 Segmentation analysis

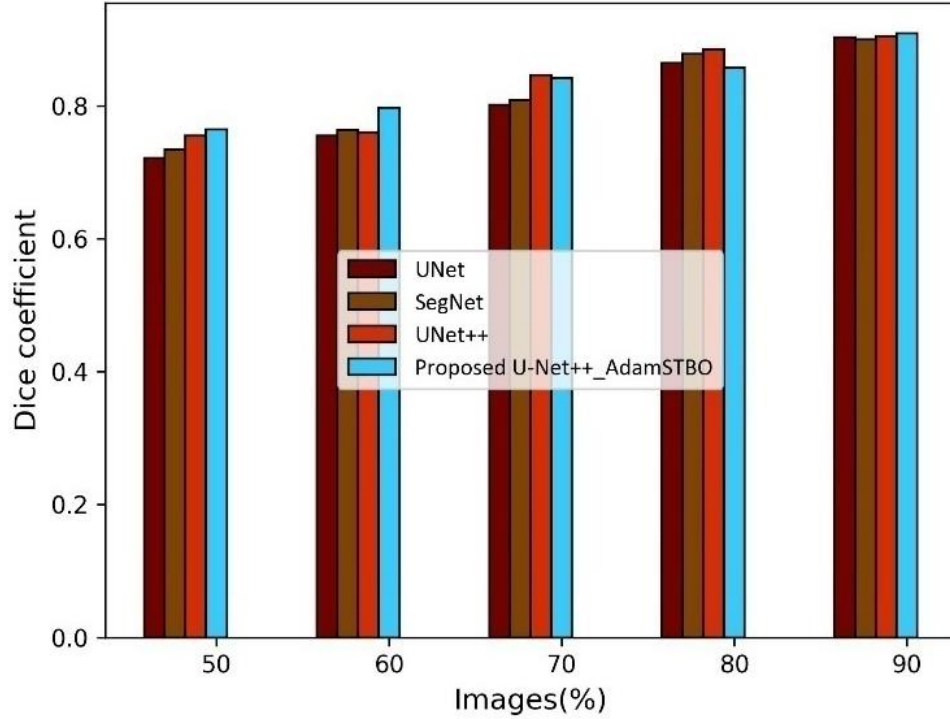


Figure 3.8: Analysis of segmentation based on dice coefficient

The segmentation analysis of AdamSTBO+UNet++ for BT segmentation and classification is performed in accordance with the dice coefficient and the images, and is given in Figure 3.8. The AdamSTBO+UNet++ attained the dice coefficient of 0.909 when the segmentation technique considers 90% of images for the experimentation. For the meantime, the dice coefficient of comparative segmentation methods, like UNet [100], SegNet [101] and UNet++ [93] got the dice coefficient of 0.903, 0.899 and 0.904.

3.4.5 Comparative discussion

The comparative discussion of BT segmentation and classification technique, namely AdamSWO-DCNN and AdamSTBO+UNet++ with respect to the evaluation metrics is clearly explained in this part. Here, the segmentation and classification performance are done by adjusting the training data and k-fold value. Based on the two analysis, AdamSWO-DCNN attained the higher performance than the comparative techniques. Here, the AdamSWO-DCNN attained the accuracy, NPV,

PPV, TNR and TPR of 0.928, 0.918, 0.925, 0.929 and 0.929. Moreover, the corresponding existing values are given in Table 3.1.

Table 3.1: Comparative discussion

| Variations | Metrics | FCNN+C RF+ DBN [50] | Deep learning +DBN [52] | Bayesian fuzzy+ DBN [62] | DeepCNN +DBN [54] | Proposed Method |
|------------------------------------|----------|---------------------------|-------------------------------|--------------------------------|----------------------|--------------------|
| For Training data = (90%) | Accuracy | 0.893 | 0.920 | 0.915 | 0.898 | 0.928 |
| | NPV | 0.890 | 0.912 | 0.911 | 0.895 | 0.918 |
| | PPV | 0.892 | 0.903 | 0.920 | 0.896 | 0.925 |
| | TNR | 0.896 | 0.920 | 0.907 | 0.925 | 0.929 |
| | TPR | 0.882 | 0.890 | 0.921 | 0.908 | 0.929 |
| K-fold value = (9) | Accuracy | 0.913 | 0.910 | 0.905 | 0.904 | 0.926 |
| | NPV | 0.910 | 0.915 | 0.901 | 0.901 | 0.922 |
| | PPV | 0.897 | 0.917 | 0.903 | 0.902 | 0.924 |
| | TNR | 0.871 | 0.893 | 0.902 | 0.896 | 0.928 |
| | TPR | 0.916 | 0.897 | 0.911 | 0.894 | 0.929 |

In Table 3.2, the segmentation result obtained by the AdamSTBO+UNet++ is exposed. Here, the AdamSTBO+UNet++ attained the dice coefficient of 0.909, and the existing techniques achieved the dice coefficient of 0.903, 0.899 and 0.904.

Table 3.2: Analysis of Segmentation technique

| Variation | Metrics | UNet [100] | SegNet [101] | UNet++ [93] | Proposed Method |
|-----------|---------------------|------------|-----------------|-------------|-----------------|
| Image% | Dice coefficient | 0.903 | 0.899 | 0.904 | 0.909 |

From the Table 3.1 and Table 3.2, the attained values of both AdamSTBO+UNet++ and AdamSWO-DCNN is higher than the existing techniques due to the efficacy of invented model.

3.5 Summary

This chapter presents the proposed AdamSWO-DCNN and AdamSTBO+UNet++ for BT segmentation and classification. Here, the BT segmentation is completed by the UNet++ model and its weight are tuned by the AdamSTBO algorithm. The AdamSTBO algorithm is the hybridization of Adam optimizer with the STBO algorithm. Likewise, the BT classification is done by the DCNN model in which its weight is modified by the AdamSWO algorithm for

attaining the improved classification performance. Furthermore, the AdamSWO algorithm is designed by modifying the SWO algorithm with the Adam Optimizer. Furthermore, SWO is designed by joining the merits of SSA and WWO algorithm. For further improving the classification accuracy, the AdamSWO-DCNN method extracts the more relevant features, such as CNN, LOOP, LGP, PHoG and GLCM.

Implementing and fine-tuning the proposed techniques require specialized knowledge in optimization algorithms, deep learning, and medical image analysis. Healthcare professionals without expertise in these areas may find it challenging to utilize or customize the techniques. Training deep learning models like UNet++ and DCNNs with optimization algorithms can be computationally intensive, requiring high-performance hardware resources. This may limit the accessibility of the techniques to institutions with adequate computational infrastructure.

CHAPTER

4

Optimizing Brain Health with ASO-DRN Technique for MRI based Brain Tumor Classification

4.1 Introduction

Brain Tumor (BT) is considered as the main organ of human body since it controls and coordinates all the functions of the body. Due to various reasons, sometimes the brain cells grow abnormally resulting in the formation of a tumor [102]. This unusual growth of abnormal cells affects the brain functions and thus the patient's health will be heavily deteriorated. An accurate segmentation of BT from the input image is an important task in cancer detection and its treatment. The manual segmentation of BT is laborious; hence the researchers are interested to invent automatic BT segmentation approaches. Various traditional BT segmentation techniques mainly concentrate on gliomas which are mainly occur in adults [103, 104].

This chapter proposes an Adaptive Salp swarm Optimization (ASO)-trained Deep Residual Network (DRN) for classifying brain tumor with MRI images. The utilization of Adaptive Salp Swarm Optimization (ASO) to train the Deep Residual Network (DRN) allows for adaptive tuning of the network parameters, potentially improving convergence speed and solution quality. This adaptive optimization approach enhances the robustness and effectiveness of the classification system. ASO dynamically adjusts the optimization process based on the current state of the training process, allowing for adaptive tuning of the network parameters. This enables the optimization algorithm to respond to changes in the optimization landscape, potentially improving convergence speed and solution quality. By adaptively tuning the network parameters during training, ASO helps the model to navigate complex optimization spaces more effectively, reducing the risk of getting

stuck in local optima. This enhanced robustness improves the model's ability to generalize well to unseen data and handle variations in the input distribution.

The adaptive optimization approach employed by ASO can enhance the generalization performance of the classification system by improving its ability to learn from diverse and complex datasets [105, 106]. This enables the model to generalize well to unseen data and handle variations in the input distribution, resulting in more robust and reliable classification performance across different scenarios [107, 108]. The proposed technique can be applied to various types of brain tumors detected through MRI imaging, making it a versatile tool for diagnosing different pathological conditions affecting the brain [109]. The versatility of the proposed technique in diagnosing various types of brain tumors detected through MRI imaging is a significant advantage [110]. Brain tumors can manifest in diverse forms, including gliomas, meningiomas, pituitary tumors, and metastatic tumors, among others. The proposed technique's ability to classify different types of brain tumors ensures comprehensive coverage, enabling clinicians to accurately diagnose and differentiate between various pathological conditions affecting the brain [111].

The technique's versatility allows it to be tailored to different clinical applications, enhancing its utility and effectiveness [112, 113]. MRI imaging is often complemented by other imaging modalities such as computed tomography (CT) [114, 115], positron emission tomography (PET) [116], and functional MRI (fMRI). The proposed technique's versatility extends to its integration with multimodal imaging data, enabling comprehensive analysis and diagnosis of brain tumors across multiple imaging modalities [117].

This chapter is having following key benefits:

- (i) ASO-DRN technique is proposed for segmentation and classification of MRI images for identifying the brain cancer. This method is different because it uses a new technique called ASO to train a DRN classifier. This classifier is trained to spot cancer in the brain effectively.
- (ii) Proposed ASO is a special kind of optimization technique which providing more reliable diagnostic results. It is implemented by blending an adaptive concept

with the Salp Swarm Algorithm (SSA) and Deep Residual Network. This combination helps to make the training process more effective to identify the brain tumor area and segment it more precisely.

- (iii) The proposed technique reduces the reliance on manual diagnosis, which can be prone to errors and subjective interpretation. This automation streamlines the diagnostic process and enhances efficiency.

The chapter is arranged as, section 4.2 gives challengers of brain tumor detection, section 4.3 details the proposed work, the outcomes of the proposed work along with its discussion are discussed in section 4.4, and finally in section 4.5, the conclusion is elaborated.

4.2 Challenges

The list of the challenges while designing the BT segmentation and classification is as follows:

- (i) Brain tumors can exhibit diverse characteristics, including size, shape, and location. The ASO-DRN technique's adaptability allows it to effectively classify different types of brain tumors, ranging from benign to malignant, regardless of their specific features.
- (ii) As new imaging technologies emerge and our understanding of brain tumors evolves, the proposed techniques can be scaled and adapted to incorporate advancements in medical imaging and machine learning. This scalability ensures that the techniques remain relevant and applicable in the face of evolving clinical needs and technological developments.
- (iii) MRI imaging protocols can vary between different healthcare institutions, imaging centres, and MRI machine manufacturers. These variations can include differences in imaging sequences, parameters, and acquisition techniques. The proposed techniques are versatile and can be adapted to different MRI imaging protocols, allowing them to be effectively utilized in diverse clinical settings without significant modifications.

4.3 Proposed ASO-DRN for brain tumor classification

This section shows the devised ASO-DRN for brain cancer classification from images of MRI. The developed ASO-DRN for classifying brain cancers is implemented through the following stages. Initially, the input MRI image is acquired from a database. The acquired image is then pre-processed using Gaussian filter [119] to remove unwanted noise from it further, brain tumor segmentation is performed on the pre-processed image using SegNet [81]. This segmentation process is adopted for segmenting the desired brain part from the image. Then in the feature extraction phase, Convolutional neural network (CNN) features [47] and gray level co-occurrence matrix (GLCM) texture features [112] are extracted from the segmented image. The extracted features from the image are the finally fed to the DRN [120] classifier which is trained using the proposed ASO for brain tumor detection. The proposed ASO is devised using the SSA [73] and adaptive concept. The illustrative diagram of the proposed ASO-DRN for classifying tumors of brain is displayed in Figure 4.1.

4.3.1 Image acquisition

For brain tumor diagnosis, the MRI images will be acquired from a dataset. Here, the dataset used is denoted as ‘D’ which contains ‘n’ number of MRI images. The dataset ‘D’ can be expressed in the following representation.

$$D = \{I_1, I_2, \dots, I_m, \dots, I_n\} \quad (4.1)$$

wherein, I_m represents the m^{th} image which is regarded for tumor detection.

4.3.2 Pre-processing of image

The chosen image I_m considered for detection is pre-processed by the Gaussian filter [119] for removing noise from it. Gaussian filters work on the basis of Gaussian distribution which is more effective in smoothing images. The Gaussian distribution’s probability density function $P(I_m)$ is given below [45].

$$P(I_m) = \frac{1}{\sqrt{2\pi\xi^2}} e^{-\frac{(I_m - \mu)^2}{2\xi^2}} \quad (4.2)$$

where, ξ characterizes for standard deviation which measures the amount of smoothing to be done, μ denotes the mean value. The filtered image is symbolized as I_p .

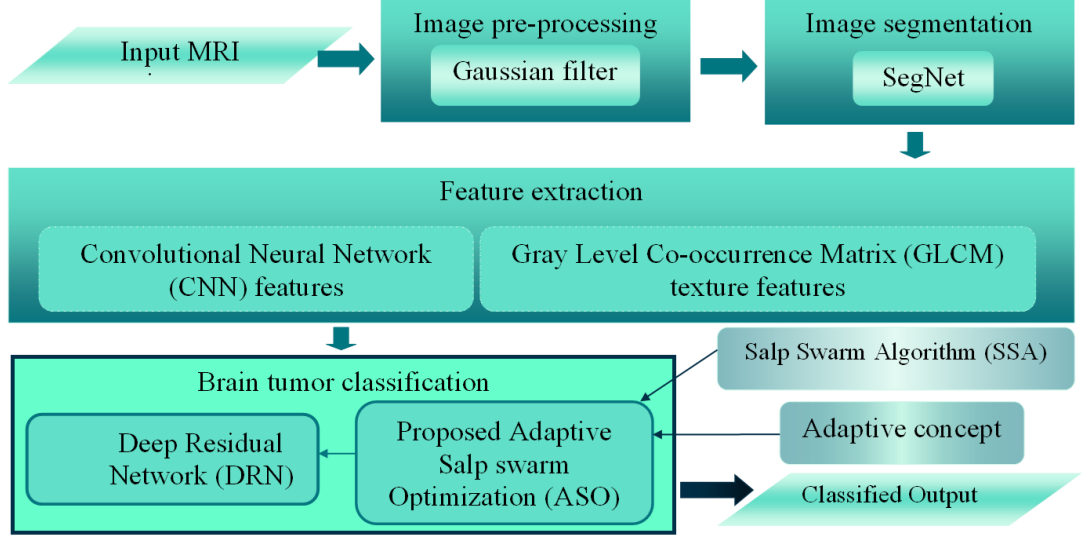


Figure 4.1: Illustrative diagram of the devised ASO-DRN for classifying brain tumors

4.3.3 Segmentation of image

The denoised I_p image is given to a segmentation model for segmenting the images. Here, segmentation is carried out by SegNet [81] which consists of an encoder and decoder setup with a pixel-wise classification layer. The encoder system is used for generating the feature maps, while the decoder system up samples the generated feature maps by utilizing the stored pooled indices.

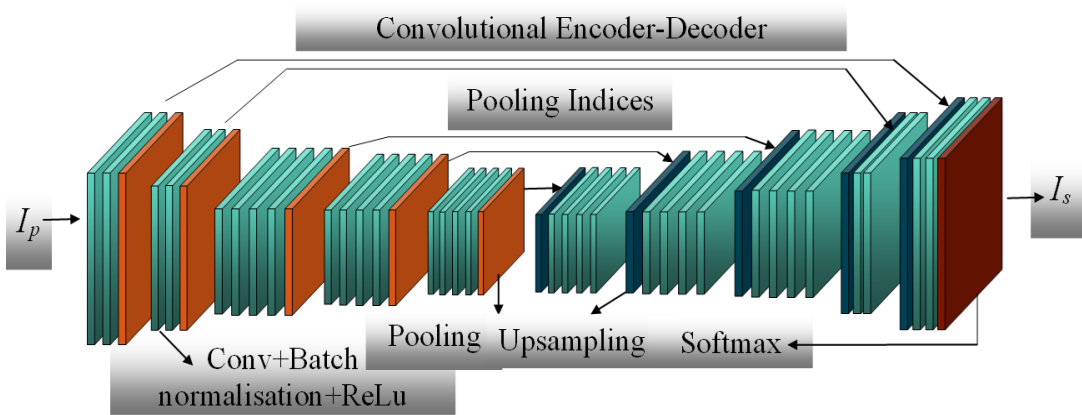


Figure 4.2: SegNet architecture

The output of the decoder system is finally passed to the soft-max classifier layer for producing pixel-wise class probabilities. SegNet is considered here because it

doesn't require resources with high computation. The architecture of SegNet is provided in the Figure 4.2. The resultant image obtained from the SegNet is called as segmented image, which is I_s .

4.3.4 Feature extraction

Here, the features will be excerpted from I_s . Mainly CNN and GLCM texture features are considered for extraction.

(a) Convolutional neural network (CNN) features

CNNs [47] are deep neural networks comprising of three different layers, such as Fully Connected (FC) layers, pooling layers, and convolutional layers. The convolutional layer present in the CNN architecture is dedicated to excerpt the features from I_s and the extracted CNN feature is termed as f_1 .

(b) Gray level co-occurrence matrix (GLCM) texture features

GLCM [121] is a proven statistical technique utilized for extracting textural features from various images. Here, four features namely Angular Second Moment (ASM), Inverse Difference Moment (IDM), correlation, and entropy are considered for extraction and they are denoted by the following notations f_4, f_5, f_3 , and f_2 respectively.

(c) Angular Second Moment (ASM)

ASM is also referred to as Uniformity. As the name indicates it measures the uniformity of the image texture. It is a measure of the sum of squares of normalized value $F(i, j)$ of the grey tone present at positions i and j of the kernel. It is given by equation 4.3 [62].

$$f_2 = \sum_{i=0}^{M-1} \sum_{j=0}^{M-1} F(i, j)^2 \quad (4.3)$$

where, f_2 denotes ASM and M is the number of grey tones in the kernel.

(d) Inverse Difference Moment (IDM)

IDM measures the local homogeneity present between two pixels in the image. It is denoted as f_3 and is calculated as follows [62].

$$f_3 = \sum_{i=0}^{M-1} \sum_{j=0}^{M-1} \frac{F(i, j)}{1 + (i - j)^2} \quad (4.4)$$

(e) Entropy

Entropy is the amount of randomness or disorder Ness present in the image. It is implied as f_4 and is formulated as,

$$f_4 = \sum_{i=0}^{M-1} \sum_{j=0}^{M-1} F(i, j) * \log(F(i, j)) \quad (4.5)$$

(f) Correlation

Correlation can be termed as a measure that measures the amount of likeliness between two pixels. It is represented as f_5 in the below equation.

$$f_5 = \sum_{i=0}^{M-1} \sum_{j=0}^{M-1} \frac{(i - \mu_i)(j - \mu_j)}{\sqrt{(\sigma_i)(\sigma_j)}} \quad (4.6)$$

wherein, μ_i and μ_j represents the mean of grey tones present at i^{th} and j^{th} position respectively; σ_j and σ_i refers to the standard deviation of the grey levels at j^{th} and i^{th} position correspondingly.

The feature vector F generated is shown below and this is further inputted to the brain tumor classification model.

$$F = \{f_1, f_2, f_3, f_4, f_5\} \quad (4.7)$$

4.3.5 Classification of brain tumor

The brain tumor classification is performed by the DRN [16] classifier network. The feature vector F acquired from the previous phase is given as an input to the DRN framework. By analyzing F , the classifier detects whether tumors are present in the brain or not. DRN framework is utilized here because it can overcome the gradient problem, produce results with high accuracy and make the training process faster. The architecture of DRN is provided in the subsequent part.

(a) DRN's architecture:

The DRN is made up of various layers, such as linear classifier, average pooling layers (AvgPool), residual blocks, and convolutional layers. These layers are briefly described below. DRNs architecture is provided in Figure 4.3.

(i) Convolutional Layer

The feature vector F is inputted to the convolutional layer. Here, a filter also called kernel is used to slide over the entire image both horizontally and vertically to produce feature map. This layer extracts features from the image by convolving the kernel with the image. The computation technique of Conv1d and Conv2d is given by equations 4.8 and 4.9.

$$Conv1d(F) = \sum_{q=0}^{o-1} H_q * F \quad (4.8)$$

$$Conv2d(F) = \sum_{pos1=0}^{p_1-1} \sum_{pos2=0}^{p_1-1} X_{pos1, pos2} \cdot F_{(xx+pos1), (yy+pos2)} \quad (4.9)$$

Herein, H_q implies the size of the kernel for q^{th} neuron; o implies the dimension of feature vector F ; X represents $p_1 \times p_1$ kernel matrix; $pos1$ and $pos2$ denotes the position in the matrix; and xx and yy records the coordinates in the 2D input.

(ii) Pooling layer

Following the convolutional layer, a pooling layer is present for decreasing the feature map dimensions obtained from the convolutional layer. This layer avoids overfitting occurring in neural networks. The equation of average pooling (AvgPool) is provided beneath.

$$\text{Width of the output 2D matrix, } out_{width} = \frac{in_{width} - ke_{width}}{ie} + 1 \quad (4.10)$$

$$\text{Height of the output 2D matrix, } out_{height} = \frac{in_{height} - ke_{height}}{ie} + 1 \quad (4.11)$$

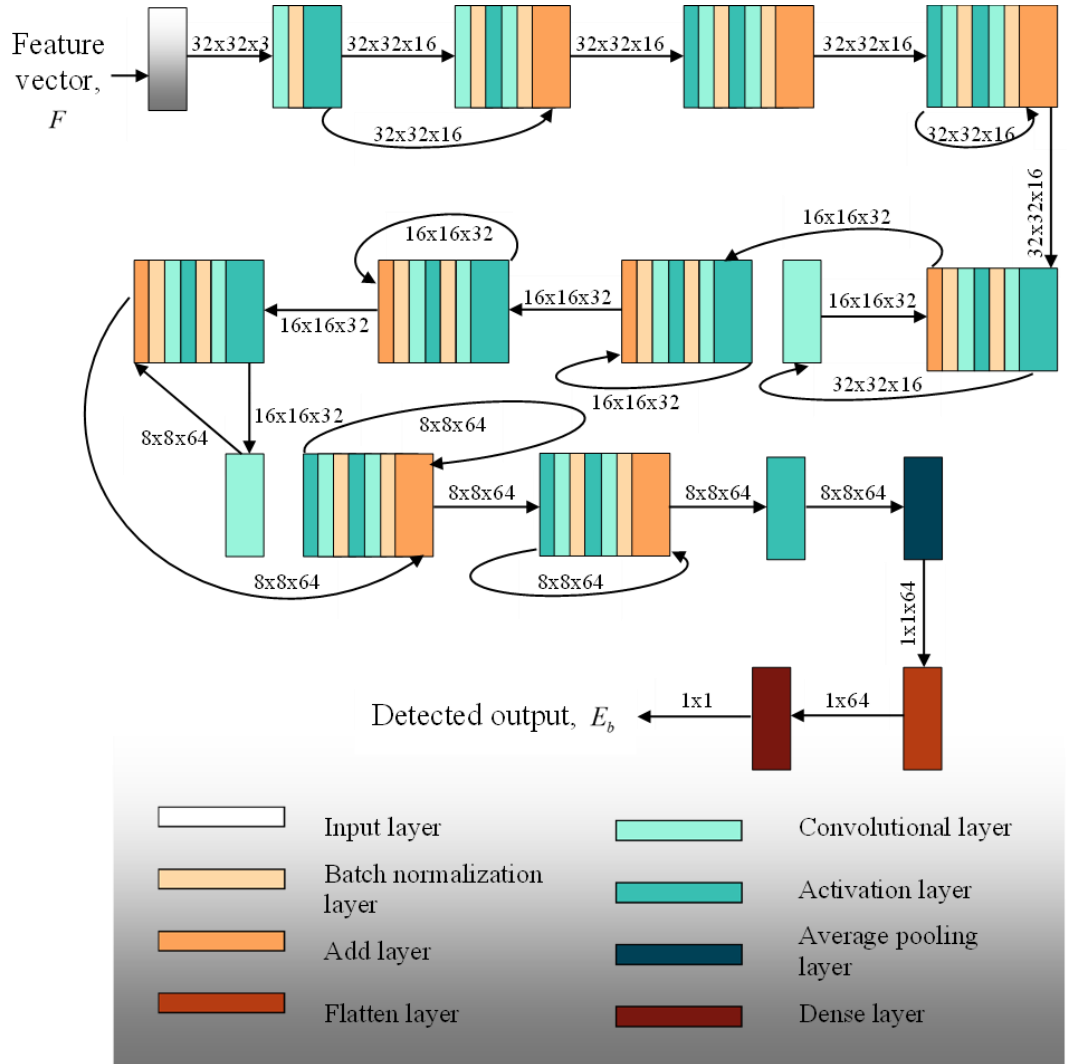


Figure 4.3: DRN architecture

The height of the input matrix is characterized as in_{height} , while the width is symbolized as in_{width} . The height and width of the kernel matrix is ke_{height} and ke_{width} .

(iii) Activation function

To achieve convergence faster, an activation function called Rectified Linear Unit (ReLU) is built after the convolutional layer. This ReLU increases the non-linearity associated with the features.

$$\text{ReLU}(F) = \begin{cases} 0, & \text{if } F < 0 \\ F, & \text{if } F \geq 0 \end{cases} \quad (4.12)$$

(iv) Batch normalization

This technique is basically used to divide the large learning data into small parts and the training the model on these divided parts to converge faster and reduce the complexity in computation.

(v) Residual block

Residual block skips one or two layers of the DRN network for accomplishing high accuracy by overcoming the degradation experienced by the network. It applies identity function to the output of any layer and passes the result to input of any layer by skipping some of the layers in between.

When the number of neurons contained in the output and input layer are same, then the output ‘out’ of the residual block is expressed in equation (4.13), which is

$$out = A(in) + in \quad (4.13)$$

In the above equation, in depicts the residual block’s input whereas the function $A(in)$ depicts the relationship of mapping between input and output.

On the other hand, when the output and input dimensions are different, a factor called ‘ c ’ is introduced in the above equation that gets multiplied with the input for making both the input and output dimensions same. It is shown below.

$$out = A(in) + (in * c) \quad (4.14)$$

(vi) Linear classifier

The linear classifier is employed to classify the results with the help of FC layer and Softmax function. The computation of FC is given by,

$$FC = WM_{Q \times C} F_{C \times T} + B_{Q \times T} \quad (4.15)$$

The computation of Softmax is given by,

$$\text{Softmax}(g_f) = \frac{e^{g_f}}{\sum_h^{\dim_{ot}} e^{g_h}}, f = 1, 2, \dots, \dim_{ot} \quad (4.16)$$

The weight matrix with $Q \times C$ dimension is denoted as $WM_{Q \times C}$, the feature map with $C \times T$ dimension is given as $F_{C \times T}$, and B acts as the bias. g_f acts as one of the

output layer elements and \dim_{ot} denotes the dimension of DRN's output E_b . The optimized weights and bias are computed by the devised ASO algorithm.

(b) ASO algorithm:

This algorithm is devised by combining adaptive concept and SSA [122]. The adaptive concept is incorporated into the SSA to adapt to the changes both in input and output. The SSA optimization technique is developed based on the inspiration gained from the swarming behavior of salps. To model the behavior of salp swarms mathematically, the population of salp is categorized into followers and leaders. The leaders lead the swarm whereas the followers follow the leaders. The mathematical model of SSA is detailed here.

(i) Initialization

Consider the population of salp as A which contains 'y' number of members is initiated initially. A is expressed as mentioned below.

$$A = \{A_1, A_2, \dots, A_x, \dots, A_y\} \quad (4.17)$$

Here, A_x is considered as the member at x^{th} position.

(ii) Fitness calculation

The fitness of every individual salp in the population is formulated on the basis of the Mean Squared Error (MSE) as given below.

$$MSE = \frac{1}{d} \sum_{b=1}^d (E_b^* - E_b)^2 \quad (4.18)$$

In the equation mentioned above, d denotes the number of samples considered for training, E_b^* implies the expected result and E_b denotes the actual output obtained by DRN.

(iii) Leader position updation

The leader's location is updated only based on the location of source of food. The location of the first leader " A_z^1 " in the z^{th} dimension is updated based on the value of r_l , which is considered a random variable.

When $r_3 \geq 0$, the position of the leader is given by,

$$A_z^1 = Y_z + r_1 ((up_z - low_z) r_2 + low_z) \quad (4.19)$$

When $r_3 < 0$, the leader position is updated as mentioned below,

$$A_z^1 = Y_z - r_1 ((up_z - low_z) r_2 + low_z) \quad (4.20)$$

Herein, Y_z is the food source's position in the z^{th} dimension; r_1 and r_2 are considered as random variables; low_z and up_z mentions the lower and upper bound of z^{th} dimension. r_2 is the most significant variable in SSA since it balances exploitation and exploration and is made adaptive by using the following formula.

$$r_2 = 4 - \left(\frac{curr_{it}}{2 * max_{it}} \right) * r_3; \quad (4.21)$$

where, $curr_{it}$ is the current iteration, the value of r_2 and r_3 lies in the range $[0 - 4]$, and $[0 - 1]$, respectively and max_{it} is the maximum number of iterations.

(iv) Update follower position

The v^{th} follower's position in u^{th} dimension, A_u^v is expressed by the below-mentioned equation,

$$A_u^v = \frac{1}{2} (A_u^v + A_u^{v-1}) \quad (4.22)$$

wherein, $v \geq 2$.

(v) Feasibility check

If the fitness of the updated position is found lower than the previously updated one, then the present updated position will be the newly updated position, else, the updated position in the previous iteration will serve as the new updated position.

(vi) Termination

The position will be updated until the maximum number of iterations is attained. The best optimal solution obtained is used as bias and weights in the DRN network.

Algorithm 4.1: Pseudocode of ASO algorithm

| |
|--|
| Initialize population of salp agents A with random positions as ‘y’ numbers. |
| Evaluate fitness of each salp agent using fitness function (MSE) equation (4.18) |
| Set initial parameters (e.g., step size, convergence criteria) |
| Repeat until convergence or maximum iterations reached: |
| For each salp agent: |
| Update ladder position based on adaptive step size and search strategy using equation (4.19) |
| Evaluate fitness of updated position using objective function using equation (4.20) |
| Update personal best position and fitness of salp agent if improved using equation (4.21) |
| Update global best position and fitness if improved using equation (4.22) |
| Update adaptive parameters based on performance of salp agents |
| End loop |
| End loop |
| Return global best position (optimized parameters) as solution |

4.4 Results and Discussion

The developed ASO-DRN [123] is examined by considering different evaluation metrics and its performance is compared with the prevailing tumor prediction strategies, and these are brought up in this division. Brain Tumor Segmentation (BraTS) 2018 [82] Challenge dataset is utilized to develop the model. This dataset provides multimodal 3D MRIs, such as FLAIR, T2, T1c, and T1 annotated by physicians [124].

4.4.1 Experimental results

The results obtained by experimenting the devised model is exhibited in Figure 4.4. The given input MRI image to the ASO-DRN is displayed in Figure 4.4 (a); the pre-processed image of the input is depicted in Figure 4.4 (b); and in Figure 4.4 (c) the segmented image is displayed.

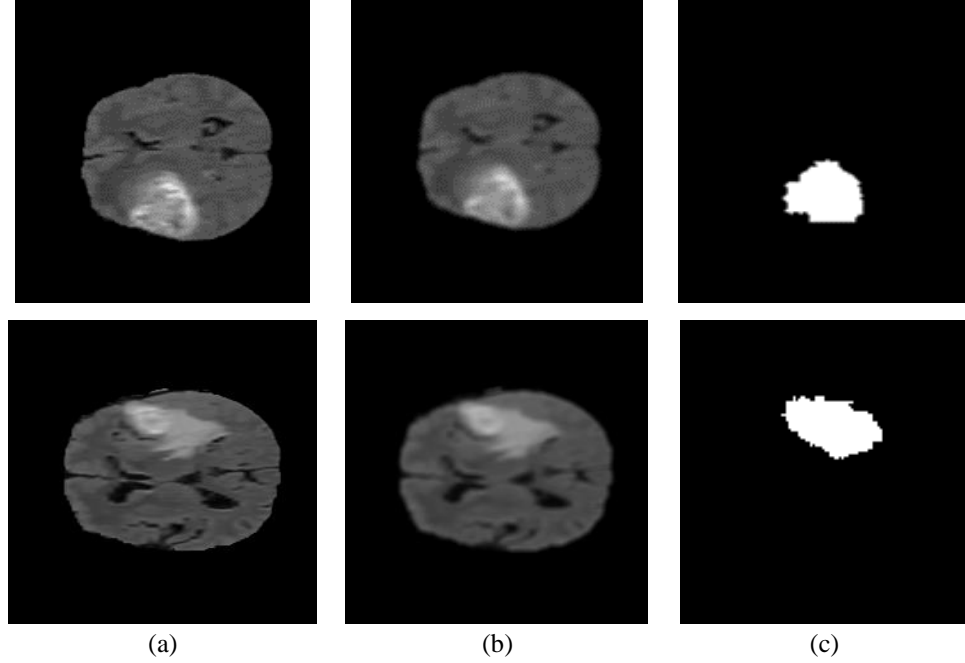


Figure 4.4: Image results showing (a) Input MRI image, (b) Pre-processed image, (c) Segmented image

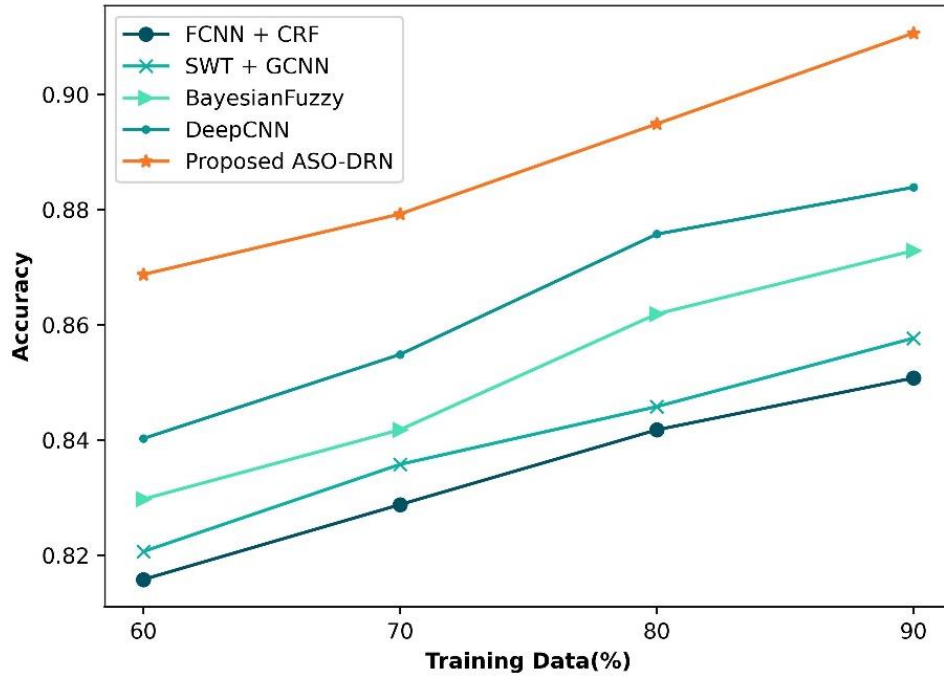
4.4.2 Comparative assessment

The developed technique's performance is evaluated based on TNR, TPR and accuracy. These metrics are already defined in chapter 2. The developed brain tumor detection model is compared with various techniques like FCNN+CRF [50], SWT+GCNN [105], BayesianFuzzy [62], and DeepCNN [54] in order to analyses its performance over them. This assessment deals with the performance comparison of various techniques for brain cancer classification with the proposed one based on k-value and training data.

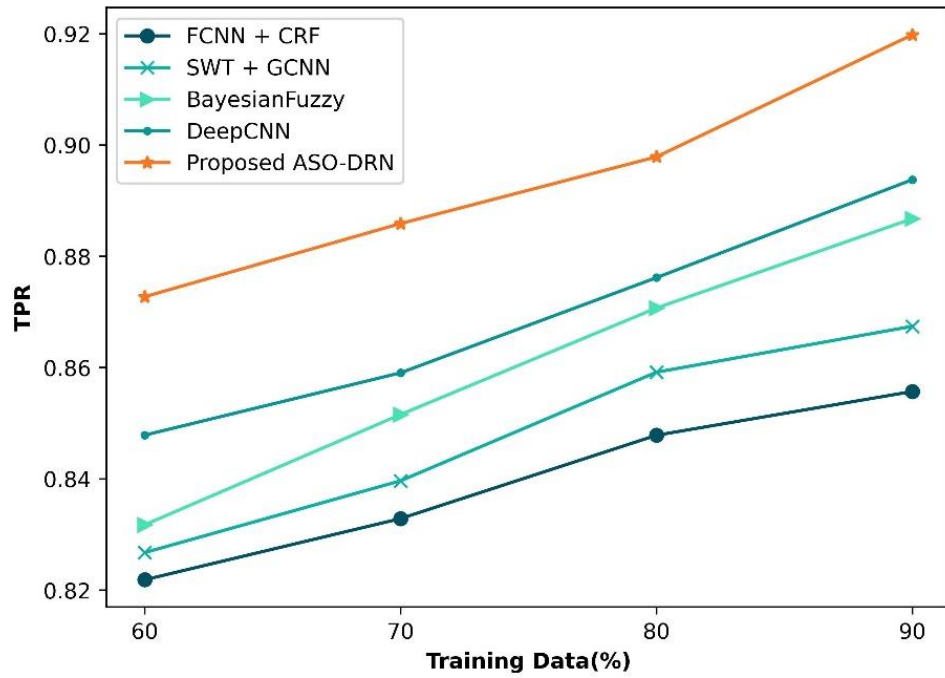
(a) Comparative investigation on training data

The performance of the proposed ASO-DRN is comparatively analysed here based on the training data and is depicted in the Figure 4.5. The Figure 4.5 (a) displays the accuracy assessment of the implemented ASO-DRN. When the training data is 90%, the obtained accuracy of the BayesianFuzzy, the implemented technique, SWT+GCNN, FCNN+CRF, and DeepCNN is 0.873, 0.911, 0.858, 0.851, and 0.884 respectively. The accuracy of the ASO-DRN is improved by 2.94% than the DeepCNN model. The analysis based on the value of TPR is given in Figure 4.5 (b). The TPR of the BayesianFuzzy is 0.887, SWT+GCNN is 0.867, DeepCNN is

0.894, FCNN+CRF is 0.856 and the devised ASO-DRN is 0.920 when the training data is 90%. The TPR of the ASO-DRN is enhanced by 3.59% than the BayesianFuzzy framework.



(a)



(b)

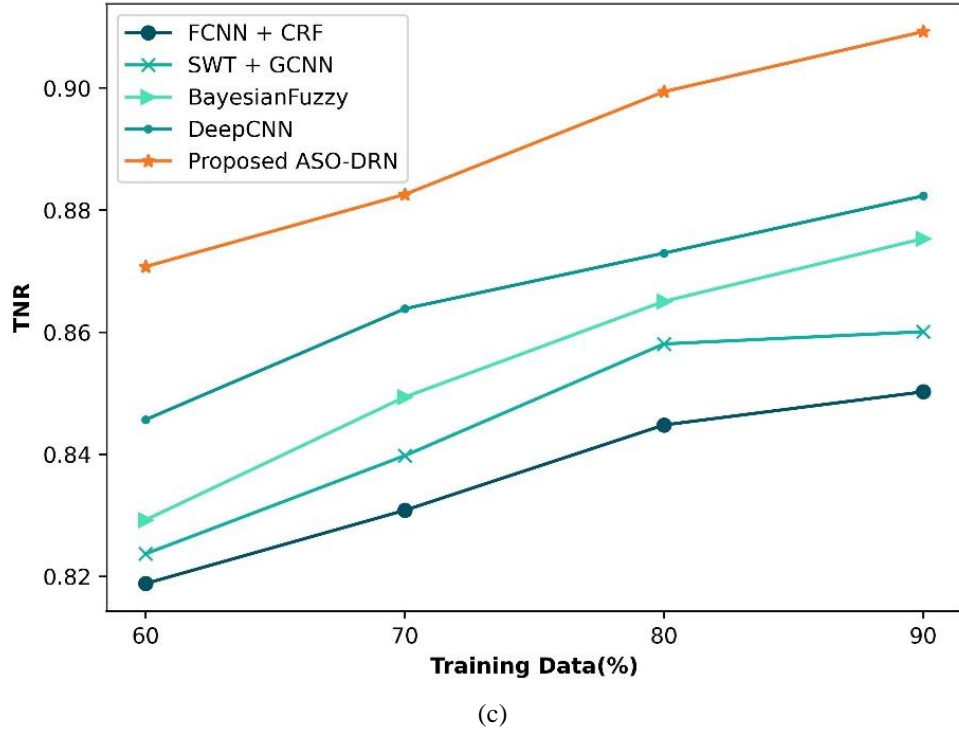


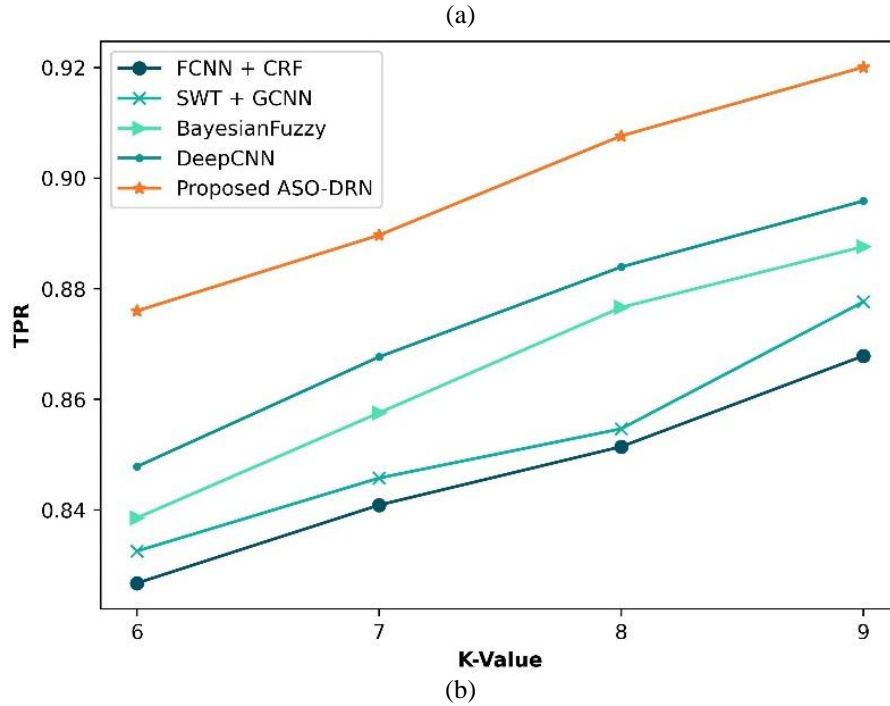
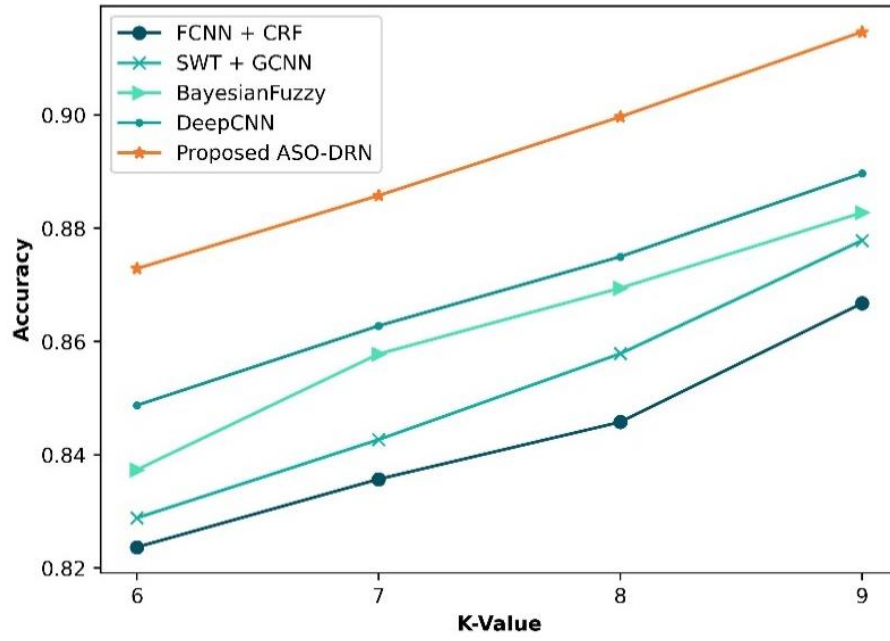
Figure 4.5: Comparative investigation of (a) accuracy, (b) TPR, and (c) TNR of the implemented ASO-DRN with other techniques on the basis of the training data

The analysis of TNR is depicted in Figure 4.5 (c). When the training data is 90%, the TNR of the BayesianFuzzy is 0.875, SWT+GCNN is 0.860, DeepCNN is 0.882, FCNN+CRF is 0.850, and the devised ASO-DRN is 0.909. The TNR of the ASO-DRN is improved by 6.49%, 5.41%, 3.73%, and 2.96% than the FCNN+CRF, SWT+GCNN, BayesianFuzzy, and DeepCNN model.

(b) Comparative assessment based on k-value

The proposed framework's performance is analyzed in comparison with other technologies on the basis of k-value in this analysis which is portrayed in Figure 4.6. The investigation of the implemented framework's accuracy is displayed in Figure 4.6 (a). When the k-value is 9, the accuracy obtained by the ASO-DRN, FCNN+CRF, SWT+GCNN, BayesianFuzzy, and DeepCNN is 0.915, 0.867, 0.878, 0.883, and 0.890 respectively. The accuracy of the ASO-DRN is enhanced by 5.24% than the FCNN+CRF scheme. The comparative investigation of TPR is shown in Figure 4.6 (b). The TPR of the DeepCNN is 0.896, FCNN+CRF is 0.868, BayesianFuzzy is 0.888, SWT+GCNN is 0.878, and the devised technique is 0.920 when k-value is 9. The TPR achieved by the ASO-DRN is found to be 4.61% better

than the SWT+GCNN scheme. The comparative analysis based on TNR is depicted in Figure 4.6 (c). When k-value is equal to 9, the corresponding TNR value of the SWT+ GCNN, FCNN+CRF, DeepCNN, BayesianFuzzy, and the proposed one are 0.873, 0.867, 0.896, 0.884, and 0.917. The value of TNR obtained by the ASO-DRN scheme is 5.46%, 4.87%, 3.61%, and 2.36% better than the existing FCNN+CRF, SWT+GCNN, BayesianFuzzy, and DeepCNN schemes.



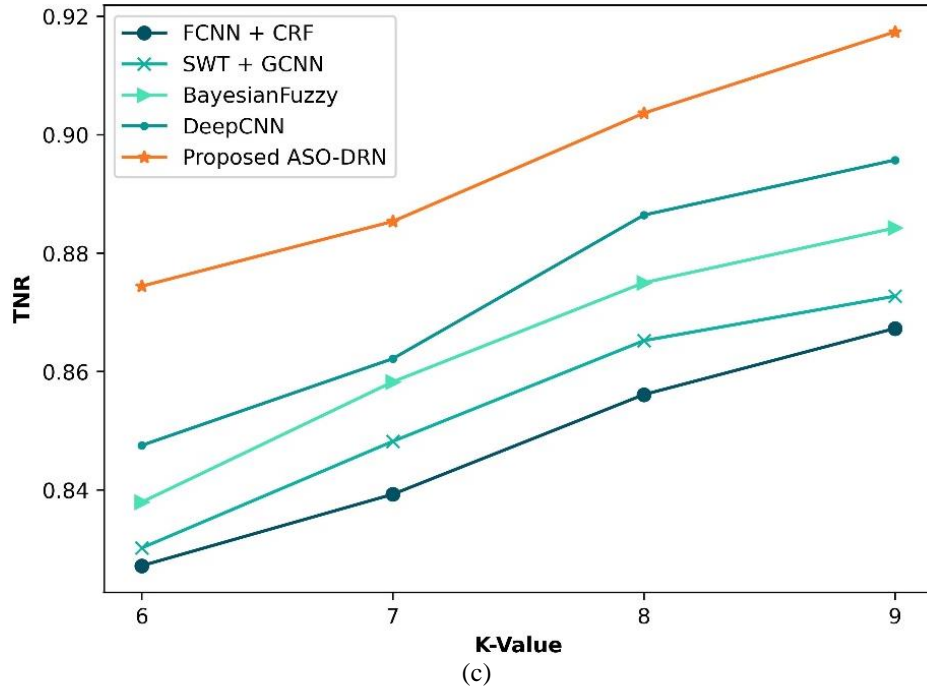


Figure 4.6: Analysis of (a) accuracy, (b) TPR, and (c) TNR of various techniques on the basis of k-value

4.4.3 Comparative discussion

The presented ASO-DRNs performance based on distinct validation metrics like TNR, accuracy, and TPR is comparatively discussed here with prevailing tumor detection schemes. Table 4.1 presents the comparison of the developed technique based on the k-value of 9 and training data of 90%. From the table, it is seen that high TPR, TNR, and accuracy achieved by the implemented ASO-DRN is 0.920, 0.917, and 0.915 correspondingly. Huge improvement in performance is seen in the proposed ASO-DRN framework because of the utilization of the novel ASO technique and application of DRN for classification.

Table 4.1: Comparative discussion of the proposed technique

| Variations | Metrics | FCNN+C RF+ DBN [50] | SWT+ GCNN [112] | Bayesian fuzzy+ DBN [62] | DeepCNN +DBN [54] | Proposed Method |
|------------------------------------|----------|---------------------------|-----------------------|--------------------------------|----------------------|--------------------|
| K-fold value = (9) | Accuracy | 0.867 | 0.878 | 0.883 | 0.890 | 0.915 |
| | TNR | 0.867 | 0.873 | 0.884 | 0.896 | 0.917 |
| | TPR | 0.868 | 0.878 | 0.888 | 0.896 | 0.920 |
| For Training data = (90%) | Accuracy | 0.851 | 0.858 | 0.873 | 0.884 | 0.911 |
| | TNR | 0.850 | 0.860 | 0.875 | 0.882 | 0.909 |
| | TPR | 0.856 | 0.867 | 0.887 | 0.894 | 0.920 |

4.5 Summary

In this chapter, a DRN model optimized with ASO algorithm is developed for classifying brain tumors at an earlier stage with the aid of images taken from MRI. The unwanted noise is removed from the images using Gaussian filter in the pre-processing phase and the segmentation is carried out by SegNet. Further, in the feature extraction module, GLCM and CNN features are determined. Based upon the extracted features, brain tumor classification is executed by the DRN model. The DRN classifier was tuned by the proposed ASO algorithm, which incorporates adaptive concept as well as the SSA technique.

Due to this improved performance, the proposed technique can be customized and fine-tuned to address specific diagnostic needs or clinical requirements. Whether detecting primary tumors, metastatic lesions, or monitoring treatment response. Implementing and fine-tuning deep learning models like DRN with optimization algorithms such as ASO may require specialized expertise in machine learning and medical image analysis. Healthcare professionals without this expertise may find it challenging to utilize or customize the technique. The performance of the technique depends heavily on the quality and quantity of the training data. The effectiveness of the classification may vary when applied to datasets with different characteristics or imaging conditions.

CHAPTER

5

Advancement in Clinical Diagnostics using Adaptive ASWO_Dbne Alexnet for Brain Tumor Technique

5.1 Introduction

In recent years, the most recognized, challengeable and time-consuming task in clinical image processing applications is brain tumor classification. Magnetic Resonance Imaging (MRI) is a successful clinical diagnosing tool that deliver efficacious identification of unusual tissues [125]. Since dimension of the carcinoma in brain image is heterogeneous for diverse patients, it is very difficult to identify the brain tumor. Moreover, the minute details in the brain cannot be obtained due to various reasons, such as cluttered background and low illumination thereby, degrading the image quality [126]. To overcome such issues, novel Adaptive Adam Salp Water Optimization (Adaptive ASWO_DbneAlexnet) is proposed for brain tumor classification.

The technique utilizes U-Net++ [127] for precise segmentation of tumor-affected areas in brain MRI images. This ensures that only relevant regions are considered during the classification process, improving the accuracy of tumor classification. U-Net++ is well-known for its ability to accurately localize and segment objects of interest in medical images, including brain tumors in MRI scans. By precisely delineating tumor-affected areas [128], U-Net++ ensures that only relevant regions are considered during the subsequent classification process, reducing the risk of false positives and improving overall accuracy. Precise segmentation with U-Net++ helps reduce false positives by accurately delineating tumor boundaries and excluding non-tumor regions from consideration during the classification process [129, 130]. This improves the specificity of the classification model, leading to more reliable and clinically relevant results. The Adaptive ASWO optimizer, derived from Adam optimizer and Salp Water Optimization (SWO), allows for adaptive tuning of the

DbneAlexnet model. This adaptive optimization approach enhances the robustness and convergence speed of the model, leading to improved classification performance.

The benefaction of this chapter is highlighted as follows:

- **Proposed Adaptive ASWO_DbneAlexnet:** A potent system is built to classify the brain tumor using DbneAlexnet and fine tuning of this efficient classifier model is carried out based on hybrid optimization, referred as Adaptive ASWO.
- **Proposed Adaptive ASWO:** The Adaptive ASWO algorithm is developed by integrating the Adam optimizer and SWO with adaptive concept. SWO is developed by integrating SSA and WWO.

The chapter is arranged as follows: the section 5.2 describes the challenges for classifying the tumor based on assessment of traditional techniques, and the proposed model along with the structural overview of network and its algorithmic procedure is given in 5.3 section. The results are discussed in 5.4 section, and the conclusion is given in 5.5.

5.2 Challenges

Some of the highlighted issues experienced in the previous works are enlisted as follows:

- (i) Imbalanced training data problem was solved partially by FCNN-CRF model. Moreover, the approach failed to construct fully 3D network as it highly enhances the performance of tumor segmentation.
- (ii) The SWT + GCNN model designed in did not degrade the image quality but, utilization of limited number of datasets is a major issue.
- (iii) Accurate segmentation of brain glioma employing MRI is extremely important in medical diagnosis and effective decision making for personalized treatment. However, abundant rough data generated by MRI blocks accurate segmentation in a limited span. Hence, automatic or semi-automatic segmentation model is necessary.

5.3 Proposed adaptive ASWO_Dbnealexnet for brain tumor classification

The major motto of this investigation is to propose an effective model named Adaptive ASWO_DbneAlexnet for brain tumor categorization. Initially MRI image acquired from specific data set illustrated in [96] is considered as the input and this MRI image is preprocessed to eradicate the artifacts present in the image by using ABF [131] at pre-processing module. Here, U-Net++ is employed to segment the pre-processed image which will improve the segmentation quality of the varying-size objects at the segmentation module. Moreover, the feature extraction is carried out from segmented image to refine the appropriate features, like convolutional neural network (CNN) features [95], LOOP [96] and gray level co-occurrence matrix (GLCM) [112]. Lastly, Brain tumor classification is accomplished using DbneAlexnet [132], which is trained by Adaptive ASWO. However, Adaptive ASWO is achieved by the combination of Adam algorithm [133] with Salp Water Optimization (SWO) and Adaptive concept. Moreover, SWO is the unification Salp Swarm Algorithm (SSA) [122] and the Water Wave Optimization (WWO). Figure 5.1 represents the pictorial view of Adaptive ASWO_DbneAlexnet for brain tumor classification.

5.3.1 Acquisition of input MRI

Assume the brain tumor dataset as B illustrated in [82] with q count of samples and the expression for this dataset is stated as follows,

$$B = \{ I_1, I_2, I_3, \dots, I_p, \dots, I_q \} \quad (5.1)$$

Here, I_p refers p^{th} MRI sample and all over count of samples in B^{th} repository is set as I_q .

5.3.2 Adaptive bilateral filter-based pre-processing

The I_p is applied over ABF, which accomplishes pre-processing step to extent the image quality by reducing unwanted distortions. The ABF technique [134] is highly

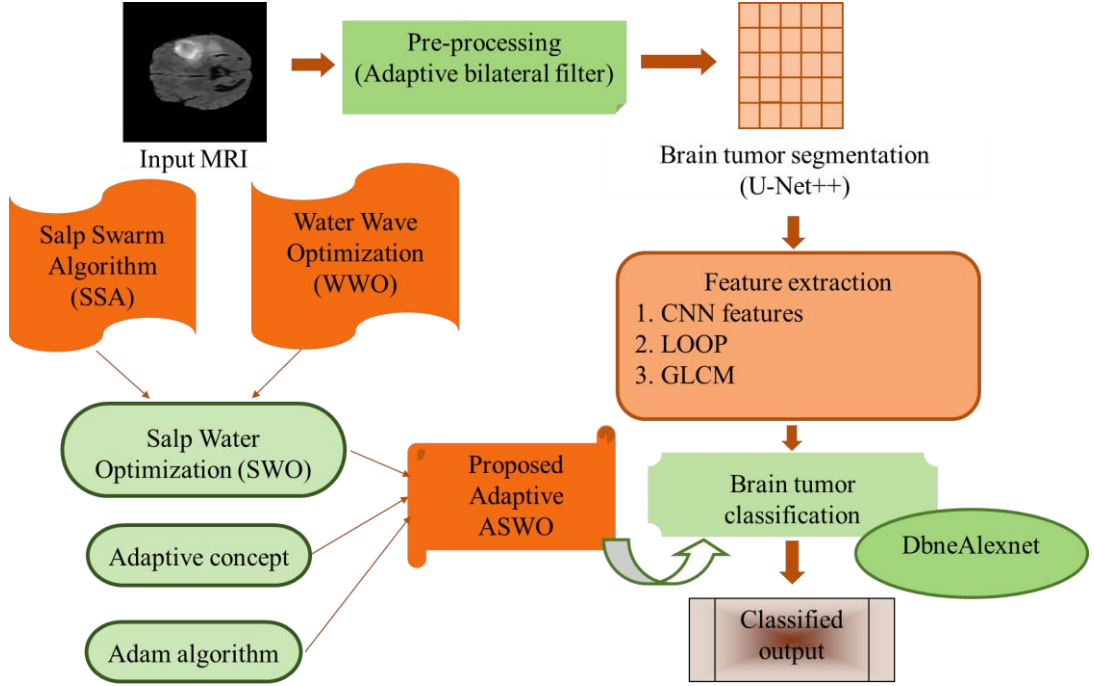


Figure 5.1: Diagrammatic illustration of proposed Adaptive ASWO_DbneAlexnet for brain tumor classification

capable to smooth out the noise while improving textures and edges in the image. The restored images by ABF are sharper than that of bilinear filter [135]. The expression for ABF is given by,

$$\hat{h}[U_0, V_0; U, V] = \left\{ \mathfrak{R}_{U_0, V_0}^{-1} \exp \left(-\frac{(U - U_0)^2 + (V - V_0)^2}{2\sigma_d^2} \right) \exp \left(-\frac{(A[U, V] - A[U_0 - V_0] - \zeta[U_0, V_0])^2}{2\sigma_{\mathfrak{R}}^2} \right) \right\}, [U, V] \in \phi_{U_0, V_0} \quad (5.2)$$

Here, ζ is made as adaptive and $\sigma_{\mathfrak{R}}$ converts the bilateral filter into successful, which has the ability of sharpening and smoothing. The resultant of pre-processing is denoted as P_p .

5.3.3 Tumor segmentation using U-Net++

The pre-processed result P_p is fed into U-Net++, where the accurate region of presence of tumor is segmented effectively. The ultimate motive of U-Net++ [136] is to carry out the instance and semantic segmentation by reducing unknown structural depth with an effective combination of U-Nets [137] of different sizes. In fact, there

is no need for deep supervision. However, t promoted the model pruning resulting in a speedup with minimum flop in performance.

(a) Network connectivity:

Let us assume the outcome of node $Y^{m,n}$ as $y^{m,n}$ in which m denotes down-sampling layer with encoder and n signifies conv layer of dense component with skip connection [138]. The arrangement of feature maps is expressed by $y^{m,n}$ is defined as follows,

$$y^{m,n} = \begin{cases} H\left(D\left(y^{m-1,n}\right)\right), & n = 0 \\ H\left(\left[y^{m,a}\right]_{a=0}^{n-1}, \Xi\left(y^{m+1,n-1}\right)\right), & n > 0 \end{cases} \quad (5.3)$$

Here, $H(\cdot)$ is a convolution mechanism succeeded by an activation parameter. Here, up-sampling and down-sampling layer are respectively symbolized as $\Xi(\cdot)$ and $D(\cdot)$. Moreover, the concatenation layer is expressed as $[]$.

(b) Deep supervision

Here, a 1×1 convolution with c kernels is used succeeded by a sigmoid parameter to the results from nodes $Y^{0,1}, Y^{0,2}, Y^{0,3}$ and $Y^{0,4}$, such that c refers the count of classes found in the given dataset. In addition, hybrid segmentation loss is considered to have smooth gradient and also to handle the unevenness. The loss is mathematically calibrated as,

$$Loss(Y, \tau) = \frac{1}{N} \sum_{cc=1}^c \sum_{M=1}^N \left(b_{M,cc} \log_{\tau_{M,cc}} + \frac{2b_{\tau,cc} \tau_{M,cc}}{b_{M,cc}^2 + \tau_{M,cc}^2} \right) \quad (5.4)$$

Here, $b_{M,cc} \in Y$ and $\tau_{M,cc} \in \tau$ implies the target labels as well as the detected probabilities for class cc . N implies the count of pixels within single batch. The whole error factor is described as the weighted aggregation of hybrid loss from individual decoders.

(c) Model Pruning

Due to deep supervision, U-Net++ is implemented in two mechanisms, such as ensemble model and pruned mode. The former model collected and averaged the

segmentation outcomes from all branches, while in the latter mode segmentation outcome is chosen from single segmentation branch. The segmented output by U-Net++ is symbolized as S_p . Figure 5.2 signifies the architectural overview of U-Net++.

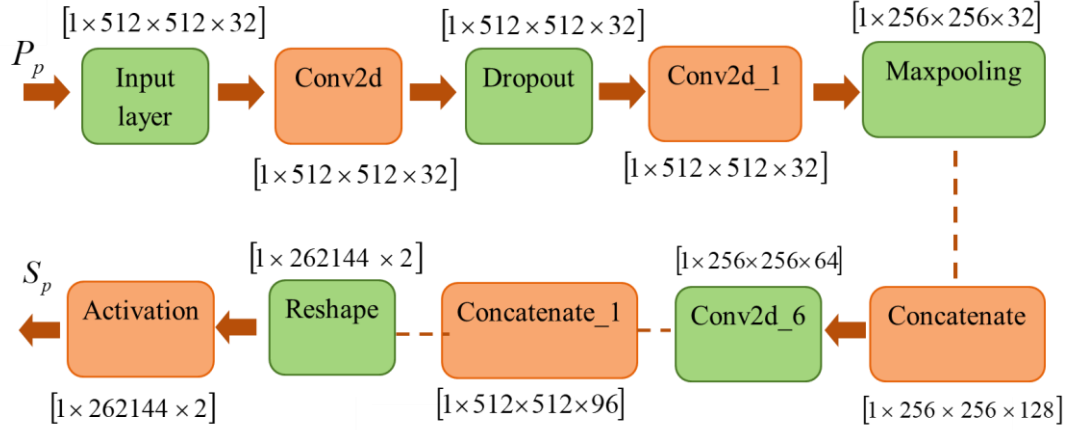


Figure 5.2: Overview of U-Net++

(d) Feature extraction

Feature extraction [139] serves an indispensable role in all image processing tasks as it effectively retains the appropriate feature for further classification process. The extracted features are described as follows,

(i) Convolutional neural network (CNN) features

The purpose of the conv layer [140] is to refine the features from image. It consists of multiple layers of conv kernels, each of which similar to its weight and deviation parameter.

(ii) LOOP

LOOP is the unification of Local Binary Pattern (LBP) [141] and Local Directional Pattern (LDP) [142] that counterparts the limitations faced while preserving the strength of an image. Let I_e be the image intensity I at pixel (u_e, v_e) and I_θ ($\theta = 0, 1, \dots, 7$) be the pixel intensity omitting the middle pixel I_e . The Kirsch masks are arranged in the movement of such eight neighborhood pixels as

$I_e (e=0,1,...,7)$. The Kirsch result is utilized to allocate the decimal-to-binary weightage. The LOOP descriptor is shown as follows,

$$LOOP(u_e, v_e) = \sum_{\theta=0}^7 C(I_\theta - I_e) \cdot 2^{w_\theta} \quad (5.5)$$

Here,

$$C(u) = \begin{cases} 1 & \text{if } u \geq 0 \\ 0 & \text{otherwise} \end{cases} \quad (5.6)$$

The LOOP is signified as F_2 .

(iii) Gray level co-occurrence matrix (GLCM)

Texture features can be easily obtained using GLCM features [143] and it is a matrix of how various groups of a pixel in grey levels present in an image. The extracted GLCM features are Angular Second Moment (ASM) [144], Inverse Difference Moment (IDM) [145], Entropy [146] and Correlation [147].

(e) Brain tumor classification using Adaptive ASWO_DbneAlexnet

The F_p is applied over classification step to categorize tumor into normal and abnormal conditions using DbneAlexnet. The classification process will help the clinical experts to determine the location, intensity, diameter and kind of tumor in a quick way [148]. Accurate classification of brain tumor assists the doctor to provide personalized treatments to the tumor affected patients.

(i) Architecture of DbneAlexnet

DbneAlexNet is an extended version of AlexNet mainly employed for accurate classification process. Here, two very small filters of (3×3) is employed. The purpose of utilizing this filter size is that it captures the picture from all rotations, such as top, bottom, left and right. An eLU activation layer is adopted and Unlike ReLU, eLU activation factor set up the activation mechanisms as it has the negative measures [149]. Another layer used in this structure is Batch Normalization (BatchNorm) layer that solves the internal covariate shift owing to changes of distribution of input. In order to regularize CNN models, dropout is used. This layer eliminates the unevenly chosen neurons while training. This degrades the involvement of such neurons while

doing front propagation and the weight upgrades will not be done on the neuron while performing retro-propagation. The architecture of DbneAlexnet is shown in Figure 5.3. The outcome of DbneAlexnet is signified as J_p .

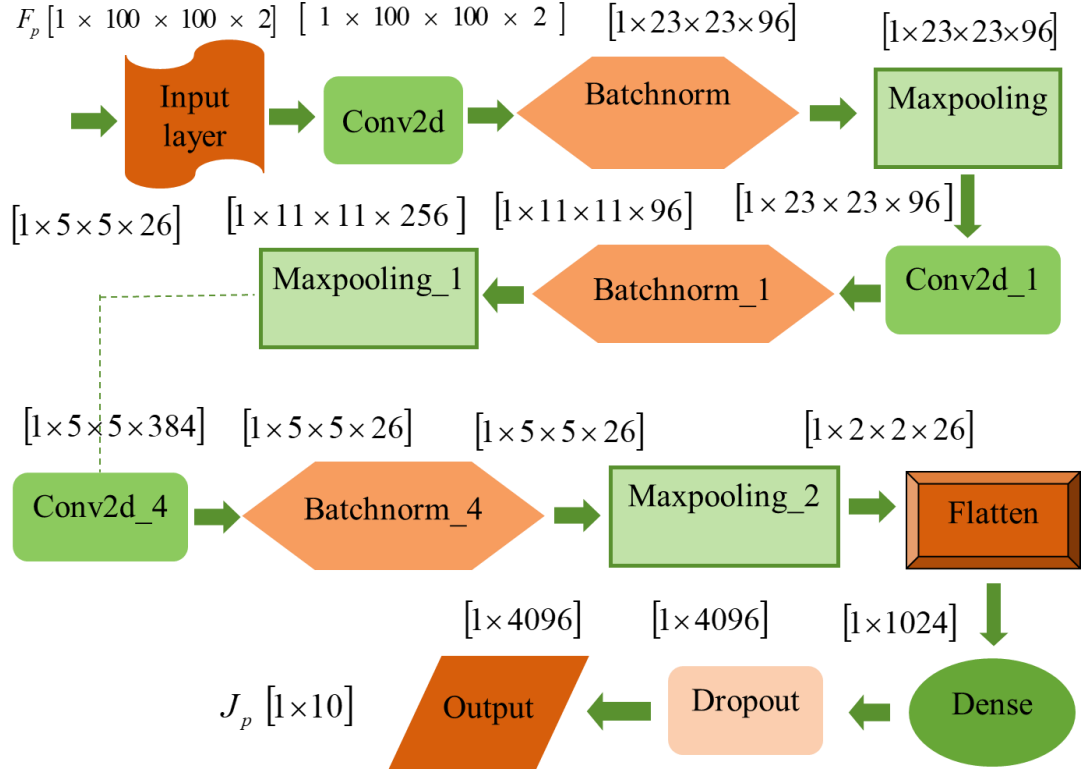


Figure 5.3: Architecture of DbneAlexnet

(ii) Fine tuning of DbneAlexnet using adaptive ASWO

The hyper parameter of DbneAlexnet is fine-tuned using designed Adaptive ASWO, which is the unification of Adaptive concept with Adam and SWO. However, SWO is achieved by incorporating SSA and WWO [150].

(a) Salp position encoding

To attain the suitable solution in a M - search area [151] and it is given by, $M = [1 \times \ell]$.

(b) Fitness function

It is termed as the variation among actual outcome and predicted outcome of classification, which is expressed as,

$$\mathfrak{J} = \frac{1}{q} \sum_{p=1}^q [TAR_p^* - J_p]^2 \quad (5.7)$$

(c) Algorithmic steps

SSA [123] is inspired from the swarming nature of salps when roaming and foraging in oceans. On the other hand, WWO [70] is an evolutionary algorithm that follows the wave-inspired operators, such as propagation, refraction and breaking. By incorporating these two algorithms with Adaptive concept can enhance the convergence speed and provides better classification accuracy without compromising the image quality [152].

Step 1: Initialize the salp population

The salp population is randomly initiated in a M - search space with bb samples and it is expressed as follows,

$$s = \{s_1, s_2, \dots, s_{aa}, \dots, s_{bb}\} \quad (5.8)$$

Here, s_{bb} denotes the overall Salp populations.

Step 2: Determine the fitness

To calculate the optimal solution for a precise classification task and it is generally calibrated by Eq. (5.7).

Step 3: Upgrade the location of leader Salp

The population is firstly partitioned into two groups, such as leader and follower. The salp at the front of the chain is considered as leader, whereas the remnant salps are declared as follower. As the name states, the leader guides the salp group and follower follows the leader. The leader salp's location is given in expression as,

$$s_h^1 = \begin{cases} M_h + r_1 ((UB_h - LB_h)r_2 + LB_h) & r_3 \geq 0 \\ M_h - r_1 ((UB_h - LB_h)r_2 + LB_h) & r_3 < 0 \end{cases} \quad (5.9)$$

Here, s_h^1 refers the location of initial salp in h^{th} dimension and food source in j^{th} size is stated as M_h . The upper and lower variable is defined as UB and LB , respectively. r_1, r_2 , and r_3 are uneven numbers. The coefficient r_1 is the significant factor in SSA and it is given by,

$$r_1 = 2e^{-\left(\frac{4t}{t_{\max}}\right)^2} \quad (5.10)$$

Step 4: Renew the follower salp's location

The follower salp's location is upgraded by incorporating the WWO equation with adaptive concept. The standard expression for follower salp is given by,

$$s_h^g = \frac{1}{2} (s_h^g + s_h^{g-1}) \quad (5.11)$$

The upgraded equation of adaptive SWO is defined below,

$$s_h^g(t+1) = s_h^g(t) - \text{Gaussian}(0,1) \alpha L_h \quad (5.12)$$

Here, α is made as adaptive,

$$\alpha = k_{\max} - \left(\frac{t}{t_{\max}} * \beta \right) rand \quad (5.13)$$

Here, k_{\max} refers the maximum wave height, present iteration is denoted as t and maximum iteration is specified as t_{\max} . Moreover, *rand* is a random number that lies in the range of $[-1, 1]$.

Step 5: Termination

The above-mentioned procedures are repeated over and over until it satisfies pre-defined condition and pseudo code of Adaptive ASWO is specified in Algorithm 5.1.

Algorithm 5.1: Algorithm for Adaptive ASWO

| |
|---|
| Initialize the salp population M - search space with bb samples |
| Calculate the fitness by equitation (5.7) |
| The location of leader salp given by equitation (5.9) |
| Upgrade r_1 (coefficient of upper and lower variable) using equitation (5.10) |
| for each salp (s_g) |
| If ($g = 1$) |
| Upgrade the leader salp's location by Eq. (5.9) |
| else |
| Upgrade follower salp's location by Eq. (5.12) |
| End if |
| End for |
| Revise the salps depending upon upper and lower bound variables |
| Return M |

5.4 Results and discussion

This segment discusses the outcomes of Adaptive ASWO_DbneAlexnet in regard of evaluation measures.

5.4.1 Experimental results

Figure 5.4 represents the experimental results of Adaptive ASWO_DbneAlexnet. Figure 5.4 (a) and (b) illustrates input and pre-processed image. Figure 5.4 (c) implies segmented outcomes, whereas LOOP is depicted in Figure 5.4 (d).

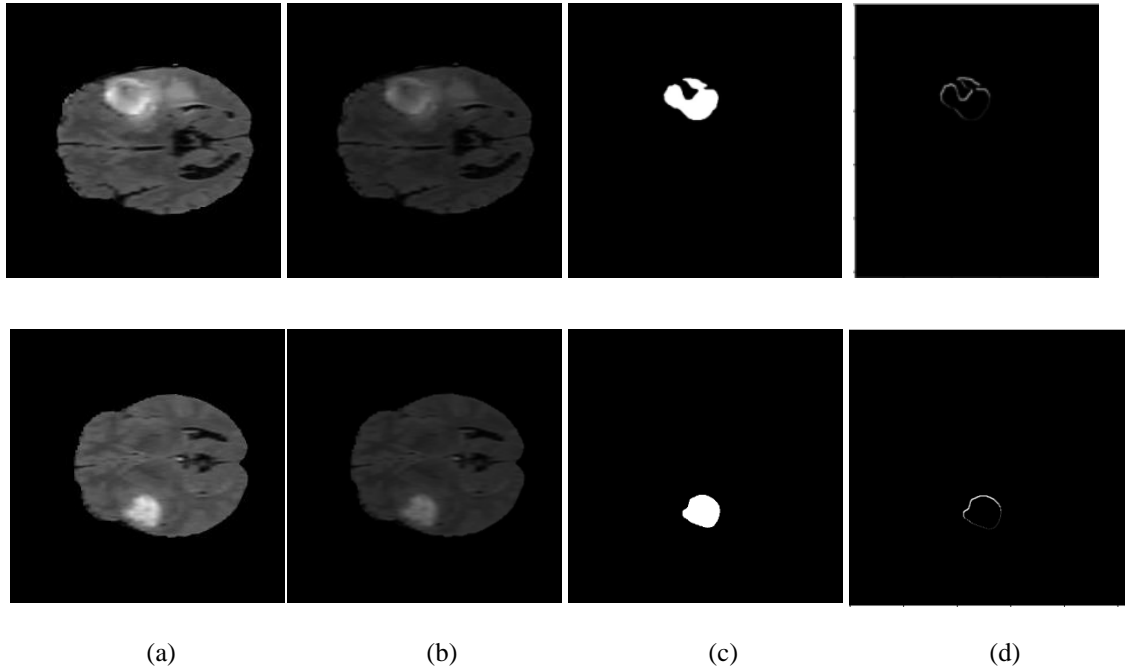


Figure 5.4: Experimental outcomes, (a) input image, (b) pre-processed result, (c) segmented outcome, (d) LOOP feature

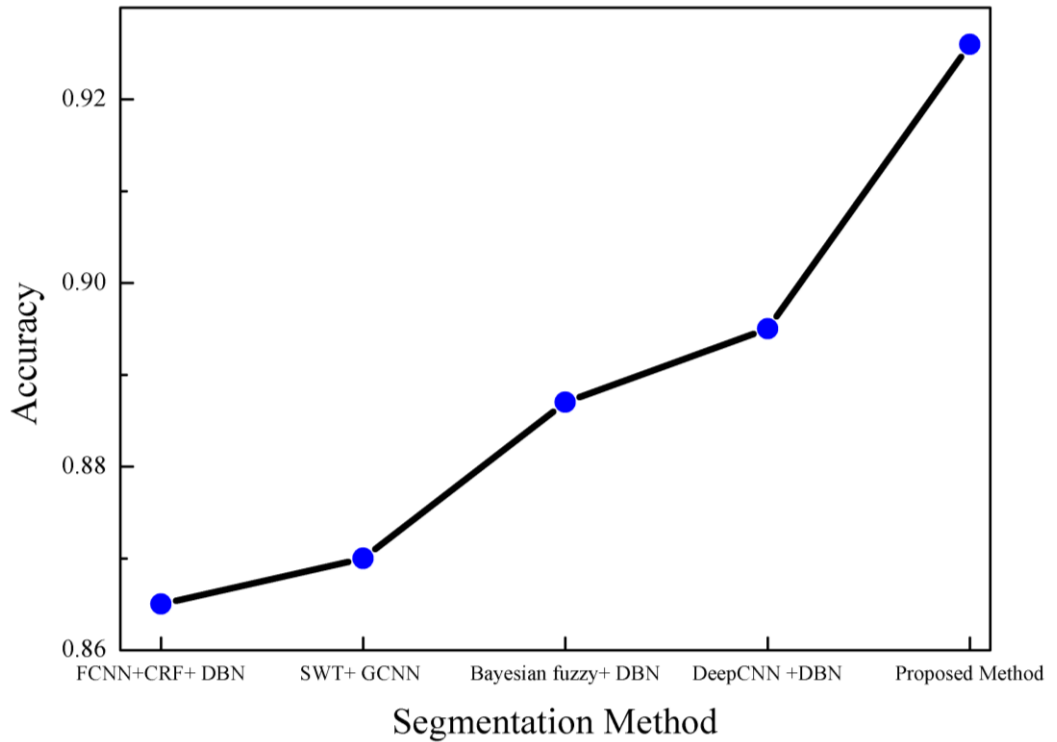
5.4.2 Comparative evaluation

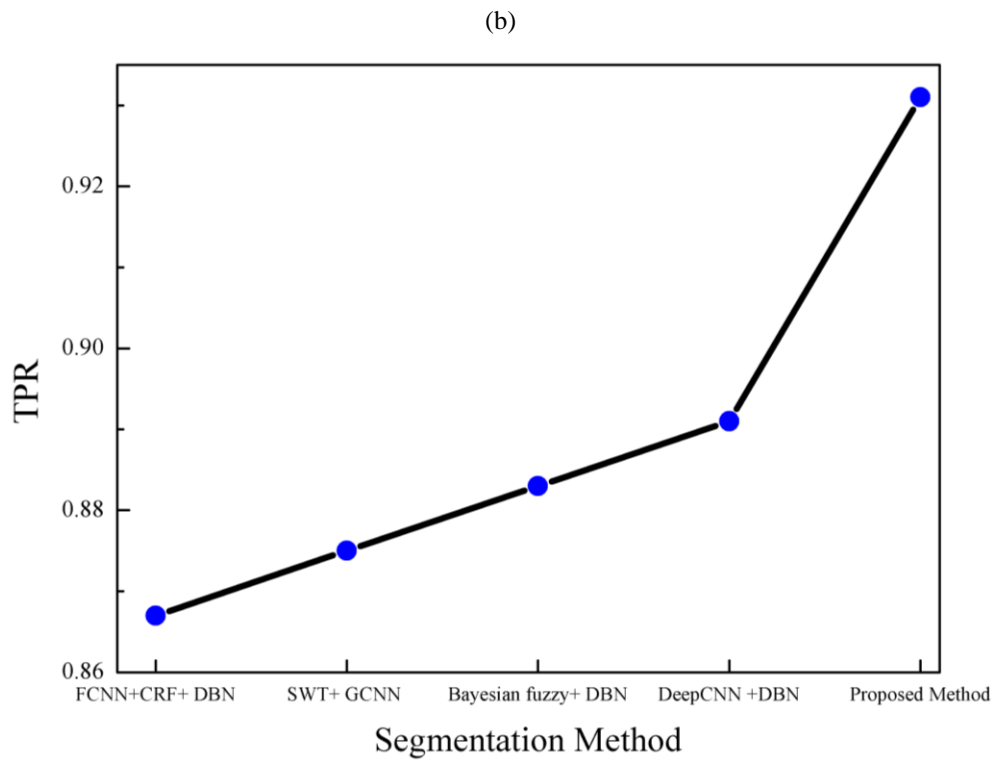
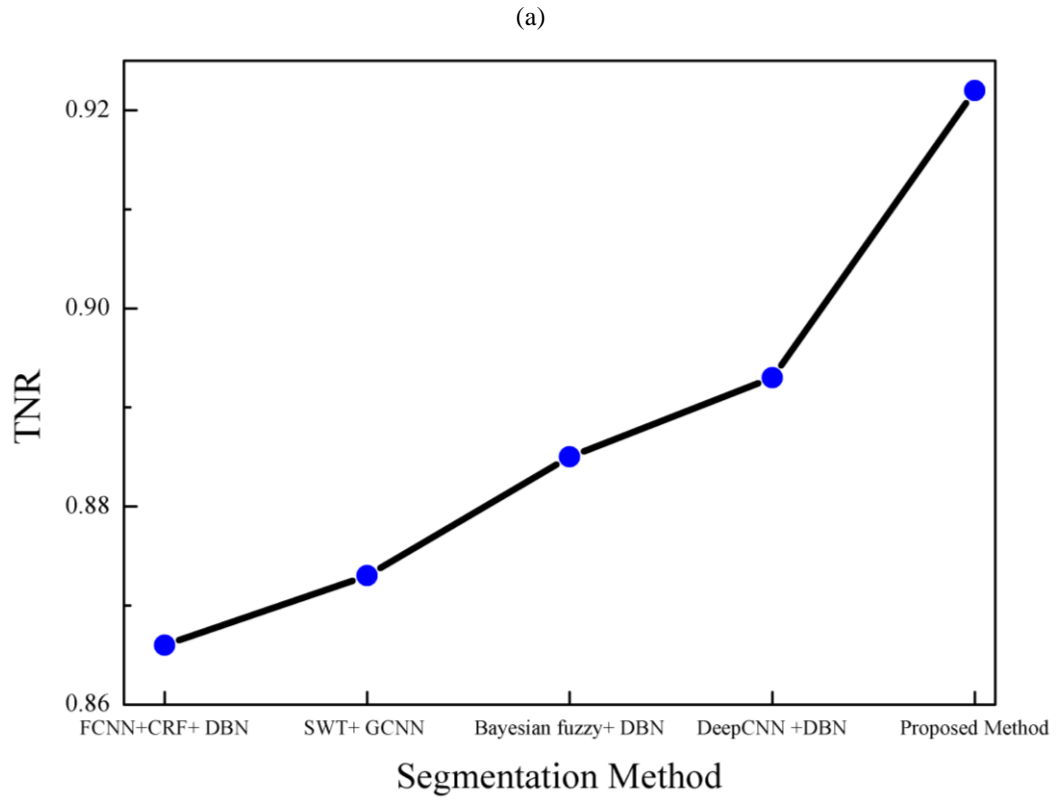
The performance metrics employed for assessment purpose are accuracy, TPR and TNR. These metrics are already defined in chapter 2. The performance of Adaptive ASWO_DbneAlexnet is assessed using the existing techniques, such as FCNN + CRF [50], SWT + GCNN [112], Bayesian fuzzy [62] and Deep CNN [54]. This segment delineates the estimation of Adaptive ASWO_DbneAlexnet with in regard of various estimation measures. Multimodal brain tumor segmentation

challenge (BRATS) 2018 [82] dataset will be provided with training, validation and testing data.

(a) Evaluation with training data

Figure 5.5 specifies estimation of adaptive ASWO_DbneAlexnet in terms of different evaluation indicators. Figure 5 (a) signifies the estimation of accuracy. If 90% data is considered, accuracy yielded by Adaptive ASWO_DbneAlexnet is 0.926 that reveals the gain of 6.5865 for FCNN + CRF, 5.997% for SWT + GCNN, 4.149 for bayesian fuzzy, 3.370% and for Deep CNN, 2.784%.. However, the traditional schemes obtained accuracy value of 0.865 for FCNN + CRF, 0.870 for SWT + GCNN, 0.887 for bayesian fuzzy, 0.895 for Deep CNN. Figure 5.5 (b) illustrates the estimation of adaptive ASWO_DbneAlexnet in regard of TPR. By considering the data=90%, TPR shown by designed technique is 0.931, whereas TNR gained by adaptive ASWO_DbneAlexnet is 0.922 illustrated in Figure 5.5 (c). Nonetheless, improvement resulted by designed model to that of former methodologies are 5.390, 4.041, 3.209 and 2.656 respectively.



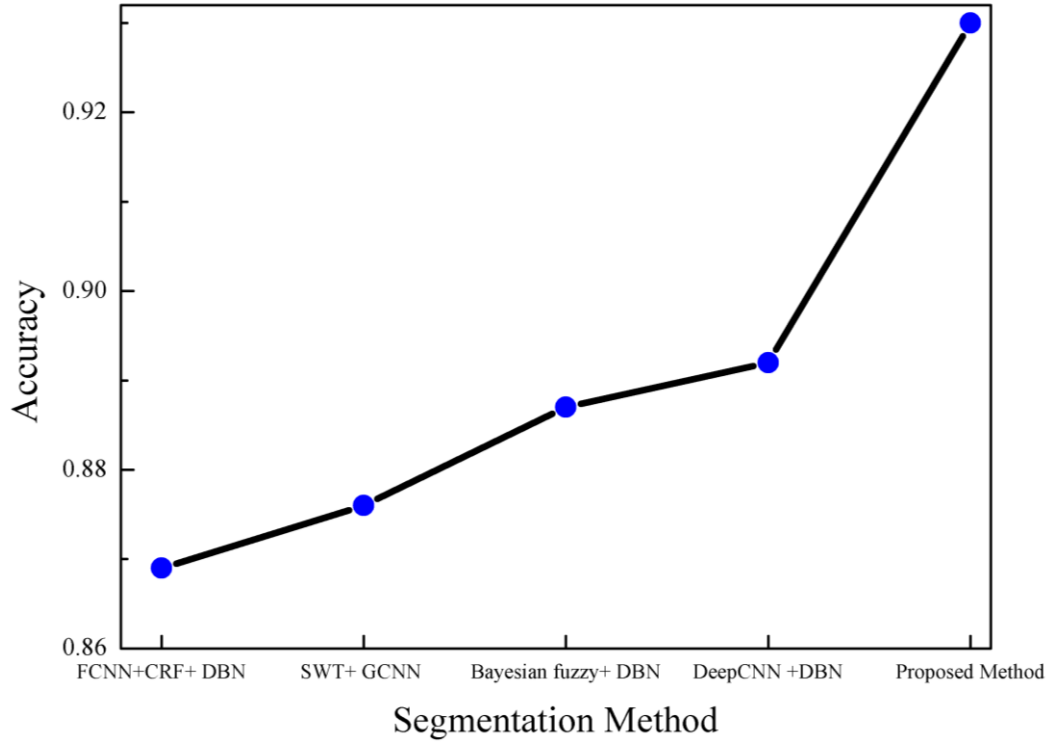


(c)

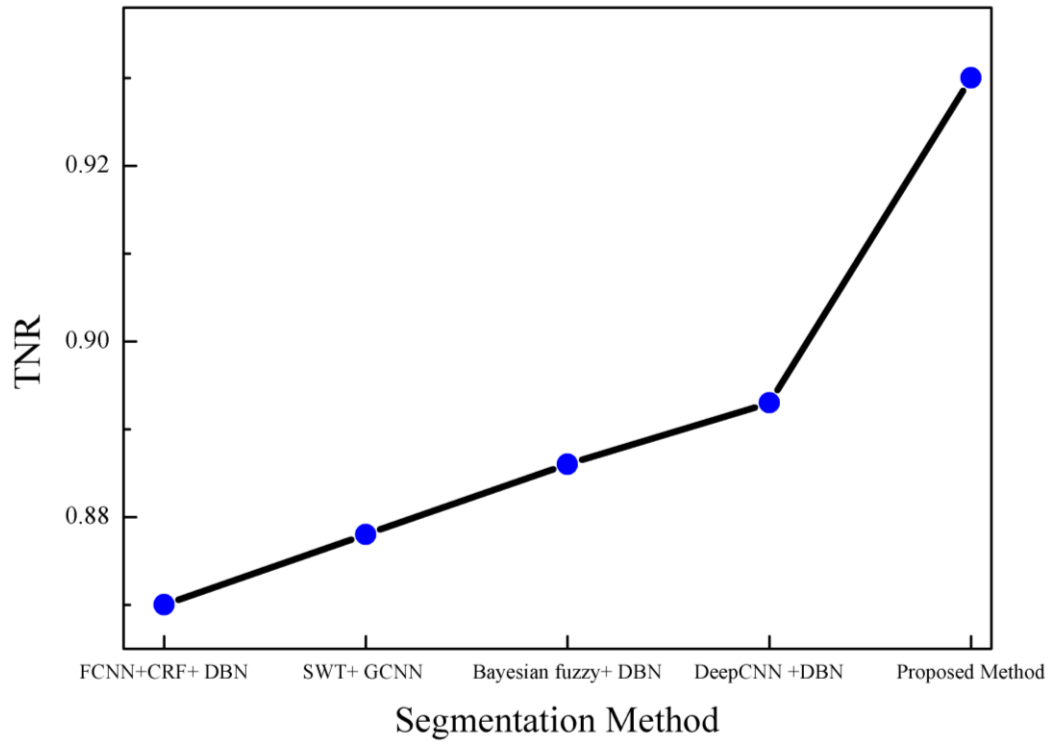
Figure 5.5: Estimation with training data, (a) Accuracy, (b) TPR, (c) TNR

(b) Evaluation with k-value

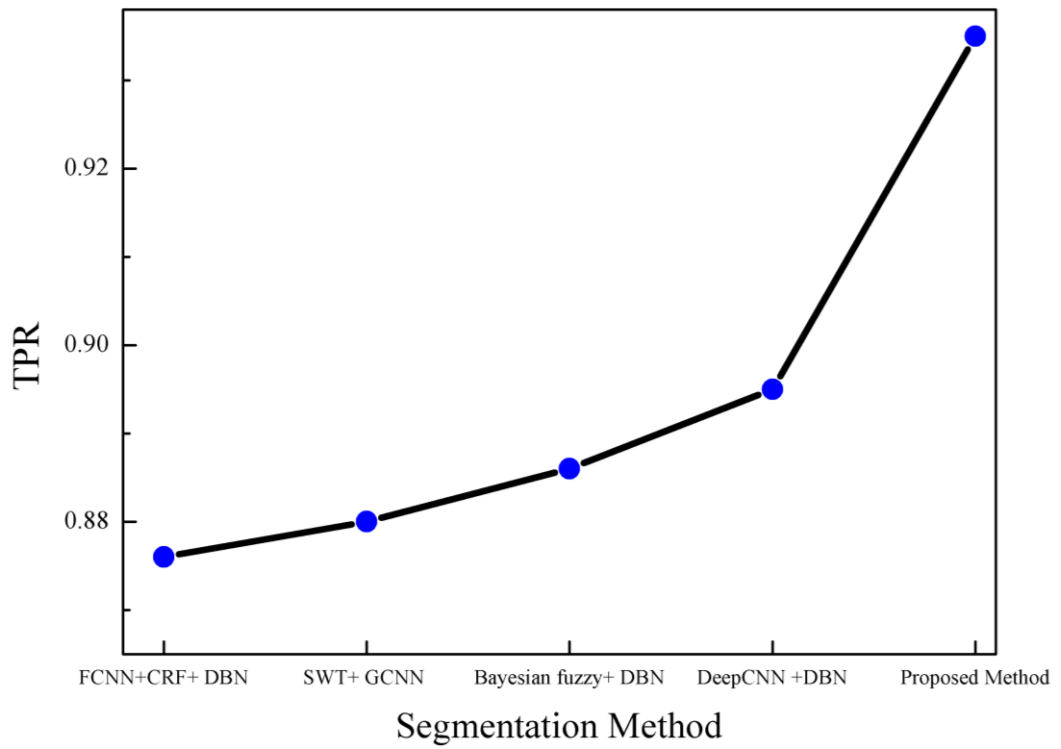
Figure 5.6 represents comparative estimation done by adaptive ASWO_DbneAlexnet in respect to indicators by measuring the k-value. Figure 5.6 (a) portrays estimation of accuracy. If 9 is assumed as k-value, adaptive ASWO_DbneAlexnet offered the accuracy as 0.930 that results the performance gain of 6.467%, 5.708%, 4.595% and 4.053%. Figure 5.6 (b) shows the estimation of devised technique in accordance to TPR. If the k-value is 9, TPR of modelled approach is 0.935 and the TNR is specified in Figure 5.6 (c). By assuming k-value as 9, TNR delivered by adaptive ASWO_DbneAlexnet is 0.930, while the preceding techniques offered the TNR as 0.870 for FCNN + CRF, 0.878 for SWT + GCNN, 0.886 for bayesian fuzzy, 0.893 and for deep CNN.



(a)



(b)



(c)

Figure 5.6: Estimation with K-value, (a) Accuracy, (b) TPR, (c) TNR

(c) Comparative discussion

Table 5.1 specifies discussion of adaptive ASWO_DbneAlexnet. From the discussion, it is known that adaptive ASWO_DbneAlexnet has received the remarkable results with 93.00% of accuracy, 93.50% of TPR and 93.00% of TNR.

Table 5.1: Comparative Discussion

| | Metrics/ Methods | FCNN + CRF [50] | SWT + GCNN [112] | Bayesian fuzzy [62] | Deep CNN [54] | Proposed Adaptive ASWO_ DbneAlexnet |
|----------------------|-----------------------------|--------------------------------|---------------------------------|--------------------------------|------------------------------|--|
| Training data=90% | Accuracy | 86.50% | 87.00% | 88.70% | 89.50% | 92.60% |
| | TPR | 86.70% | 87.50% | 88.30% | 89.10% | 93.10% |
| | TNR | 86.60% | 87.30% | 88.50% | 89.30% | 92.20% |
| K-value=9 | Accuracy | 86.90% | 87.60% | 88.70% | 89.20% | 93.00% |
| | TPR | 87.60% | 88.00% | 88.60% | 89.50% | 93.50% |
| | TNR | 87.00% | 87.80% | 88.60% | 89.30% | 93.00% |

5.5 Summary

Brain tumors are the deadly illness that is prevalently detected in all age groups leading to sudden death if left untreated on time. Manual diagnosis of brain tumors always needs medical experts and high experience to clearly diagnose the brain tumors. Moreover, these human assessments are inefficient and highly prone to errors and also take high time for processing. Huge variations in tumor kinds also include additional complexity. By taking this into concern, adaptive ASWO_DbneAlexnet is designed for tumor categorization. First of all, MRI is pre-processed by ABF in order to demolish the artifacts available in image. After that, U-Net++ is utilized to segment pre-processed image, which will improve the segmentation quality. Once the image is segmented, features like CNN, LOOP and GLCM texture features are refined effectively. Thereafter, brain tumor classification is conducted utilizing DbneAlexnet and it is finely adjusted based on adaptive ASWO. However, adaptive ASWO is attained by blending the adam optimizer and SWO with adaptive concept.

The technique integrates various optimization algorithms and deep learning architectures such as U-Net++ and DbneAlexnet, leveraging the strengths of each component to achieve superior classification results. This integration enhances the

versatility and effectiveness of the classification system. The proposed technique contributes to ongoing research efforts in medical imaging and machine learning by introducing innovative approaches to brain tumor classification. It serves as a valuable tool for researchers studying neurological disorders and developing advanced diagnostic methods for clinical applications.

CHAPTER

6

Conclusion and Scope for Future Studies

A brain tumor classification method using Deep Belief Network (DBN) is proposed to enhance detection performance, resolving the issues occurred during detection by conventional methods. The method employs a newly developed algorithm called SWO for training the classifier and optimizing weights. Pre-processing eliminates artifacts and noise, SegNet facilitates segmentation, and CNN features are extracted for subsequent classification by DBN. The training of DBN is accomplished using SWO, a combination of WWO and SSA algorithms. Experimentation on BRATS 2018 and BRATS 2020 datasets demonstrates superior performance in terms of specificity, accuracy and sensitivity.

Secondly, two novel methods, AdamSWO-DCNN and AdamSTBO+UNet++, for brain tumor (BT) segmentation and classification are developed. The UNet++ model is utilized for BT segmentation, with its weights optimized by the AdamSTBO algorithm, which combines Adam optimizer with the STBO algorithm. Similarly, BT classification is performed using the DCNN model, with weight modification achieved through the AdamSWO algorithm, a fusion of SWO and Adam Optimizer. The AdamSWO-DCNN method enhances classification accuracy by extracting relevant features like CNN, LOOP, LGP, PHoG, and GLCM. Experimental results indicate superior performance compared to existing techniques.

A DRN model optimized using the ASO algorithm for early-stage brain tumor classification using MRI images is also developed. Pre-processing involves noise removal with a gaussian filter, followed by segmentation using SegNet. Feature extraction includes GLCM and CNN features, enabling brain tumor classification by the DRN model. The ASO algorithm tunes the DRN classifier, achieving high TNR, TPR and accuracy, surpassing the existing technologies.

Also, to address the challenges like imbalanced training data and risk of false positives, the Adaptive ASWO_DbneAlexnet model is developed for tumor categorization. The process involves pre-processing of MRI images with adaptive bilateral filtering (ABF) to remove artifacts, followed by segmentation using U-Net++. Subsequent feature refinement includes CNN, LOOP and GLCM texture features. Tumor classification is performed using DbneAlexnet, fine-tuned with adaptive ASWO, a hybrid of Adam optimizer and SWO with adaptive elements. This adaptive optimization approach enhances the robustness and convergence speed of the model, leading to improved classification performance.

In conclusion, the investigations into MRI brain tumor segmentation using optimization-based deep learning classifiers underscores the promising potential of these methodologies in medical imaging analysis. Through analysis, the effectiveness of optimization techniques within deep learning frameworks in accurately segmenting tumor regions from MRI scans is demonstrated. The application of these classifiers shows significant advancements in precision and efficiency, offering valuable insights into the potential for improved diagnostic and treatment planning in neuroimaging.

As automated techniques become more prevalent in clinical settings, there is a growing need for explainable and interpretable AI models. Future research could explore methods to make the decision-making process of AI models transparent and understandable to healthcare professionals, enhancing trust and acceptance of automated techniques in medical practice. Future research could explore methods to make the decision-making process of AI models transparent and understandable to healthcare professionals, enhancing trust and acceptance of automated techniques in medical practice. Overall, the dissertation lays a strong foundation for future research in the field of medical image processing and machine learning, introducing novel automated brain tumor detection and classification techniques for practical clinical applications.

References:

- [1] V. Hlavac, “Fundamentals of Image Processing,” *Optical and Digital Image Processing: Fundamentals and Applications*, pp. 71–96, 2011, doi: 10.1002/9783527635245.ch4.
- [2] R. C. Gonzalez and R. E. Woods, *Digital Image Processing*, 4th ed. Pearson, 2018.
- [3] J. Tavares, “Image Processing and Analysis: Applications and Trends,” AES-ATEMA International Conference Series - Advances and Trends in Engineering Materials and their Applications, 2010.
- [4] S. Bauer, R. Wiest, L.-P. Nolte, and M. Reyes, “A Survey of MRI-based Medical Image Analysis for Brain Tumor Studies A Survey of MRI-based Medical Image Analysis for Brain Tumor Studies 2”, doi: 10.7892/boris.15734.
- [5] S. E. Forshult, *Magnetic Resonance Imaging - MRI – An Overview*. Karlstad University Studies, 2007.
- [6] M. Idrees, “An Overview on MRI Physics and it’s Clinical Applications,” vol. 4, no. 4, pp. 185–193, 2014.
- [7] Y. Guan *et al.*, “A framework for efficient brain tumor classification using MRI images,” *Mathematical Biosciences and Engineering*, vol. 18, no. 5, pp. 5790–5815, 2021, doi: 10.3934/MBE.2021292.
- [8] A. Işin, C. Direkoğlu, and M. Şah, “Review of MRI-based Brain Tumor Image Segmentation Using Deep Learning Methods,” in *Procedia Computer Science*, Elsevier B.V., 2016, pp. 317–324. doi: 10.1016/j.procs.2016.09. 407.
- [9] E. C. Holland, “Progenitor cells and glioma formation.” 2001 Dec;14(6):683-8. doi: 10.1097/00019052-200112000-00002.
- [10] H. Mohsen, E.-S. A. El-Dahshan, E.-S. M. El-Horbaty, and A.-B. M. Salem, “Classification using deep learning neural networks for brain tumors,” *Future Computing and Informatics Journal*, vol. 3, no. 1, pp. 68–71, 2018, doi: 10.1016/j.fcij.2017.12.001.
- [11] A. Islam, S. M. S. Reza, and K. M. Iftekharuddin, “Multifractal texture estimation for detection and segmentation of brain tumors,” *IEEE Trans Biomed Eng*, vol. 60, no. 11, pp. 3204–3215, 2013, doi: 10.1109/TBME.2013.2271383.
- [12] S. Hussain, S. M. Anwar, and M. Majid, “Segmentation of glioma tumors in brain using deep convolutional neural network,” *Neurocomputing*, vol. 282, pp. 248–261, 2018, doi: 10.1016/j.neucom.2017.12.032.
- [13] R. Rajasree and C. C. Columbus, “Brain Tumour Image Segmentation and Classification System Based on the Modified Adaboost Classifier.” [Online]. Available: <https://www.researchgate.net/publication/327033395>
- [14] A. Rehman, S. Naz, M. I. Razzak, F. Akram, and M. Imran, “A Deep Learning-Based Framework for Automatic Brain Tumors Classification

- Using Transfer Learning,” *Circuits Syst Signal Process*, vol. 39, no. 2, pp. 757–775, Feb. 2020, doi: 10.1007/s00034-019-01246-3.
- [15] W. Zhang *et al.*, “Deep convolutional neural networks for multi-modality iso-intense infant brain image segmentation,” *Neuroimage*, vol. 108, pp. 214–224, 2015, doi: 10.1016/j.neuroimage.2014.12.061.
 - [16] M. Soltaninejad *et al.*, “Automated brain tumour detection and segmentation using super pixel-based extremely randomized trees in FLAIR MRI,” *Int J Comput Assist Radiol Surg*, vol. 12, no. 2, pp. 183–203, 2017, doi: 10.1007/s11548-016-1483-3.
 - [17] M. Alfonse and A.-B. M. Salem, “An Automatic Classification of Brain Tumors through MRI Using Support Vector Machine,” 2016.
 - [18] N. Ghassemi, A. Shoeibi, and M. Rouhani, “Deep neural network with generative adversarial networks pre-training for brain tumor classification based on MR images,” *Biomed Signal Process Control*, vol. 57, Mar. 2020, doi: 10.1016/j.bspc.2019.101678.
 - [19] A. Gooya *et al.*, “GLISTR: Glioma image segmentation and registration,” *IEEE Trans Med Imaging*, vol. 31, no. 10, pp. 1941–1954, 2012, doi: 10.1109/TMI.2012.2210558.
 - [20] M. S. Islam, “Local gradient pattern-A novel feature representation for facial expression recognition,” 2014.
 - [21] A. Sehgal, S. Goel, P. Mangipudi, A. Mehra, and D. Tyagi, “Automatic brain tumor segmentation and extraction in MR images,” *Conference on Advances in Signal Processing, CASP 2016*, pp. 104–107, 2016, doi: 10.1109/CASP.2016.7746146.
 - [22] M. Ben Naceur, R. Saouli, M. Akil, R. Kachouri, M. Ben, and M. Ben naceur, “Fully Automatic Brain Tumor Segmentation using End-to-End Incremental Deep Neural Networks in MRI images,” *Comput Methods Programs Biomed*, vol. 166, 2018, doi: 10.1016/j.cmpb.2018.09.007.
 - [23] C. Patil *et al.*, “Early Detection of Alzheimer’s Disease Using Image Processing on MRI Scans,” *IEEE International Conference on Signal Processing, Informatics, Communication and Energy Systems*, pp. 1–4, 2015, doi: 10.1109/SPICES35288.2015.
 - [24] D. Bhattacharyya and T. H. Kim, “Brain tumor detection using MRI image analysis,” *Communications in Computer and Information Science*, vol. 151 CCIS, no. PART 2, pp. 307–314, 2011, doi: 10.1007/978-3-642-20998-7_38.
 - [25] R. D. Fields, “Change in the brain’s white matter,” *Sciencemag*, vol. 330, pp. 768–769, 2010, doi: 10.1126/science.1199139.
 - [26] P. Ghosal, S. Reddy, C. Sai, V. Pandey, J. Chakraborty, and D. Nandi, “A Deep Adaptive Convolutional Network for Brain Tumor Segmentation from Multimodal MR Images,” *IEEE Region 10 Annual International Conference, Proceedings, TENCON*, pp. 1065–1070, 2019, doi: 10.1109/TENCON.2019.8929402.

- [27] S. Iqbal, M. U. Ghani, T. Saba, and A. Rehman, "Brain tumor segmentation in multi-spectral MRI using convolutional neural networks (CNN)," *Microsc Res Tech*, vol. 81, no. 4, pp. 419–427, 2018, doi: 10.1002/jemt.22994.
- [28] M. Havaei *et al.*, "Brain tumor segmentation with Deep Neural Networks," *Med Image Anal*, vol. 35, pp. 18–31, Jan. 2017, doi: 10.1016/j.media.2016.05.004.
- [29] N. Arunkumar *et al.*, "K-Means clustering and neural network for object detecting and identifying abnormality of brain tumor," *Soft comput*, vol. 23, no. 19, pp. 9083–9096, 2019, doi: 10.1007/s00500-018-3618-7.
- [30] Y. Xiao, J. Wu, Z. Lin, and X. Zhao, "A semi-supervised deep learning method based on stacked sparse auto-encoder for cancer prediction using RNA-seq data," *Comput Methods Programs Biomed*, vol. 166, pp. 99–105, 2018, doi: 10.1016/j.cmpb.2018.10.004.
- [31] M. Goetz *et al.*, "DALSA: Domain adaptation for supervised learning from sparsely annotated MR images," *IEEE Trans Med Imaging*, vol. 35, no. 1, pp. 184–196, 2016, doi: 10.1109/TMI.2015.2463078.
- [32] F. Xing, Y. Xie, and L. Yang, "An automatic learning-based framework for robust nucleus segmentation," *IEEE Trans Med Imaging*, vol. 35, no. 2, pp. 550–566, 2016, doi: 10.1109/TMI.2015.2481436.
- [33] B. S. M. Po-Yu Kao, Thuyen Ngo, Angela Zhang, Jefferson W. Chen, "Brain Tumor Segmentation and Tractographic Feature Extraction from Structural MR Images for Overall Survival Prediction," *Springer Nature Switzerland AG*, vol. 2, pp. 380–392, 2019, doi: 10.1007/978-3-030-11726-9.
- [34] M. M. Thaha, K. P. M. Kumar, B. S. Murugan, S. Dhanasekaran, P. Vijayakarthish, and A. S. Selvi, "Brain Tumor Segmentation Using Convolutional Neural Networks in MRI Images," *J Med Syst*, vol. 43, no. 9, 2019, doi: 10.1007/s10916-019-1416-0.
- [35] S. Sajid, S. Hussain, and A. Sarwar, "Brain Tumor Detection and Segmentation in MR Images Using Deep Learning," *Arab J Sci Eng*, vol. 44, no. 11, pp. 9249–9261, Nov. 2019, doi: 10.1007/s13369-019-03967-8.
- [36] A. Mukaram, "An Automatic Brain Tumour Detection, Segmentation and Classification Using MRI Image," vol. 6, no. 5, pp. 54–65, 2017.
- [37] F. Isensee *et al.*, "Brain tumor segmentation using large receptive field deep convolutional neural networks," in *Informatik aktuell*, Kluwer Academic Publishers, 2017, pp. 86–91. doi: 10.1007/978-3-662-54345-0_24.
- [38] K. Kamnitsas *et al.*, "Efficient multi-scale 3D CNN with fully connected CRF for accurate brain lesion segmentation," *Med Image Anal*, vol. 36, pp. 61–78, 2017, doi: 10.1016/j.media.2016.10.004.
- [39] R. Lavanyadevi, M. Machakowsalya, J. Nivethitha, and A. N. Kumar, "Brain Tumor Classification and Segmentation in MRI Images using PNN."
- [40] S. U. Khan, N. Islam, Z. Jan, I. Ud Din, and J. J. P. C. Rodrigues, "A novel deep learning-based framework for the detection and classification of breast

- cancer using transfer learning,” *Pattern Recognit Lett*, vol. 125, pp. 1–6, 2019, doi: 10.1016/j.patrec.2019.03.022.
- [41] L. C. Chen, G. Papandreou, I. Kokkinos, K. Murphy, and A. L. Yuille, “DeepLab: Semantic Image Segmentation with Deep Convolutional Nets, Atrous Convolution, and Fully Connected CRFs,” *IEEE Trans Pattern Anal Mach Intell*, pp. 1–14, 2016, doi: 10.1109/TPAMI.2017.2699184.
 - [42] I. Hong, Y. Hwang, and D. Kim, “Efficient deep learning of image denoising using patch complexity local divide and deep conquer,” *Elsevier*, vol. 96, pp. 1–18, 2019, doi: 10.1016/j.patcog.2019.06.011.
 - [43] N. J. Tustison *et al.*, “Optimal Symmetric Multimodal Templates and Concatenated Random Forests for Supervised Brain Tumor Segmentation (Simplified) with ANTsR,” *Neuroinformatics*, vol. 13, no. 2, pp. 209–225, 2015, doi: 10.1007/s12021-014-9245-2.
 - [44] M. Prastawa, E. Bullitt, S. Ho, and G. Gerig, “A brain tumor segmentation framework based on outlier detection,” *Med Image Anal*, vol. 8, no. 3, pp. 275–283, 2004, doi: 10.1016/j.media.2004.06.007.
 - [45] A. Chaddad, “Automated feature extraction in brain tumor by magnetic resonance imaging using gaussian mixture models,” *Int J Biomed Imaging*, vol. 2015, 2015, doi: 10.1155/2015/868031.
 - [46] S. Damodharan and D. Raghavan, “Combining Tissue Segmentation and Neural Network for Brain Tumor Detection,” 2015.
 - [47] Q. Ain, M. A. Jaffar, and T. S. Choi, “Fuzzy anisotropic diffusion-based segmentation and texture-based ensemble classification of brain tumor,” *Applied Soft Computing Journal*, vol. 21, pp. 330–340, 2014, doi: 10.1016/j.asoc.2014.03.019.
 - [48] I. E. Kaya, A. Ç. Pehlivanlı, E. G. Sekizkardeş, and T. Ibrikci, “PCA based clustering for brain tumor segmentation of T1w MRI images,” *Comput Methods Programs Biomed*, vol. 140, pp. 19–28, Mar. 2017, doi: 10.1016/j.cmpb.2016.11.011.
 - [49] H. Li, A. Li, and M. Wang, “A novel end-to-end brain tumor segmentation method using improved fully convolutional networks,” *Comput Biol Med*, vol. 108, pp. 150–160, May 2019, doi: 10.1016/j.compbimed.2019.03.014.
 - [50] X. Zhao, Y. Wu, G. Song, Z. Li, Y. Zhang, and Y. Fan, “A deep learning model integrating FCNNs and CRFs for brain tumor segmentation,” *Med Image Anal*, vol. 43, pp. 98–111, Jan. 2018, doi: 10.1016/j.media.2017.10.002.
 - [51] M. Mittal, L. M. Goyal, S. Kaur, I. Kaur, A. Verma, and D. Jude Hemanth, “Deep learning based enhanced tumor segmentation approach for MR brain images,” *Applied Soft Computing Journal*, vol. 78, pp. 346–354, May 2019, doi: 10.1016/j.asoc.2019.02.036.
 - [52] T. Yang, J. Song, and L. Li, “A deep learning model integrating SK-TPCNN and random forests for brain tumor segmentation in MRI,” *Biocybern Biomed Eng*, vol. 39, no. 3, pp. 613–623, 2019, doi: 10.1016/j.bbe.2019.06.003.

- [53] J. Tong, Y. Zhao, P. Zhang, L. Chen, and L. Jiang, "MRI brain tumor segmentation based on texture features and kernel sparse coding," *Biomed Signal Process Control*, vol. 47, pp. 387–392, 2019, doi: 10.1016/j.bspc.2018.06.001.
- [54] H. Chen, Z. Qin, Y. Ding, L. Tian, and Z. Qin, "Brain tumor segmentation with deep convolutional symmetric neural network," *Neurocomputing*, vol. 392, pp. 305–313, Jun. 2020, doi: 10.1016/j.neucom.2019.01.111.
- [55] J. Hu, L. Mou, A. Schmitt, and X. X. Zhu, "FusioNet: A two-stream convolutional neural network for urban scene classification using PolSAR and hyperspectral data," *2017 Joint Urban Remote Sensing Event, JURSE 2017*, no. 3, pp. 3–6, 2017, doi: 10.1109/JURSE.2017.7924565.
- [56] T. Sun, Y. Wang, J. Yang, and X. Hu, "Convolution Neural Networks with Two Pathways for Image Style Recognition," *IEEE Transactions on Image Processing*, vol. 26, no. 9, pp. 4102–4113, 2017, doi: 10.1109/TIP.2017.2710631.
- [57] P. Kumar Mallick, S. H. Ryu, S. K. Satapathy, S. Mishra, G. N. Nguyen, and P. Tiwari, "Brain MRI Image Classification for Cancer Detection Using Deep Wavelet Autoencoder-Based Deep Neural Network," *IEEE Access*, vol. 7, pp. 46278–46287, 2019, doi: 10.1109/ACCESS.2019.2902252.
- [58] P. Moeskops, M. A. Viergever, A. M. Mendrik, L. S. De Vries, M. J. N. L. Benders, and I. Isgum, "Automatic Segmentation of MR Brain Images with a Convolutional Neural Network," *IEEE Trans Med Imaging*, vol. 35, pp. 1–11, 2016, doi: 10.1109/TMI.2016.2548501.
- [59] R. Thillaikkarasi and S. Saravanan, "An Enhancement of Deep Learning Algorithm for Brain Tumor Segmentation Using Kernel Based CNN with M-SVM," *J Med Syst*, vol. 43, no. 4, Apr. 2019, doi: 10.1007/s10916-019-1223-7.
- [60] M. Alfonse and A.-B. M. Salem, "An Automatic Classification of Brain Tumors through MRI Using Support Vector Machine," *Egyptian Computer Science Journal*, vol. 40, no. 03, pp. 1110–2586, 2016.
- [61] P. Kumar and B. Vijayakumar, "Brain Tumour Mr Image Segmentation and Classification Using by PCA and RBF Kernel Based Support Vector Machine," *Middle-East Journal of Scientific Research*, vol. 23, no. 9, pp. 2106–2116, 2015, doi: 10.5829/idosi.mejsr.2015.23.09.22458.
- [62] P. M. Siva Raja and A. V. rani, "Brain tumor classification using a hybrid deep autoencoder with Bayesian fuzzy clustering-based segmentation approach," *Biocybern Biomed Eng*, vol. 40, no. 1, pp. 440–453, Jan. 2020, doi: 10.1016/j.bbe.2020.01.006.
- [63] Y. Xue, W. Jia, X. Zhao, and W. Pang, "An Evolutionary Computation Based Feature Selection Method for Intrusion Detection," *Security and Communication Networks*, vol. 2018, 2018, doi: 10.1155/2018/2492956.
- [64] M. I. Sharif, J. P. Li, M. A. Khan, and M. A. Saleem, "Active deep neural network features selection for segmentation and recognition of brain tumors using MRI images," *Pattern Recognit Lett*, vol. 129, pp. 181–189, Jan. 2020, doi: 10.1016/j.patrec.2019.11.019.

- [65] J. Bernal *et al.*, “Deep convolutional neural networks for brain image analysis on magnetic resonance imaging: a review,” *Artif Intell Med*, vol. 95, pp. 64–81, 2019, doi: 10.1016/j.artmed.2018.08.008.
- [66] M. Angulakshmi and G. G. Lakshmi Priya, “Automated brain tumour segmentation techniques— A review,” *Int J Imaging Syst Technol*, vol. 27, no. 1, pp. 66–77, 2017, doi: 10.1002/ima.22211.
- [67] T. Y. Lin, P. Goyal, R. Girshick, K. He, and P. Dollar, “Focal Loss for Dense Object Detection,” *International Conference on Computer Vision*, pp. 2999–3007, 2017, doi: 10.1109/ICCV.2017.324.
- [68] S. Bai, Z. Li, and J. Hou, “Learning two-pathway convolutional neural networks for categorizing scene images,” *Multimed Tools Appl*, vol. 76, no. 15, pp. 16145–16162, 2017, doi: 10.1007/s11042-016-3900-6.
- [69] S. Lokesh, P. Malarvizhi Kumar, M. Ramya Devi, P. Parthasarathy, and C. Gokulnath, “An Automatic Tamil Speech Recognition system by using Bidirectional Recurrent Neural Network with Self-Organizing Map,” *Neural Comput Appl*, vol. 31, no. 5, pp. 1521–1531, 2019, doi: 10.1007/s00521-018-3466-5.
- [70] Y. J. Zheng, “Water wave optimization: A new nature-inspired metaheuristic,” *Comput Oper Res*, vol. 55, pp. 1–11, 2015, doi: 10.1016/j.cor.2014.10.008.
- [71] X. Zhao, H. Li, L. Wu, and Y. Qi, “Enterprise-level amount of energy saved targets in China: Weaknesses and a way forward,” *J Clean Prod*, vol. 129, pp. 75–87, 2016, doi: 10.1016/j.jclepro.2016.04.116.
- [72] Z. Akkus, A. Galimzianova, A. Hoogi, D. L. Rubin, and B. J. Erickson, “Deep Learning for Brain MRI Segmentation: State of the Art and Future Directions,” *J Digit Imaging*, vol. 30, no. 4, pp. 449–459, 2017, doi: 10.1007/s10278-017-9983-4.
- [73] S. Mirjalili, A. H. Gandomi, S. Z. Mirjalili, S. Saremi, H. Faris, and S. M. Mirjalili, “Salp Swarm Algorithm: A bio-inspired optimizer for engineering design problems,” *Advances in Engineering Software*, vol. 114, pp. 163–191, Dec. 2017, doi: 10.1016/j.advengsoft.2017.07.002.
- [74] U. Zahid *et al.*, “BrainNet: Optimal Deep Learning Feature Fusion for Brain Tumor Classification,” *Comput Intell Neurosci*, vol. 2022, 2022, doi: 10.1155/2022/1465173.
- [75] S. Bauer, R. Wiest, L.-P. Nolte, and M. Reyes, “A survey of MRI-based medical image analysis for brain tumor studies,” *Phys Med Biol*, vol. 58, no. 13, pp. R97–R129, Jul. 2013, doi: 10.1088/0031-9155/58/13/R97.
- [76] S. E. Forshult, *Magnetic Resonance Imaging - MRI – An Overview*. Karlstad University Studies, 2007.
- [77] E. C. Holland, “Progenitor cells and glioma formation.”
- [78] G. E. Hinton and S. Osindero, “A Fast-Learning Algorithm for Deep Belief Nets Yee-Whye Teh.”
- [79] V. Badrinarayanan, A. Kendall, and R. Cipolla, “SegNet: A Deep Convolutional Encoder-Decoder Architecture for Image Segmentation,”

- IEEE Trans Pattern Anal Mach Intell*, vol. 39, no. 12, pp. 2481–2495, Dec. 2017, doi: 10.1109/TPAMI.2016.2644615.
- [80] A. Raza *et al.*, “A Hybrid Deep Learning-Based Approach for Brain Tumor Classification,” *Electronics (Switzerland)*, vol. 11, no. 7, Apr. 2022, doi: 10.3390/electronics11071146.
 - [81] H. H. Sultan, N. M. Salem, and W. Al-Atabany, “Multi-Classification of Brain Tumor Images Using Deep Neural Network,” *IEEE Access*, vol. 7, pp. 69215–69225, 2019, doi: 10.1109/ACCESS.2019.2919122.
 - [82] B. 2018 Dataset, “Section for Biomedical Image Analysis (SBIA).” [Online]. Available: <https://www.med.upenn.edu/sbia/brats2018/data.html>
 - [83] BRATS 2020 dataset, “[https://www.med.upenn.edu/cbica/brats2020/.](https://www.med.upenn.edu/cbica/brats2020/)”
 - [84] D. P. Kingma and J. Ba, “Adam: A Method for Stochastic Optimization,” Dec. 2014, [Online]. Available: <http://arxiv.org/abs/1412.6980>
 - [85] Z. Zhou, M. M. R. Siddiquee, N. Tajbakhsh, and J. Liang, “UNet++: Redesigning Skip Connections to Exploit Multiscale Features in Image Segmentation,” *IEEE Trans Med Imaging*, vol. 39, no. 6, pp. 1856–1867, Jun. 2020, doi: 10.1109/TMI.2019.2959609.
 - [86] B. H. Menze *et al.*, “The Multimodal Brain Tumor Image Segmentation Benchmark (BRATS),” *IEEE Trans Med Imaging*, vol. 34, no. 10, pp. 1993–2024, Oct. 2015, doi: 10.1109/TMI.2014.2377694.
 - [87] A. Pradhan, D. Mishra, K. Das, G. Panda, S. Kumar, and M. Zymbler, “On the classification of MR images using ‘elm-ssa’ coated hybrid model,” *Mathematics*, vol. 9, no. 17, Sep. 2021, doi: 10.3390/math9172095.
 - [88] A. V. N. Reddy *et al.*, “Analyzing MRI scans to detect glioblastoma tumor using hybrid deep belief networks”, doi: 10.1186/s40537-020-00311-y.
 - [89] D. R. Nayak, N. Padhy, P. K. Mallick, D. K. Bagal, and S. Kumar, “Brain Tumour Classification Using Noble Deep Learning Approach with Parametric Optimization through Metaheuristics Approaches,” *Computers*, vol. 11, no. 1, Jan. 2022, doi: 10.3390/computers11010010.
 - [90] R. F. Mansour, J. Escorcia-Gutierrez, M. Gamarra, V. G. Díaz, D. Gupta, and S. Kumar, “Artificial intelligence with big data analytics-based brain intracranial hemorrhage e-diagnosis using CT images,” *Neural Comput Appl*, vol. 35, no. 22, pp. 16037–16049, Aug. 2023, doi: 10.1007/s00521-021-06240-y.
 - [91] P. Carvalho, D. Ranjan Nayak, N. Padhy, P. K. Mallick, M. Zymbler, and S. Kumar, “Brain Tumor Classification Using Dense Efficient-Net,” 2022, doi: 10.3390/axioms11010034.
 - [92] T. Wang, H. Feng, S. Li, and Y. Yang, “Medical Image Denoising Using Bilateral Filter and the K-SVD Algorithm,” in *Journal of Physics: Conference Series*, Institute of Physics Publishing, May 2019. doi: 10.1088/1742-6596/1229/1/012007.
 - [93] F. Hoorali, H. Khosravi, and B. Moradi, “Automatic Bacillus anthracis bacteria detection and segmentation in microscopic images using UNet+.,”

- J Microbiol Methods*, vol. 177, p. 106056, Oct. 2020, doi: 10.1016/j.mimet. 2020.106056.
- [94] M. Dehghani, E. Trojovská, and T. Zušćák, “A new human-inspired metaheuristic algorithm for solving optimization problems based on mimicking sewing training,” *Sci Rep*, vol. 12, no. 1, p. 17387, Oct. 2022, doi: 10.1038/s41598-022-22458-9.
 - [95] R. Yao, N. Wang, Z. Liu, P. Chen, and X. Sheng, “Intrusion detection system in the advanced metering infrastructure: A cross-layer feature-fusion CNN-LSTM-based approach,” *Sensors (Switzerland)*, vol. 21, no. 2, pp. 1–17, Jan. 2021, doi: 10.3390/s21020626.
 - [96] T. Chakraborti, B. McCane, S. Mills, and U. Pal, “LOOP Descriptor: Local Optimal-Oriented Pattern,” *IEEE Signal Process Lett*, vol. 25, no. 5, pp. 635–639, May 2018, doi: 10.1109/LSP.2018.2817176.
 - [97] N. Gour and P. Khanna, “Automated glaucoma detection using GIST and pyramid histogram of oriented gradients (PHOG) descriptors,” *Pattern Recognit Lett*, vol. 137, pp. 3–11, Sep. 2020, doi: 10.1016/j.patrec.2019.04.004.
 - [98] N. Zulpe and V. Pawar, “GLCM Textural Features for Brain Tumor Classification,” 2012. [Online]. Available: www.IJCSI.org
 - [99] S. Sugave and B. Jagdale, “Monarch-EWA: Monarch-Earthworm-Based Secure Routing Protocol in IoT,” *Comput J*, vol. 63, no. 6, pp. 817–831, Jun. 2020, doi: 10.1093/comjnl/bxz135.
 - [100] M. S. I. Khan *et al.*, “Accurate brain tumor detection using deep convolutional neural network,” *Comput Struct Biotechnol J*, vol. 20, pp. 4733–4745, Jan. 2022, doi: 10.1016/j.csbj.2022.08.039.
 - [101] S. Alqazzaz, X. Sun, X. Yang, and L. Nokes, “Computational Visual Media Automated brain tumor segmentation on multi-modal MR image using SegNet,” vol. 5, no. 2, pp. 209–219, 2019, doi: 10.1007/s41095-019-0139-y.
 - [102] J. Jung and B.-C. Ahn, “Current Radiopharmaceuticals for Positron Emission Tomography of Brain Tumors,” *Brain Tumor Res Treat*, vol. 6, no. 2, 2018, doi: 10.14791/btrt.2018.6. e13.
 - [103] M. Heinsch *et al.*, “Supporting friends and family of adults with a primary brain tumour: A systematic review,” *Health and Social Care in the Community*, vol. 30, no. 3. 2022. doi: 10.1111/hsc.13586.
 - [104] Y. Guan *et al.*, “A framework for efficient brain tumor classification using MRI images,” *Mathematical Biosciences and Engineering*, vol. 18, no. 5, pp. 5790–5815, 2021, doi: 10.3934/MBE.2021292.
 - [105] R. Salgotra, U. Singh, S. Singh, G. Singh, and N. Mittal, “Self-adaptive salp swarm algorithm for engineering optimization problems,” *Appl Math Model*, vol. 89, 2021, doi: 10.1016/j.apm.2020.08.014.
 - [106] M. Khajehzadeh, A. Iraj, A. Majdi, S. Keawsawasvong, and M. L. Nehdi, “Adaptive Salp Swarm Algorithm for Optimization of Geotechnical

- Structures,” *Applied Sciences (Switzerland)*, vol. 12, no. 13, 2022, doi: 10.3390/app12136749.
- [107] F. Sha, S. M. Zandavi, and Y. Y. Chung, “Fast deep parallel residual network for accurate super resolution image processing,” *Expert Syst Appl*, vol. 128, 2019, doi: 10.1016/j.eswa.2019.03.032.
 - [108] L. Peng, Y. Na, D. Changsong, L. I. Sheng, and M. Hui, “Research on classification diagnosis model of psoriasis based on deep residual network,” *Digital Chinese Medicine*, vol. 4, no. 2, 2021, doi: 10.1016/j.dcmmed.2021.06.003.
 - [109] K. Muhammad, S. Khan, J. Del Ser, and V. H. C. D. Albuquerque, “Deep Learning for Multigrade Brain Tumor Classification in Smart Healthcare Systems: A Prospective Survey,” *IEEE Trans Neural Netw Learn Syst*, vol. 32, no. 2, pp. 507–522, Feb. 2021, doi: 10.1109/TNNLS.2020.2995800.
 - [110] L. H. Shehab, O. M. Fahmy, S. M. Gasser, and M. S. El-Mahallawy, “An efficient brain tumor image segmentation based on deep residual networks (ResNets),” *Journal of King Saud University - Engineering Sciences*, vol. 33, no. 6, 2021, doi: 10.1016/j.jksues.2020.06.001.
 - [111] S. Siuly, Y. Guo, O. F. Alcin, Y. Li, P. Wen, and H. Wang, “Exploring deep residual network-based features for automatic schizophrenia detection from EEG,” *Phys Eng Sci Med*, vol. 46, no. 2, 2023, doi: 10.1007/s13246-023-01225-8.
 - [112] S. A. Alazawi, N. Mezaal Shati, and A. H. Abbas, “Texture features extraction based on GLCM for face retrieval system,” vol. 7, no. 3, pp. 1459–1467, 2019, [Online]. Available: <http://pen.ius.edu.ba>
 - [113] R. Su, T. Liu, C. Sun, Q. Jin, R. Jennane, and L. Wei, “Fusing convolutional neural network features with hand-crafted features for osteoporosis diagnoses,” *Neurocomputing*, vol. 385, pp. 300–309, Apr. 2020, doi: 10.1016/j.neucom.2019.12.083.
 - [114] R. Chrzan, A. Gleń, A. Bryll, and A. Urbanik, “Computed tomography assessment of brain atrophy in centenarians,” *Int J Environ Res Public Health*, vol. 16, no. 19, 2019, doi: 10.3390/ijerph16193659.
 - [115] Q. D. Buchlak *et al.*, “Charting the potential of brain computed tomography deep learning systems,” *Journal of Clinical Neuroscience*, vol. 99, 2022, doi: 10.1016/j.jocn.2022.03.014.
 - [116] I. N. Fleming *et al.*, “Imaging tumour hypoxia with positron emission tomography,” *British Journal of Cancer*, vol. 112, no. 2, 2015, doi: 10.1038/bjc.2014.610.
 - [117] O. Ronneberger, P. Fischer, and T. Brox, “U-net: Convolutional networks for biomedical image segmentation,” in *Lecture Notes in Computer Science (including subseries Lecture Notes in Artificial Intelligence and Lecture Notes in Bioinformatics)*, Springer Verlag, 2015, pp. 234–241. doi: 10.1007/978-3-319-24574-4_28.
 - [118] R. Anitha, D. B. Dasari, P. S. S. Vivek, N. M. L. Kakarla, and M. S. Kumar, “A novel adaptive dual swarm intelligence-based image quality enhancement approach with the modified SegNet -RBM-based Alzheimer

- Segmentation and classification,” *Multimed Tools Appl*, 2023, doi: 10.1007/s11042-023-16486-4.
- [119] A. Kumar and S. S. Sodhi, “Comparative analysis of gaussian filter, median filter and denoise autoencoder,” in *Proceedings of the 7th International Conference on Computing for Sustainable Global Development, INDIA Com 2020*, 2020. doi: 10.23919/INDIACom49435.2020.9083712.
 - [120] Z. Chen, Y. Chen, L. Wu, S. Cheng, and P. Lin, “Deep residual network-based fault detection and diagnosis of photovoltaic arrays using current-voltage curves and ambient conditions,” *Energy Convers Manag*, vol. 198, Oct. 2019, doi: 10.1016/j.enconman.2019.111793.
 - [121] Z. Xing and H. Jia, “Multilevel Color Image Segmentation Based on GLCM and Improved Salp Swarm Algorithm,” *IEEE Access*, vol. 7, 2019, doi: 10.1109/ACCESS.2019.2904511.
 - [122] L. Abualigah, M. Shehab, M. Alshinwan, and H. Alabool, “Salp swarm algorithm: a comprehensive survey,” *Neural Computing and Applications*, vol. 32, no. 15. Springer, pp. 11195–11215, Aug. 01, 2020. doi: 10.1007/s00521-019-04629-4.
 - [123] P. S. Bidkar, R. Kumar, and A. Ghosh, “SegNet and Salp Water Optimization-driven Deep Belief Network for Segmentation and Classification of Brain Tumor,” *Gene Expression Patterns*, vol. 45, 2022, doi: 10.1016/j.gep.2022.119248.
 - [124] S. Bauer, R. Wiest, L.-P. Nolte, and M. Reyes, “A Survey of MRI-based Medical Image Analysis for Brain Tumor Studies A Survey of MRI-based Medical Image Analysis for Brain Tumor Studies 2.” [Online]. Available: <http://boris.unibe.ch/61011/>
 - [125] M. E. Mayerhoefer, S. J. Archibald, C. Messiou, A. Staudenherz, D. Berzaczy, and H. Schöder, “MRI and PET/MRI in hematologic malignancies,” *Journal of Magnetic Resonance Imaging*, vol. 51, no. 5. 2020. doi: 10.1002/jmri.26848.
 - [126] A. M. Hashan, E. Agbozo, A. A. K. Al-Saeedi, S. Saha, A. Haidari, and M. N. F. Rabi, “Brain Tumor Detection in MRI Images Using Image Processing Techniques,” in *Proceedings - ISAMSR 2021: 4th International Symposium on Agents, Multi-Agents Systems and Robotics*, 2021. doi: 10.1109/ISAMSR53229.2021.9567799.
 - [127] Y. Xu, S. Hou, X. Wang, D. Li, and L. Lu, “A Medical Image Segmentation Method Based on Improved UNet 3+ Network,” *Diagnostics*, vol. 13, no. 3, 2023, doi: 10.3390/diagnostics13030576.
 - [128] K. Trebing, T. Stańczyk, and S. Mehrkanoon, “SmaAt-UNet: Precipitation nowcasting using a small attention-UNet architecture,” *Pattern Recognit Lett*, vol. 145, 2021, doi: 10.1016/j.patrec.2021.01.036.
 - [129] P. K. Jain *et al.*, “Attention-Based UNet Deep Learning Model for Plaque Segmentation in Carotid Ultrasound for Stroke Risk Stratification: An Artificial Intelligence Paradigm,” *J Cardiovasc Dev Dis*, vol. 9, no. 10, 2022, doi: 10.3390/jcdd9100326.

- [130] K. Kamnitsas *et al.*, “DeepMedic for Brain Tumor Segmentation.” [Online]. Available: <https://github.com/Kamnitsask/deepmedic>
- [131] B. Zhang and J. P. Allebach, “Adaptive bilateral filter for sharpness enhancement and noise removal,” *IEEE Transactions on Image Processing*, vol. 17, no. 5, pp. 664–678, May 2008, doi: 10.1109/TIP.2008.919949.
- [132] H. Alaeddine and M. Jihene, “Deep Batch-normalized eLU AlexNet for Plant Diseases Classification,” in *18th IEEE International Multi-Conference on Systems, Signals and Devices, SSD 2021*, Institute of Electrical and Electronics Engineers Inc., Mar. 2021, pp. 17–22. doi: 10.1109/SSD52085.2021.9429404.
- [133] P. S. Bidkar, R. Kumar, and A. Ghosh, “Hybrid Adam Sewing Training Optimization Enabled Deep Learning for Brain Tumor Segmentation and Classification using MRI Images,” *Comput Methods Biomech Biomed Eng Imaging Vis*, vol. 11, no. 5, 2023, doi: 10.1080/21681163.2023.2199891.
- [134] B. H. Chen, Y. S. Tseng, and J. L. Yin, “Gaussian-adaptive bilateral filter,” *IEEE Signal Process Lett*, vol. 27, 2020, doi: 10.1109/LSP.2020.3024990.
- [135] M. Padlia and J. Sharma, “Fractional Sobel filter-based brain tumor detection and segmentation using statistical features and SVM,” in *Lecture Notes in Electrical Engineering*, Springer Verlag, 2019, pp. 161–175. doi: 10.1007/978-981-13-0776-8_15.
- [136] S. Gowroju, Aarti, and S. Kumar, “Robust Pupil Segmentation using UNET and Morphological Image Processing,” in *2021 International Mobile, Intelligent, and Ubiquitous Computing Conference, MIUCC 2021*, 2021. doi: 10.1109/MIUCC52538.2021.9447658.
- [137] Y. Chen *et al.*, “ANT-UNet: Accurate and Noise-Tolerant Segmentation for Pathology Image Processing,” *ACM J Emerg Technol Comput Syst*, vol. 18, no. 2, 2022, doi: 10.1145/3451213.
- [138] J. Zhang, Q. Qin, Q. Ye, and T. Ruan, “ST-Unet: Swin Transformer boosted U-Net with Cross-Layer Feature Enhancement for medical image segmentation,” *Comput Biol Med*, vol. 153, 2023, doi: 10.1016/j.combiomed.2022.106516.
- [139] Y. Wang, Y. Yang, and P. Zhang, “Gesture feature extraction and recognition based on image processing,” *Traitement du Signal*, vol. 37, no. 5, 2020, doi: 10.18280/ts.370521.
- [140] G. Wang, W. Li, S. Ourselin, and T. Vercauteren, “Automatic brain tumor segmentation using cascaded anisotropic convolutional neural networks,” in *Lecture Notes in Computer Science (including subseries Lecture Notes in Artificial Intelligence and Lecture Notes in Bioinformatics)*, Springer Verlag, 2018, pp. 178–190. doi: 10.1007/978-3-319-75238-9_16.
- [141] Z. Wei and X. Zhang, “Feature extraction and retrieval of ecommerce product images based on image processing,” *Traitement du Signal*, vol. 38, no. 1, 2021, doi: 10.18280/TS.380119.
- [142] M. S. Nixon and A. S. Aguado, *Feature extraction and image processing for computer vision*. 2019. doi: 10.1016/C2017-0-02153-5.

- [143] G. Kumar and P. K. Bhatia, "A detailed review of feature extraction in image processing systems," in *International Conference on Advanced Computing and Communication Technologies, ACCT*, 2014. doi: 10.1109/ACCT.2014.74.
- [144] M. S. Nixon and A. S. Aguado, *Feature Extraction and Image Processing for Computer Vision*. 2012. doi: 10.1016/C2011-0-06935-1.
- [145] S. Singh, N. Mittal, and H. Singh, "Multi-focus Image Fusion Based on Multiresolution Pyramid and Bilateral Filter," *IETE Journal of Research*, vol. 68, no. 4. 2022. doi: 10.1080/03772063.2019.1711205.
- [146] P. Mohanaiah, P. Sathyanarayana, and L. Gurukumar, "Image Texture Feature Extraction Using GLCM Approach," *International Journal of Scientific & Research Publication*, vol. 3, no. 5, 2013.
- [147] B. Van Ginneken, A. F. Frangi, J. J. Staal, B. M. Ter Haar Romeny, and M. A. Viergever, "Active shape model segmentation with optimal features," *IEEE Trans Med Imaging*, vol. 21, no. 8, 2002, doi: 10.1109/TMI.2002.803121.
- [148] A. Çınar and S. A. Tuncer, "Classification of lymphocytes, monocytes, eosinophils, and neutrophils on white blood cells using hybrid Alexnet-GoogleNet-SVM," *SN Appl Sci*, vol. 3, no. 4, 2021, doi: 10.1007/s42452-021-04485-9.
- [149] N. A. Muhammad, A. A. Nasir, Z. Ibrahim, and N. Sabri, "Evaluation of CNN, alexnet and GoogleNet for fruit recognition," *Indonesian Journal of Electrical Engineering and Computer Science*, vol. 12, no. 2, 2018, doi: 10.11591/ijeecs.v12.i2.pp468-475.
- [150] Y. J. Zheng, X. Q. Lu, Y. C. Du, Y. Xue, and W. G. Sheng, "Water wave optimization for combinatorial optimization: Design strategies and applications," *Applied Soft Computing Journal*, vol. 83, 2019, doi: 10.1016/j.asoc.2019.105611.
- [151] I. Singh, G. Goyal, and A. Chandel, "AlexNet architecture based convolutional neural network for toxic comments classification," *Journal of King Saud University - Computer and Information Sciences*, 2022, doi: 10.1016/j.jksuci.2022.06.007.
- [152] H. C. Chen *et al.*, "AlexNet Convolutional Neural Network for Disease Detection and Classification of Tomato Leaf," *Electronics (Switzerland)*, vol. 11, no. 6, 2022, doi: 10.3390/electronics11060951.
- [153] Irmak, E. "Multi-Classification of Brain Tumor MRI Images Using Deep Convolutional Neural Network with Fully Optimized Framework," *Iran J Sci Technol Trans Electr Eng* vol. 45, pp. 1015–1036 , 2021, doi: 10.1007/s40998-021-00426-9

BIO-DATA OF THE CANDIDATE

Name of Candidate : Pravin Shivaji Bidkar

Date of Birth : 17/05/1984

Contact : +91 8378997119
pravin.bidkar@gmail.com

Permanent Address : 'Yashwant', Rukadi Fata,
A/P: Atigre, Tal: Hatkanangle,
Dist: Kolhapur, Maharashtra,
Pin: 416118.

Married : Yes

Educational Details

(a) B.E. : Dr. D. Y. Patil College of Engineering and
Technology, Kolhapur, Maharashtra, India.

(b) M.Tech. : Walchand College of Engineering, Sangli,
Maharashtra, India.

(c) Ph.D. Course work : SGPA of 8.33.

Present Occupation Details

Organization : Sanjay Ghodawat University, Kolhapur.

Rank : Assistant Professor, Department of E&C.

Job Profile : Teaching and learning process of assigned
courses.

LIST OF PUBLICATIONS

Journal Publications:

- [1] **Pravin Shivaji Bidkar**, Ram Kumar, Abhijyoti Ghosh, "SegNet and Salp Water Optimization-driven Deep Belief Network for Segmentation and Classification of Brain Tumor", *Gene Expression Patterns*, Volume 45, 2022, 119248, <https://doi.org/10.1016/j.gep.2022.119248>. [ISSN 1567-133X] [Impact factor 1.2 (Elsevier)].
- [2] **Pravin Shivaji Bidkar**, Ram Kumar, Abhijyoti Ghosh, "Hybrid Adam Sewing Training Optimization Enabled Deep Learning for Brain Tumor Segmentation and Classification using MRI Images", *Computer Methods in Biomechanics and Biomedical Engineering: Imaging & Visualization*, vol. 11, no. 5, pp. 1921 - 1936, 2023. DOI: 10.1080/21681163.2023.2199891 [ISSN Print- 2168- 1163 Online-2168-1171] [Impact factor 1.6 (Taylor & Francis)].

Conferences Publications:

- [1] **Pravin Bidkar**, Ram Kumar, Abhijyoti Ghosh, "Automatic Segmentation Techniques for Brain Cancer Detection from MR Images", *International conference on soft computing and signal processing, ICSCSP 2020*, Hyderabad, August 21-22, 2020, vol 2, pp 465 – 473, Springer Singapore. **(Paper presented)**
- [2] **Pravin Bidkar**, Ram Kumar, Abhijyoti Ghosh, "Adaptive Salp Swarm Optimization for Brain Tumor Classification using MRI Images", *International conference on engineering informatics, ICEI 2023*, Kolhapur, Maharashtra, November 25-26, 2023, IEEE Swinburne. **(Paper presented)**
- [3] **Pravin Bidkar**, Ram Kumar, Abhijyoti Ghosh, "ASWO_Dbnealexnet with Adaptive Technique for Brain Tumor Classification", *International Conference on Engineering Informatics, ICEI 2023*, Kolhapur, Maharashtra, November 25-26, 2023, IEEE Swinburne. **(Paper presented)**

PARTICULARS OF THE CANDIDATE

NAME OF CANDIDATE : PRAVIN SHIVAJI BIDKAR
DEGREE : Ph.D.
DEPARTMENT : ELECTRONICS AND COMMUNICATION
ENGINEERING
TITLE OF THE THESIS : ANALYSIS ON MRI BRAIN TUMOR
SEGMENTATION USING OPTIMIZATION
– BASED DEEP LEARNING CLASSIFIER
DATE OF ADMISSION : 24th JULY 2019
APPROVAL OF
RESEARCH PROPOSAL
1. DRC : 3rd MARCH 2020
2. BOS : 22nd APRIL 2020
3. SCHOOL BOARD : 13th MAY 2020
MZU REGISTRATION NO. : 1900181
Ph. D REGISTRATION : MZU/Ph. D/1558 of 24.07.2019
NO. & DATE
EXTENSION : NO

(Dr. ACHINTA BIDYA)

Head

Department of Electronics and Communication Engineering

ABSTRACT

ANALYSIS ON MRI BRAIN TUMOR SEGMENTATION USING OPTIMIZATION - BASED DEEP LEARNING CLASSIFIER

**AN ABSTRACT SUBMITTED IN PARTIAL FULFILLMENT OF
THE REQUIREMENTS FOR THE DEGREE OF DOCTOR OF
PHILOSOPHY**

PRAVIN SHIVAJI BIDKAR

MZU REGISTRATION NO.: 1900181

Ph.D. REGISTRATION NO.: MZU/Ph. D. /1558 of 24.07.2019



**DEPARTMENT OF ELECTRONICS & COMMUNICATION
ENGINEERING
SCHOOL OF ENGINEERING AND TECHNOLOGY
MARCH 2025**

**ANALYSIS ON MRI BRAIN TUMOR SEGMENTATION USING
OPTIMIZATION - BASED DEEP LEARNING CLASSIFIER**

BY

**PRAVIN SHIVAJI BIDKAR
DEPARTMENT OF ELECTRONICS & COMMUNICATION
ENGINEERING**

**Name of Supervisor : Dr. ABHIJYOTI GHOSH
Name of Joint Supervisor : Dr. RAM KUMAR**

Submitted

**In partial fulfillment of the requirement of the Degree of Doctor of Philosophy
in Electronics & Communication Engineering of Mizoram University, Aizawl**

The dissertation begins by elucidating the fundamentals of digital image processing, defining a digital image and introducing the concept of pixels as its smallest elements. It provides insight into the acquisition of Magnetic Resonance Imaging (MRI) images, detailing various modalities used. The discussion then shifts to the types of brain tumors, with a focus on gliomas, which are a leading cause of patient mortality. The importance of early tumor detection to improve patient outcomes is emphasized.

Various methods for brain tumor detection are reviewed, highlighting their limitations and the need for automated detection approaches. Manual segmentation of brain tumors is deemed laborious, prompting the exploration of automatic segmentation methods. The significance of accurate segmentation and classification in cancer detection and treatment is underscored, as it aids in identifying tumor boundaries and determining appropriate treatment strategies. The dissertation explores into automated techniques for brain tumor classification, using machine learning and deep learning methodologies. These techniques eliminate the need for expert intervention and offer improved accuracy and efficiency in tumor detection and classification. The challenges associated with achieving high accuracy in brain image classification are acknowledged, emphasizing the importance of overcoming vagueness in image interpretation. Accurate segmentation and classification are crucial for treatment planning and disease progression monitoring, enabling clinicians to precisely localize tumors and tailor treatment approaches accordingly. The dissertation underscores the essential role of automated techniques in improving diagnostic accuracy and patient outcomes in the context of brain tumor detection and treatment.

MRI has emerged as a crucial tool for brain tumor detection, offering detailed three-dimensional images without ionizing radiation. MRI works by subjecting the body to a strong magnetic field and radio pulses, which excite hydrogen nuclei, emitting signals that reveal tissue characteristics. MRI captures data from different tissue types, by adjusting magnetic fields and monitoring signal decay rates, allowing for contrast differentiation in resulting images. Different radio pulse sequences and interpretation techniques optimize image quality and aid in detecting abnormalities

like lesions and tumors with distinct relaxation times.

Brain tumor classification in MRI images is vital for treatment planning, early diagnosis, and outcome evaluation. However, classifying and diagnosing tumors from numerous images poses challenges, necessitating an automatic prediction system. This dissertation introduces a novel strategy based on Salp Water Optimization-based Deep Belief Network (SWO-based DBN) for brain tumor classification. The SWO-based DBN technique exhibits adaptability to different tumor types and imaging conditions, enabling robust performance across diverse clinical scenarios. The research makes significant contributions to the field of brain tumor detection and classification through the introduction of innovative methodologies and optimization techniques. Firstly, the proposed SegNet is utilized for brain tumor segmentation, leveraging the benefits of the SegNet architecture trained by Salp Water Optimization (SWO). SegNet's efficient storage of max-pooling indices and the utilization of a decoder network enhance segmentation performance. Secondly, the research presents the SWO-based Deep Belief Network (DBN) for brain tumor classification. This approach categorizes tumors into edema, malignant, core, and benign categories, leveraging the adaptability of SWO, which integrates Salp Swarm Algorithm (SSA) and Water Wave Optimization (WWO) techniques.

The segmentation process includes pre-processing to remove artifacts and noise, followed by segmentation using a customized SegNet based on SWO optimization. Segmented tumor regions undergo feature extraction using CNN features extracted from a convolutional layer. The classification task employs DBN to improve detection performance by deriving optimal weights using SWO. The proposed method integrates SWO with WWO and SSA to train the DBN classifier. The technique's performance relies on the quality and quantity of training data, with variations across datasets, affecting effectiveness. The success of the technique hinges on the availability of reliable training data, ensuring accurate tumor classification and effective utilization of the SWO-based DBN approach in clinical practice.

The dissertation introduces second innovative novel technique for brain tumor segmentation and classification, Adam Sewing Training Based Optimization with UNet++ (AdamSTBO+UNet++) for segmentation and Adam Salp Water Wave Optimization with Deep Convolutional Neural Network (AdamSWO-DCNN) for classification. AdamSTBO+UNet++ utilizes UNet++ for segmentation, with weights tuned by the AdamSTBO algorithm which is a hybrid of Adam optimizer and STBO. Meanwhile, AdamSWO-DCNN employs DCNN for classification, with weights adjusted by AdamSWO which is nothing but a modification of SWO with Adam Optimizer, integrating SSA and WWO. AdamSWO-DCNN further enhances accuracy by extracting relevant features like CNN, LOOP, LGP, PHoG, and GLCM.

Several challenges hinder existing approaches, including limited availability of data in clinical settings, imbalanced data in brain imaging segmentation, and variations in imaging conditions such as magnetic field strength. Furthermore, reducing computation time in segmentation tasks, particularly those involving deep learning techniques, remains a common challenge. Despite attempts to improve accuracy through methods like Bayesian fuzzy clustering, prolonged training times persist as obstacles. The AdamSTBO + UNet++ and Adam Salp Water Wave Optimization with Deep Convolution Neural Network (AdamSWO_DCNN) algorithm addresses these challenges by utilizing excess layers and regularization strategies for brain tumor segmentation and classification. The integration of the Adam optimizer with the STBO algorithm enhances the performance of segmentation. Moreover, the proposed AdamSWO_DCNN employed for brain tumor classification, utilizing the AdamSWO algorithm that combines Adam optimizer with SWO, formed by integrating SSA and WWO enhances the classification accuracy and reliability through innovative optimization strategies.

Additionally, the research introduces Adaptive Salp Swarm Optimization (ASO) with Deep Residual Network (DRN), a novel method for brain cancer identification using MRI images, which utilizes ASO to train a DRN classifier effectively. This technique enhances diagnostic accuracy and reduces reliance on manual interpretation. ASO optimizes the DRN parameters adaptively, potentially improving convergence speed and solution quality. ASO enhances the robustness and

effectiveness of the classification system, by dynamically adjusting the optimization process, navigating complex optimization spaces more effectively and reducing the risk of local optima. The proposed technique improves generalization performance by learning from diverse datasets and handling variations in input distribution, ensuring robust and reliable classification across different scenarios. Its versatility allows for diagnosing various brain tumors detected through MRI imaging, including gliomas, meningiomas, pituitary tumors, and metastatic tumors. The technique can be tailored to different clinical applications, including integration with other imaging modalities like CT and PET scans. In the proposed method, a DRN model optimized with ASO is utilized for early-stage brain tumor classification using MRI images.

Lastly, the research presents another novel technique, the Adaptive ASWO_DbneAlexnet algorithm, integrating Adam optimizer and SWO with an adaptive concept, offering more reliable diagnostic results and enhancing the efficiency of brain tumor segmentation and classification. These proposed techniques collectively streamline the diagnostic process, reduce errors, and improve efficiency in brain tumor detection and classification, ultimately advancing medical imaging and diagnostic practices. It addresses challenges posed by heterogeneous tumor dimensions and image quality degradation. This method utilizes U-Net++ for precise tumor segmentation in MRI images, improving classification accuracy by considering only relevant regions. The Adaptive ASWO optimizer, derived from Adam optimizer and SWO, enhances model robustness and convergence speed, leading to improved classification performance.

Implementing and fine-tuning these techniques requires expertise in optimization algorithms, deep learning, and medical image analysis. Healthcare professionals lacking such expertise may struggle to utilize or customize these methods. Additionally, training deep learning models with optimization algorithms demands significant computational resources, potentially limiting accessibility to institutions with adequate infrastructure. Overall, the proposed techniques integrate optimization algorithms and deep learning architectures to achieve superior classification results, contributing to ongoing research in medical image processing and machine learning, for brain tumor diagnosis and treatment planning of

neurological disorders.